



**UNIVERSIDADE FEDERAL DA BAHIA**  
**INSTITUTO DE GEOCIÊNCIAS**  
**PROGRAMA DE PESQUISA E PÓS-GRADUAÇÃO EM GEOLOGIA**  
**ÁREA DE CONCENTRAÇÃO:**  
**PETROLOGIA, METALOGÊNESE E EXPLORAÇÃO MINERAL**

**DISSERTAÇÃO DE MESTRADO**

**MINERALOGIA E GEOQUÍMICA DO DEPÓSITO DE**  
**NÍQUEL LATERÍTICO MORRO DO ENGENHO, PROVÍNCIA**  
**ALCALINA DE GOIÁS**

**EDUARDO MOUSSALLE GRISSOLIA**

SALVADOR

2022

**MINERALOGIA E GEOQUÍMICA DO DEPÓSITO DE  
NÍQUEL LATERÍTICO MORRO DO ENGENHO, PROVÍNCIA  
ALCALINA DE GOIÁS**

**Eduardo Moussalle Grissolia**

*Orientador: Prof. Dr. Aroldo Misi*

*Coorientador: Prof. Dr. Pedro Maciel de Paula Garcia*

Dissertação de Mestrado apresentada ao Programa de Pós-Graduação em Geologia do Instituto de Geociências da Universidade Federal da Bahia como requisito parcial à obtenção do Título de Mestre em Geologia, Área de Concentração: Petrologia, Metalogênese e Exploração Mineral.

SALVADOR

2022

G869 Grissolia, Eduardo Moussalle

Mineralogia e geoquímica do depósito de níquel laterítico Morro do Engenho, Província Alcalina de Goiás/ Eduardo Moussalle Grissolia. – Salvador, 2022.

73 f.

Orientador: Prof. Dr. Aroldo Misi

Dissertação (Mestrado) – Universidade Federal da Bahia. Instituto de Geociências, 2022.

1. Geologia. 2. Geoquímica. 3. Mineralogia. I. Misi, Aroldo. II. Universidade Federal da Bahia. III. Título.

CDU 551

**EDUARDO MOUSSALLE GRISSOLIA**

**MINERALOGIA, GEOQUÍMICA E VARIABILIDADE ESPACIAL DO  
DEPÓSITO DE Ni LATERÍTICO MORRO DO ENGENHO, PROVÍNCIA  
ALCALINA DE GOIÁS**

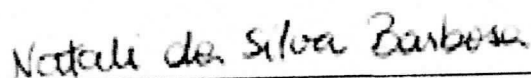
Dissertação de Mestrado apresentada ao Programa de Pós-Graduação em Geologia da Universidade Federal da Bahia como requisito para a obtenção do Título de Mestre em Geologia, Área de Concentração: Petrologia, Metalogênese e Exploração Mineral em 13/06/2022.

**DISSERTAÇÃO APROVADA PELA BANCA EXAMINADORA:**



---

**Dr. Aroldo Misi (Orientador) - UFBA**



---

**Dra. Natali da Silva Barbosa - UFBA**



---

**Dr. Marcondes Lima da Costa - UFPA**

**SALVADOR**

**2022**

*Aos meus pais, minha esposa e minhas filhas  
com muito carinho.*

## AGRADECIMENTOS

O presente trabalho foi realizado com o apoio da CAPES - Código de financiamento 001.

Dedico este trabalho aos meus pais, Sandra e Orlando (*In memoriam*) que, incansavelmente, enfrentaram todas as dificuldades para que eu e minhas irmãs pudéssemos estudar e nos formar na universidade.

À minha esposa, Larene, por todo seu apoio, incentivo e ajuda durante estes dois anos de curso. Por toda sua dedicação com nossas duas filhas pequenas, nos incontáveis momentos em que estive ausente.

Às minhas duas filhas, Maya e Paola, por serem o meu incentivo, todos os dias, para buscar o crescimento pessoal e profissional.

Ao SGB-CPRM por ter viabilizado este estudo, oferecendo todo suporte e estrutura necessários para o desenvolvimento das etapas.

Aos colegas de SGB-CPRM e equipe da Divisão de Economia Mineral e Geologia Exploratória, em especial ao meu chefe Ruben Sardou, por todo seu apoio ao longo desta etapa. Meu agradecimento fraterno aos colegas e amigos Daniel Miranda, Ricardo Wosniak, Angeval Brito, Ricardo Santiago, Alice Dias e Said Abdallah.

Meus agradecimentos ao meu orientador, Prof. Aroldo Misi e coorientador, Prof. Pedro Maciel, por todo o conhecimento compartilhado e apoio durante o desenvolvimento desta pesquisa.

## RESUMO

O depósito de níquel laterítico Morro do Engenho é resultado da atuação de processos intempéricos sobre as rochas máfico-ultramáficas alcalinas que compõem o corpo intrusivo zonado de idade cretácea, pertencente à Província Alcalina de Goiás. Historicamente, o depósito é classificado como do tipo silicático, onde a mineralização está presente principalmente, em filossilicatos como serpentina e clorita. Este estudo tem como objetivo a compreensão dos processos metalogenéticos e controles atuantes na mineralização do depósito de níquel laterítico de Morro do Engenho, através da identificação das fases minerais portadoras de Ni e caracterização litogeoquímica dos perfis de alteração. A metodologia utilizada contou com estudos de petrografia, MEV/EDS, DRX e caracterização litogeoquímica dos perfis de alteração desenvolvidos sobre cada uma das rochas parentais que compõem o corpo. O maciço intrusivo de Morro do Engenho é formado por um núcleo dunítico, circundado por uma zona peridotito/piroxenítica, uma zona gabróica alcalina e mais externamente por uma zona sienito-nefelínica. No perfil laterítico foi possível reconhecer oito horizontes de alteração, empilhados a partir do bedrock como: (i) saprock, (ii) saprólito inferior, (iii) saprólito ferruginoso, (iv) saprólito ocre, (v) zona plasmática, (vi) duricrosta laterítica, (vii) silcrete e (viii) topsoil. A mineralização de Ni está concentrada no saprólito inferior, no saprólito ferruginoso e no saprólito ocre. Os resultados apontaram para a presença de Ni em fases minerais silicáticas representadas por serpentina, clorita e esmectita, assim como em fases óxido, concentrado em oxi-hidróxidos de Fe e Mn. A área deprimida, inserida entre as duas elevações topográficas principais, apresenta os maiores enriquecimentos em Ni, os quais podem chegar até 40%. A atuação de fatores hidrodinâmicos, através de dissolução/precipitação de silicatos nos horizontes saprolíticos do núcleo dunítico, são sugeridas como possíveis agentes atuantes na remobilização do Ni, dentre outros elementos móveis, para zonas planas topograficamente. A geometria do depósito Morro do Engenho mostra que a redistribuição lateral através dos fatores hidrodinâmicos poderia também explicar a mineralização de áreas periféricas ao núcleo dunítico, compostas por perfis lateríticos derivados de piroxenito e gabro. A direção do fluxo regional de águas subterrâneas, influenciada fortemente pela topografia, também seria um fator importante na remobilização do Ni, assim como o transporte mecânico de materiais lateríticos. A mineralização dominante no depósito Morro do Engenho é do tipo silicática, concentrada em hidrossilicatos de Mg e argilominerais com participação importante de mineralização do tipo óxido, presente, sobretudo, em oxi-hidróxidos de Fe e Mn. As discussões aqui apresentadas contribuem para a compreensão dos processos metalogenéticos atuantes na gênese de depósitos de Níquel laterítico a partir de corpos máfico-ultramáficos e fornecem subsídios para campanhas de exploração de depósitos similares.

Palavras-chave: Intemperismo. Ni laterítico. Rochas máfico-ultramáficas alcalinas. Mineralização de Ni tipo silicato. Mineralização de Ni tipo óxido.

## ABSTRACT

The Morro do Engenho lateritic nickel deposit results from the action of weathering processes on the alkaline mafic-ultramafic rocks that make up the Cretaceous zoned intrusive body belonging to the Goiás Alkaline Province. Historically, the deposit is classified as a silicate one, and mineralization is present especially in phyllosilicates such as serpentine and chlorite. By identifying Ni-bearing phases and providing the lithogeochemical characterization of alteration profiles, this study aims to provide further insights into the metallogenetic processes and controls acting on the mineralization of the Morro do Engenho lateritic Ni deposit. The following methods were used: petrographic studies, SEM/EDS, XRD and lithogeochemical characterization of the alteration profiles developed on each of the parent rocks that make up the body. The Morro do Engenho intrusive massif is formed by a dunite core, surrounded by a peridotite/pyroxenite zone, an alkaline gabbro zone and more externally by a syenite-nepheline zone. The lateritic profile contained eight alteration horizons, stacked one upon another from the bedrock namely: (i) saprock, (ii) lower saprolite, (iii) ferruginous saprolite, (iv) ocher saprolite, (v) plasma zone, (vi) lateritic duricrust, (vii) silcrete and (viii) topsoil. Most Ni mineralization occurs in the lower saprolite, ferruginous saprolite and ocher saprolite zones. The findings pointed to the presence of Ni in silicate mineral phases - represented by serpentine, chlorite and smectite - as well as in oxide phases - concentrated in Fe and Mn oxyhydroxides. The depressed area, located between the two major topographic elevations, has the highest Ni enrichments, which can account for up to 40%. Hydrodynamic factors, by dissolution/precipitation of silicates in saprolite horizons of dunite core, are suggested as possible agents in the remobilization of Ni - among other mobile elements - to topographically flat zones. The geometry of the Morro do Engenho deposit show that lateral redistribution by hydrodynamic factors could also account for the mineralization of areas peripheral to the dunite core, composed of pyroxenite and gabbro-derived lateritic profiles. The direction of regional groundwater flow, strongly influenced by topography, would also be an important factor in the remobilization of Ni, as well as the mechanical transport of lateritic materials. Silicate mineralization predominates in the Morro do Engenho deposit, concentrated in Mg hydrosilicates and clay minerals; oxide mineralization also occurs, mostly in Fe and Mn oxyhydroxides. The findings discussed in this paper can broaden the understanding of metallogenetic processes involved in the genesis of lateritic nickel deposits from mafic-ultramafic bodies and provide valuable information for scientific expeditions aiming to explore similar deposits.

**Keywords:** Weathering. Niquel laterite. Alkaline mafic-ultramafic rocks. Silicate-type Ni mineralization. Oxide-type Ni mineralization.



## SUMÁRIO

<b>CAPÍTULO 1 – INTRODUÇÃO GERAL.....</b>	<b>8</b>
<b>CAPÍTULO 2 – ARTIGO: MINERALOGY AND GEOCHEMISTRY OF THE MORRO DO ENGENHO LATERITIC NICKEL DEPOSIT, GOIÁS ALKALINE PROVINCE, BRAZIL.....</b>	<b>12</b>
<b>CAPÍTULO 3 – CONCLUSÕES.....</b>	<b>61</b>
<b>APÊNDICE A – JUSTIFICATIVA DA PARTICIPAÇÃO DOS AUTORES .....</b>	<b>63</b>
<b>ANEXO A – REGRAS DE FORMATAÇÃO DA REVISTA JOURNAL OF SOUTH AMERICAN EARTH SCIENCES.....</b>	<b>64</b>
<b>ANEXO B – COMPROVANTE DE SUBMISSÃO DO ARTIGO.....</b>	<b>71</b>

# CAPÍTULO 1

## INTRODUÇÃO GERAL

---

Considerado historicamente um metal crítico na indústria de aços inoxidáveis, o níquel (Ni) vem acompanhando os avanços tecnológicos dos últimos dois séculos, tendo aplicações em uma gama crescente de produtos (Mudd & Jowitt, 2014). Embora a indústria de aços inoxidáveis represente ainda mais do que 60% do consumo global de níquel, o avanço crescente na produção de veículos elétricos, acompanhado da necessidade de fabricação de baterias cada vez mais potentes, vem provocando um aumento contínuo da demanda do metal. Estudos recentes apontam que até 2025, a indústria de baterias será responsável por cerca de 15% do consumo da produção global de níquel (König, 2021). Tais projeções ratificam a importância da busca por depósitos de níquel laterítico que, atualmente, representam 60 a 70% dos recursos globais e 60% da produção mundial deste metal (Maurizot et al., 2019; König, 2021).

Os depósitos lateríticos de níquel são gerados em condições de clima quente e úmido, tropical e paleotropical, a partir da atuação de prolongado intemperismo químico sobre rochas ultramáficas (Lelong et al. 1976; Aleva, 1994, Brand et al. 1998, Anand & Paine, 2002; Elias, 2002; Freyssinet et al. 2005; Golightly 2010; Marsh & Anderson, 2013; Butt and Cluzel, 2013). Além do clima e rocha parental, a gênese dos depósitos de Ni laterítico está intimamente relacionada a fatores como topografia, drenagem, tectônica e estruturas (Brand et al. 1998; Elias, 2002; Butt and Cluzel, 2013; Freyssinet et al. 2005). Tais fatores atuam de forma conjunta na geração dos enriquecimentos de Ni e são determinantes para a estruturação dos perfis lateríticos e tipos de mineralização gerados (Elias, 2002).

A classificação dos depósitos baseia-se no tipo de mineralização dominante e é dividida em três grupos principais, denominados: depósitos tipo óxido, depósitos tipo hidrossilicatos de Mg e depósitos tipo argilominerais (Brand et al., 1998; Gleeson et al., 1999; Freyssinet et al., 2005; Golightly, 2010; Butt e Cluzel, 2013). Os depósitos tipo óxido são dominados por oxi-hidróxidos de Fe, principalmente goethita, além de óxidos de Mn enriquecidos tanto em Ni quanto em Co (Butt e Cluzel, 2013). A mineralização tipo hidrossilicatos de Mg ocorre associada à serpentina, talco, clorita e sepiolita, coletivamente tratados como garnierita (Butt e Cluzel, 2013). No tipo argilominerais as concentrações de Ni ocorrem associadas à esmectitas dioctaédricas e trioctaédricas com altos conteúdos de Fe e Al (Tauler et al., 2017), originadas a partir de piroxênios (Colin et al. 1990). De acordo com Butt e Cluzel (2013), a definição do tipo de mineralização tem implicações importantes no aproveitamento econômico do depósito, principalmente em função do tipo de processamento de minério a ser adotado. Contudo, raramente os depósitos lateríticos de Ni apresentam apenas um tipo de mineralização, sendo necessário, desta forma, conhecer a mineralogia e a química das fases mineralizadas para determinar as melhores rotas de processamento do minério (Putzolu et. al., 2020).

No Brasil, os depósitos lateríticos representam a maioria das fontes de Ni. Segundo Costa (2016), a abundância de depósitos lateríticos tem relação com as condições climáticas favoráveis vividas durante o Cenozoico, além da presença numerosa de corpos ultramáficos no país. Os depósitos de Ni laterítico mais importantes no Brasil são Vermelho, Onça-Puma, Jacaré, Niquelândia, Barro Alto,

Crixás, Santa Fé, Montes Claros, Morro do Níquel, Liberdade, Ipanema, Pratópolis, Capitão Gervásio, Morro Sem Boné, Morro do Leme e Jacupiranga, desenvolvidos sobre rochas máfico-ultramáficas de idades pré-cambrianas a cretáceas (Costa, 2016).

O depósito de Ni laterítico de Morro do Engenho está localizado na região centro-oeste do estado de Goiás (Fig. 1a,b), e é caracterizado por perfis de alteração desenvolvidos sobre as rochas, de idade cretácea, que compõem o corpo intrusivo zonado do complexo máfico-ultramáfico alcalino homônimo (Fig. 1d). O maciço, integrante da Província Alcalina de Goiás (Fig. 1c), é formado por um núcleo dunítico, circundado por uma zona peridotito/piroxenítica, uma zona gabroica alcalina e mais externamente por uma zona sienito-nefelínica (Chaban et al., 1975).

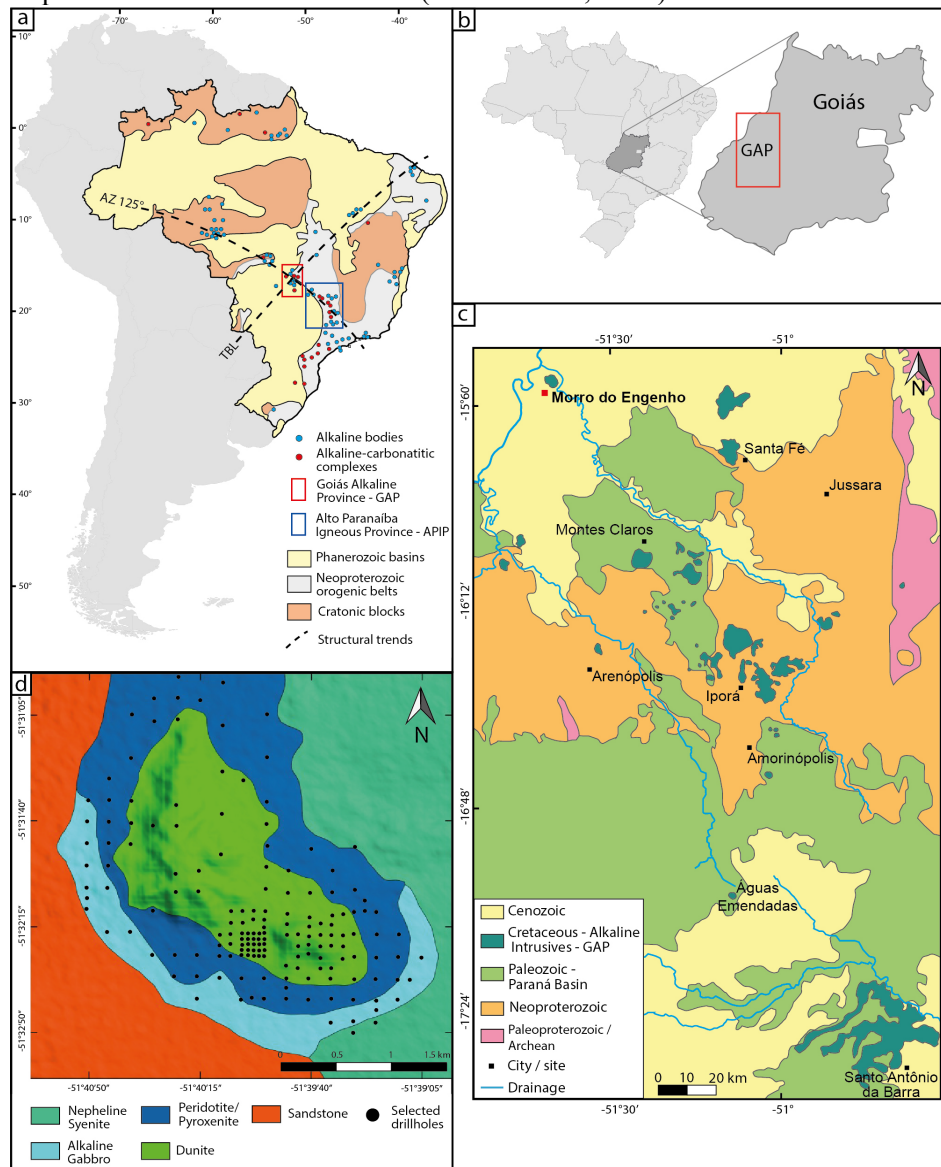


Fig. 1. a) Mapa de localização das principais ocorrências de rochas alcalinas e complexos carbonatíticos do Brasil no contexto dos *trends* estruturais regionais, do chamado “Azimute 125°” (AZ 125°) e TBL (Lineamento Transbrasiliano) e os domínios cratônicos, neoproterozoicos e fanerozoicos (adaptado de Nascimento, 2018); b) Localização da Província Alcalina de Goiás (GAP) no território do Estado de Goiás; c) Mapa geológico da Província Alcalina de Goiás exibindo a distribuição dos corpos alcalinos (adaptado de Nascimento, 2018); d) Mapa de subsuperfície do complexo máfico-ultramáfico alcalino Morro do Engenho (adaptado de Chaban et al., 1975).

Enriquecimentos de Ni associados a rochas parentais piroxeníticas e gabroicas não são comuns na literatura. A presença de zonas mineralizadas com altos teores em perfis derivados de litologias deste tipo em Morro do Engenho levanta a possibilidade de que outros agentes, além dos processos mais comuns de formação dos depósitos de Ni laterítico, tenham atuado na gênese do depósito. Exemplos como Niquelândia e Santa Fé, mostram que a ação de águas subterrâneas no transporte de soluções ricas em Ni podem produzir mineralizações em zonas topograficamente mais baixas (Colin et al., 1990; Machado et al., 2021).

O presente estudo objetiva compreender os processos metalogenéticos e controles que atuaram na mineralização do depósito de Ni laterítico de Morro do Engenho. Para tal, foram empreendidos métodos que incluem a identificação das fases minerais portadoras de minério e a caracterização litogeoquímica dos perfis de alteração desenvolvidos sobre cada uma das rochas parentais que compõem o corpo zonado, através de estudos de petrografia, difratometria de raios-X – DRX e Microscopia Eletrônica de Varredura – MEV.

Os resultados obtidos nesta pesquisa foram organizados sob a forma de artigo científico, apresentado no capítulo 2 desta dissertação. O manuscrito será submetido à revista *Journal of South American Earth Sciences*, ISSN 0895-9811, classificação B1 do Qualis Capes.

## Referências

- ALEVA, G.J.J. **Laterites: concepts, geology, morphology and chemistry**. Wageningen: ISRIC, 1994. 169 p.
- ANAND, R. R.; PAINE M. Regolith geology of the Yilgarn Craton, Western Australia: Implications for exploration. **Australian Journal of Earth Sciences**. v. 49, n.1, 3-162, 2002. DOI: 10.1046/j.1440-0952.2002.00912.x
- BRAND, N.W.; BUTT, C.R.; ELIAS, M. Nickel laterites: classification and features. **AGSO Journal of Australian Geology e Geophysics**, Symonston ACT, v. 17, n. 4, p. 81-88. 1998.
- BUTT C.R.M.; CLUZEL D. Nickel laterite ore deposits: weathered serpentinites. **Elements**, v. 9, n. 2, p.123–128, 2013.
- COLIN, F.; NAHON, D.; TRESCASES, J.J.; MELFI, A.J. Lateritic Weathering of Pyroxenites at Niquelândia, Goiás, Brazil: the supergene behavior of nickel. **Economic Geology**, Chicago, v. 85, n. 05, p.1010-1023, ago. 1990.
- COSTA, M.L. O níquel no Brasil e seus depósitos lateríticos. In: MELFI, A.J.; MISI, A.; CAMPOS, D.A.C.; CORDANI, U.G. (org.) **Recursos Minerais no Brasil: problemas e desafios**. Rio de Janeiro: Academia Brasileira de Ciências, 2016. Cap. 01, p.124-132.
- ELIAS, M. Nickel lateritic deposits – Geological overview, resources and exploitation. In: COOKE, D.; PONGRATZ, J. (ed.) **Giant Ore Deposits: characteristics, genesis and exploration**. Hobart: University of Tasmania, 2002. p. 205-220.

FREYSSINET, P.H.; BUTT, C.R.M.; MORRIS, R.C.; PIANTONE, P. Ore-forming processes related to lateritic weathering. **Economic Geology**, volume de 100° aniversário, p. 681-722, 2005.

GLEESON, S.A.; BUTT, C.R.M.; ELIAS, M.; Nickel Laterites: A Review. **SEG Discovery**, v. 54, p. 1–18, 2003. DOI: <https://doi.org/10.5382/SEGnews.2003-54.fea>.

GOLIGHTLY J.P. Progress in understanding the evolution of nickel laterite. **Society of Economic Geologists**, Inc. Special Publication, v. 15, p. 451–485, 2010.

KÖNIG, U. Nickel Laterites — Mineralogical Monitoring for Grade Definition and Process Optimization. **Minerals**, v. 11, p. 1178, 2021. DOI: <https://doi.org/10.3390/min11111178>.

LELONG, F.; TARDY, Y.; GRANDIN, G.; TRESCASES, J. J.; BOULANGE, B. Pedogenesis, chemical weathering and processes of formation of some supergene ore deposits. In: WOLF, K. H. (ed.). **Handbook of Strata-bound and Stratiform Ore Deposits**. Amsterdam, Elsevier, v. 3, P. 93–174, 1976.

MACHADO, M.; PORTO, C.; SANTORO, L.; PUTZOLU, F.; NEUMANN, R.; BASTOS NETO, A.; POLIVANOV, H.; HERRINGTON, R. The origin of supergene nickeliferous chlorite in the Santa Fé Ni-Laterite Deposit, GO, Brazil. **Brazilian Journal of Geology**, v. 51, 2021. DOI: 10.1590/2317-4889202120200119.

MARSH, E.; ANDERSON, E.; GRAY, FLOYD. **Nickel-cobalt laterites - a deposit model**: chapter H in mineral deposit models for resource assessment. Reston: USGS, 2013. (USGS Scientific Investigations Report 2010–5070–H).

MAURIZOT, P.; SEVIN, B.; ISEPPI, M.; GIBAND, T. Nickel-Bearing Laterite Deposits in Accretionary Context and the Case of New Caledonia: From the Large-Scale Structure of Earth to Our Everyday Appliances, **GSA Today**, v. 29, n. 5, p. 4–10, 2019.

MUDD, G. M. & JOWITT, S.M.; A Detailed Assessment of Global Nickel Resource Trends and Endowments. **Economic Geology**, v. 109, n. 7, p. 1813–1841, 2014. DOI: <https://doi.org/10.2113/econgeo.109.7.1813>.

PUTZOLU, F.; ABAD, I.; BALASSONE, G.; BONI, M.; CAPPELLETTI, P.; GRAZIANO, S.; MACZURAD, M.; MONDILLO, N.; NAJORKA, J. Santoro, L. (2020). Parent rock and climatic evolution control on the genesis of Ni-bearing clays in Ni-Co laterites: New inferences from the Wingellina deposit (Western Australia). **Ore Geology Reviews**, 120:103431. DOI: 10.1016/j.oregeorev.2020.103431.

TAULER, E., LEWIS, J.F., VILLANOVA-DE-BENAVENT, C.; AIGLSPERGER, T.; PROENZA, J.A.; DOMÈNECH, C.; GALLARDO, T.; LONGO, F.; GALÌ, S. Discovery of Ni-smectite-rich saprolite at Loma Ortega, Falcondo mining district (Dominican Republic): geochemistry and mineralogy of an unusual case of “hybrid hydrous Mg silicate – clay silicate” type Ni-laterite. **Miner Deposita**, v. 52, p. 1011–1030, 2017. DOI: <https://doi.org/10.1007/s00126-017-0750-8>.

**CAPÍTULO 2**

**ARTIGO – MINERALOGY AND GEOCHEMISTRY OF  
THE MORRO DO ENGENHO LATERITIC NICKEL  
DEPOSIT, GOIÁS ALKALINE PROVINCE, BRAZIL**

---

Eduardo Moussalle Grissolia <sup>a\*,b</sup>, Pedro Maciel de Paula Garcia <sup>b,c</sup>, Aroldo Misi <sup>b</sup>, Alice dos Santos  
Dias <sup>d</sup>

<sup>a</sup> Geological Survey of Brazil-CPRM, Av. Ulysses Guimarães, 2862, Salvador, BA, CEP 41213-000,  
Brazil

<sup>b</sup> Programa de Pós-Graduação em Geologia, Instituto de Geociências, Universidade Federal da Bahia,  
Salvador, BA, Brasil

<sup>c</sup> Programa de Pós-Graduação em Geociências, Faculdade de Geociências, Universidade Federal de  
Mato Grosso, Av. Fernando Corrêa da Costa 2367, Cuiabá, MT, CEP 78060-900, Brasil

<sup>d</sup> Vale, Av. Getúlio Vargas 671, Belo Horizonte, MG, CEP 30112-020, Brasil

\*Corresponding author: [eduardo.grissolia@cprm.gov.br](mailto:eduardo.grissolia@cprm.gov.br)

### **HIGHLIGHTS**

- Lateritic profiles derived from serpentized dunite, pyroxenite and gabbro containing Ni mineralization.
- Presence of oxide–silicate mineralization of Ni.
- Ni concentrations affected by hydrodynamics and mechanical transport of lateritic materials.

## ABSTRACT

The Morro do Engenho lateritic nickel deposit results from the action of weathering processes on the alkaline mafic-ultramafic rocks that make up the Cretaceous zoned intrusive body belonging to the Goiás Alkaline Province. Historically, the deposit is classified as a silicate one, and mineralization is present especially in phyllosilicates such as serpentine and chlorite. By identifying Ni-bearing phases and providing the lithogeochemical characterization of alteration profiles, this study aims to provide further insights into the metallogenetic processes and controls acting on the mineralization of the Morro do Engenho lateritic Ni deposit. The following methods were used: petrographic studies, SEM/EDS, XRD and lithogeochemical characterization of the alteration profiles developed on each of the parent rocks that make up the body. The Morro do Engenho intrusive massif is formed by a dunite core, surrounded by a peridotite/pyroxenite zone, an alkaline gabbro zone and more externally by a syenite-nepheline zone. The lateritic profile contained eight alteration horizons, stacked one upon another from the bedrock namely: (i) saprock, (ii) lower saprolite, (iii) ferruginous saprolite, (iv) ocher saprolite, (v) plasma zone, (vi) lateritic duricrust, (vii) silcrete and (viii) topsoil. Most Ni mineralization occurs in the lower saprolite, ferruginous saprolite and ocher saprolite zones. The findings pointed to the presence of Ni in silicate mineral phases - represented by serpentine, chlorite and smectite - as well as in oxide phases - concentrated in Fe and Mn oxyhydroxides. The depressed area, located between the two major topographic elevations, has the highest Ni enrichments, which can account for up to 40%. Hydrodynamic factors, by dissolution/precipitation of silicates in saprolite horizons of dunite core, are suggested as possible agents in the remobilization of Ni - among other mobile elements - to topographically flat zones. The geometry of the Morro do Engenho deposit show that lateral redistribution by hydrodynamic factors could also account for the mineralization of areas peripheral to the dunite core, composed of pyroxenite and gabbro-derived lateritic profiles. The direction of regional groundwater flow, strongly influenced by topography, would also be an important factor in the remobilization of Ni, as well as the mechanical transport of lateritic materials. Silicate mineralization predominates in the Morro do Engenho deposit, concentrated in Mg hydrosilicates and clay minerals; oxide mineralization also occurs, mostly in Fe and Mn oxyhydroxides. The findings discussed in this paper can broaden the understanding of metallogenetic processes involved in the genesis of lateritic nickel deposits from mafic-ultramafic bodies and provide valuable information for scientific expeditions aiming to explore similar deposits.

**Keywords:** Weathering. Niquel laterite. Alkaline mafic-ultramafic rocks. Silicate-type Ni mineralization. Oxide-type Ni mineralization.



## 1. Introduction

Lateritic nickel deposits are generated under tropical and paleotropical conditions by the action of prolonged chemical weathering on ultramafic rocks (Trescases, 1975; Lelong et al., 1976; Aleva, 1994, Brand et al., 1998, Anand & Paine, 2002; Elias, 2002; Freyssinet et al., 2005; Golightly 2010; Marsh & Anderson, 2013; Butt & Cluzel, 2013). Lateritic sources provide about 60 to 70% of global Ni resources (Butt & Cluzel, 2013). In Brazil, favorable climatic conditions during the Cenozoic are responsible for the abundance of lateritic deposits, which correspond to the majority of Ni sources in the country (Costa, 2016).

The importance of lateritic deposits has been steadily growing compared to sulfide deposits and they already account for approximately 60% of global nickel production (Maurizot et al., 2019). Owing to the growing production of electric vehicles, as well as the need to manufacture increasingly powerful batteries, the demand for Ni has been on a steady rise, encouraging the search for lateritic sources to supply the market (König, 2021).

In general, the genesis of Ni lateritic deposits is closely related to factors such as climate, topography, drainage, tectonics, parent rock and structures (Brand et al., 1998; Elias, 2002; Butt & Cluzel, 2013; Freyssinet et al., 2005). These factors interact for generation of Ni enrichments, and they are decisive for the structure of the resulting lateritic profiles and mineralization types (Elias, 2002). Lateritic Ni deposits are classified into three main types, namely: oxide deposits, Mg hydrosilicate deposits and clay-mineral deposits (Brand et al., 1998; Gleeson et al., 2003; Freyssinet et al., 2005; Golyghtly, 2010; Butt & Cluzel, 2013).

The Morro do Engenho deposit, located in the southwest region of the state of Goiás, is hosted by lateritic alteration profiles developed over dunites, peridotites, pyroxenites and gabbros of the Morro do Engenho alkaline mafic-ultramafic complex. Morro do Engenho has been historically classified as a silicate deposit (Chaban et al., 1975). However, the results of this study show that mineralization is also present in oxide phases. Furthermore, the presence of zones with high mineral contents in profiles derived from pyroxenitic and gabbroic parent rocks raises the possibility that other agents, in addition to the most common processes of formation of lateritic Ni deposits, have played a role in the genesis of the deposit.

Therefore the present study aims to broaden the understanding of metallogenetic processes and controls involved in the mineralization of the Morro do Engenho lateritic Ni deposit. To this end, it used methods for identification of ore-bearing mineral phases and lithochemical characterization of alteration profiles developed on each of the parent rocks that make up the zoned body, by means of petrographic studies, X-ray diffractometry (XRD) and Scanning Electron Microscopy (SEM).

## 2. Study Area

### 2.1. Regional Geology

The intrusive body that hosts the Morro do Engenho lateritic Ni deposit is associated with the alkaline magmatism event that occurred in the South American Platform during the Late Cretaceous (Almeida, 1983; Almeida, 1986; Bizzi & Vidotti, 2003; Mizusaki & Thomas Filho, 2004; Zalán & Thomaz-Filho, 2004; Gomes & Comin-Chiaramonti, 2005). This event resulted in the formation of several alkaline provinces in the marginal zones of the Paraná Basin (Fig.1a), for example, the Alto Paranaíba Igneous Province (APIP) and the Goiás Alkaline Province (GAP), where the Morro do Engenho alkaline mafic-ultramafic complex is located (Junqueira-Brod et al., 2002). K-Ar dating measurements on missourites from the Santa Fé alkaline mafic-ultramafic complex, also part of GAP,

have indicated ages of  $84.7 \pm 1.8$  and  $86.7 \pm 1.8$  Ma for these bodies (Barbour et al., 1979; Sonoki & Garda, 1988).

GAP forms an elongated strip of approximately 250 km along a N30W-trending zone, where numerous outcropping alkaline bodies are present, ranging from volcanic, subvolcanic to intrusive products (Junqueira-Brod et al., 2002). According to Almeida (1983), large faults acted as conduits for the alkaline magmatism of the Upper Cretaceous, through a tectonic rift regime, produced by sets of grabens and horsts with NNW-SSE trend. The N30W structural trend coincides with the regional alignment called Azimuth  $125^\circ$  (Bardet, 1977), which is related to the rise of the Trindade Plume, characterized as a probable source for Late Cretaceous alkaline magmatism (Gibson et al., 1995a; Ferrari & Riccomini, 1999; Assumpção et al., 2002; Alves et al., 2006). Precambrian structures of NE-SW direction, associated with the Transbrasiliiano lineament and the Arco de Bom Jardim, with S80W direction, also affect the structural control of GAP (Junqueira-Brod et al., 2002; Junqueira-Brod et al., 2005; Nascimento, 2018).

The northern portion of GAP, where the Morro do Engenho complex is located, is dominated by alkaline mafic-ultramafic complexes composed of dunites, peridotites, clinopyroxenites, alkaline gabbros, phonolite dikes, lamprophyres, alkaline picrite plugs and syenite halos (Junqueira-Brod et al., 2002; Junqueira-Brod et al., 2005). Junqueira-Brod et al. (2005) suggested that the kamafugitic/picritic magma forming the intrusive bodies in northern GAP would have ascended directly from the mantle, suffering loss of volatiles during its trajectory, and settling in the Precambrian/Phanerozoic Unconformity, at a depth of approximately 600 km. Danni (1994), through studies in dikes, plugs and sills of the Iporá region, suggested that there is a genetic affinity between these rocks and GAP's alkaline complexes, as they are related to the same alkaline-picritic parental magma that would form - in the case of alkaline complexes, through fractional crystallization - the dunite-wehrlite-clinopyroxenite-alkaline gabbro-nepheline syenite series.

Gravimetric and magnetic inversion studies by Dutra & Marangoni (2009) indicated that the Morro do Engenho intrusive body has a nearly spherical shape, with an average diameter of 10 km close to the surface and a gradual decrease in depth. Maximum depth of the body is 10 km and, according to the authors, the results of the inversions do not allow the identification of conduits to the mantle that may indicate the association of this body with plug intrusions, as proposed by Danni (1994). Such findings support the hypothesis formulated by Junqueira-Brod et al. (2005): the origin of the Morro do Engenho body would be associated with the installation of a magma chamber in the upper crust, followed by a tectonic uplift event during or after the Upper Cretaceous, which would have caused the body to ascend.

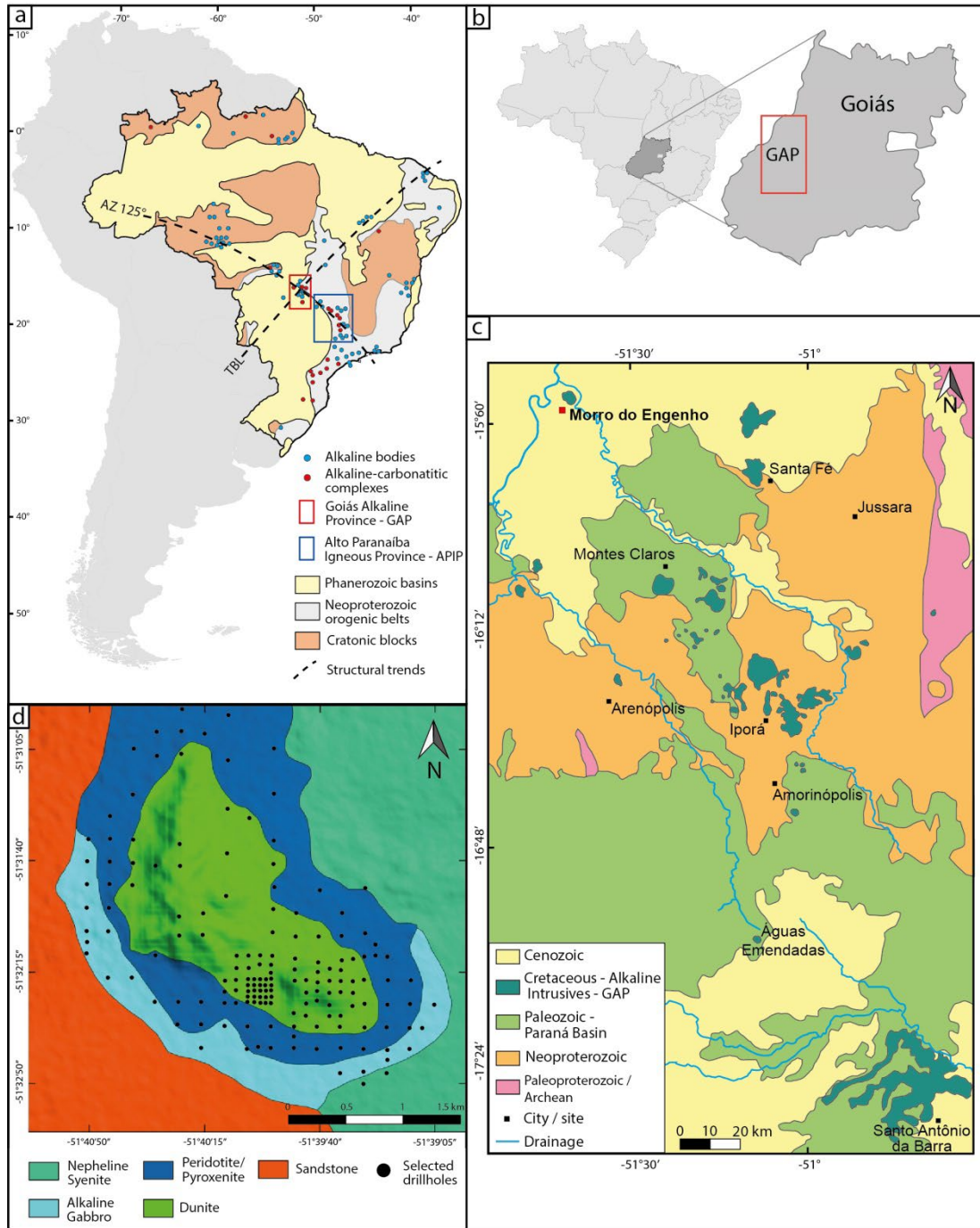


Fig. 1. A) Location map of the main occurrences of alkaline rocks and carbonatite complexes in Brazil in the context of the regional structural Azimuth 125° (AZ 125°) and Transbrasiliano (TBL) lineaments and the cratonic, neoproterozoic and phanerozoic domains (adapted from Nascimento, 2018); b) Location of the Goiás Alkaline Province (GAP) in the territory of the State of Goiás; c) Geological map of the Goiás Alkaline Province showing the distribution of alkaline bodies (adapted from Nascimento, 2018); d) Lithological map with contacts inferred from the Morro do Engenho alkaline mafic-ultramafic complex (adapted from Chaban et al., 1975).

The geomorphological evolution of the region of the Morro do Engenho complex is marked by the action of the South American and Velhas cycles (King, 1956; Braun, 1970; Oliveira, 1980). According to King (1956), Braun (1970) and Oliveira (1980), the South American cycle was marked by a prolonged period of erosion and peneplanation, which occurred during the Paleogene. This event would have caused the exhumation of alkaline bodies from the Upper Cretaceous, including the Morro do Engenho body. Oliveira (1980) described the geomorphological evolution of the study region,

suggesting that the extensive erosive period of the South American cycle would have been followed by a period of aggradational stability, in which the action of weathering processes on alkaline bodies, in tropical climate, favored lateritization on these bodies by dissolution of more soluble elements such as Mg, Ca and Si, and accumulation of less soluble elements such as Fe and Al (Freyssinet et al., 2005). As described by the author, from the Neogene onwards, the Velhas geomorphological cycle would have been responsible for a new stage of denudation of the topographic surface, in which zones with cumulative dissolved silica allowed the relief to be sustained, forming terraces and high pediplanes.

Scherer (2000) reported that during the Mesozoic, the South American platform was covered by aeolian sands from the Botucatu desert, hence its arid climate. Based on such consideration, Golightly (2010) classified the study area as a “dry to-wet” scenario.

According to the Koppen classification (Alvares et al., 2013), the current climate is tropical with dry winters; average annual precipitation ranges between 1,600 and 1,900 mm and predominantly occurs (>75%) throughout the six warmest months (October to March).

## *2.2. Geological characterization of the Morro do Engenho Alkaline Mafic-Ultramafic Complex*

The Morro do Engenho intrusive body (Fig.1c) stands out in the smooth topography of the region because of two elevations slightly oriented towards the NW-SW trend (Fig.2a), measuring about 1,400x400x120m and 400x400x90m each. It was described by Chaban et al. (1975) as a mafic-ultramafic massif with alkaline affiliation and zoned pattern formed by a dunite core, surrounded by a peridotite/pyroxenite zone, an alkaline gabbro zone and, more externally, by a syenite-nepheline zone. Basic to alkaline dikes are frequent, with compositions ranging from diabase, syenite, carbonatite and alaskite (Chaban et al., 1975; Almeida, 1983). The body is embedded in the Eodevonian units of the Paraná Basin, represented by the sandstones and shales of the Furnas formation. It shows rare features of contact metamorphism, evidenced by quartzite levels (Chaban et al., 1975). The elevations are capped by chalcedony crusts and surrounded by eluvial, colluvial, and alluvial covers, topsoil, and ferruginous crusts (Chaban et al., 1975; Berbert, 1986; Junqueira-Brod et al., 2002; Biondi, 2003; Lacerda-Filho et al., 2021).

## *2.3. Lateritic profile and Ni mineralization*

In the lateritic profile, first described by Chaban et al. (1975), five main horizons were recognized from the least altered rock. The lithological variations of the zoned body, as well as its textural-structural aspects, reveal the occurrence of significantly different lateritic profiles, depending on the lithologies of the parent rocks, which reflect variations in the control of Ni mineralization. According to the authors, the ore minerals would be serpentine, chlorite through Mg replacement in Ni in the structure of these minerals during lateritization processes, in addition to spinels (magnetite and chromite).

## **3. Materials and Methods**

### *3.1. Sampling*

The lateritic profile of the Morro do Engenho deposit was studied using the collection of core samples from the Morro do Engenho Project, which are stored and preserved by the Geological Survey of Brazil – CPRM. Based on the geological, mineralogical and geochemical terminologies and understandings of Aleva (1994), Egleton (2001), Anand & Paine (2002), Freyssinet et al., (2005), Watling et al., (2011) and Butt & Cluzel (2013), the lateritic horizons were analyzed further, after observations of 162 drill holes, with an average depth of 35m (minimum depth of 4.5m and maximum

depth of 125m of the drill holes). Further analyses of these horizons focused only on the ultramafic units, since there is no development of lateritic profiles on the alkaline syenitic unit, nor on the sedimentary host.

Sixty-eight drill holes were selected for representative sampling of the 5 domains present in the area. The database had 1265 samples, distributed among the different horizons of the lateritic profiles, which provided information about variations in color, plasticity, texture and grain size at different depths.

### 3.2. Whole-rock chemistry

Whole-rock chemical analyses were performed at the SGS-Geosol Laboratory, in Vespasiano, Brazil. The samples were dried at 105°C, crushed to 3 mm in a crusher, homogenized, quartered and pulverized to a fraction <150#. The concentrations of major and minor elements were determined using XRF (XRF79C) with Li tetraborate fusion. Trace elements were determined by ICP-OES/ICP-MS (ICM14B, ICM40B), with aqua regia or multi-acid digestion. Rare earth elements were determined by ICP-OES/ICP-MS (IMS95A, ICP95A), with lithium metaborate fusion.

To quantify the effects of lateritization processes along the lateritic profiles, the the Ultramafic Index of Alteration (UMIA) was calculated (Babechuk et al., 2014; Aiglsperger et al., 2016; Putzolu et al., 2021). The UMIA index is calculated using the molar ratios between the oxides of major elements, defined by the following formula:

$$UMIA = 100 \times [(Al_2O_3 + Fe_2O_3(T)) / (SiO_2 + MgO + Al_2O_3 + Fe_2O_3(T))]$$

### 3.3 Density Measurements (Dry bulk sample)

Density tests were carried out for 118 samples that were representative of the different horizons of the lateritic profiles, developed on each of the lithotypes that make up the Morro do Engenho mafic-ultramafic zoned body. Holes at the greatest depths of each of the lithological zones enabled the collection of samples with the lowest possible degree of alteration. The procedures were performed in accordance with ASTM C 914-95 (ASTM, 2004). The samples of disaggregated materials underwent compaction processes in specific bottles for weighing and calculating the densities according to the formula:

$$\text{Density (g/cm}^3\text{)} = P_s / V_f$$

where  $P_s$  = sample mass in the standard bottle (g) and  $V_f$  = volume of the standard flask ( $\text{cm}^3$ , or ml).

Samples of compact to semi-compact materials were first dried in an oven at 110 °C and weighed on a balance to determine dry weight. Shortly afterwards, they were waterproofed by coating their outer surface with PVC film, and then weighed again. Then, the PVC-coated samples were placed in a basket and immersed in water. The weight of the immersed samples was determined to enable the calculation of the respective density values using the following formula:

$$\text{Density (g/cm}^3\text{)} = W/W-S$$

where  $W$  = dry sample mass (g) and  $S$  = immersed sample mass (g).

### 3.4. Mass balance

Mass balance was determined using the methodology described by Brimhall and Dietrich (1987) and Brimhall et al. (1991). Volumetric variations in each change horizon were calculated by the authors using the following equation:

$$\varepsilon_{i,w} = ((\delta_p C_{i,p}) / (\delta_w C_{i,w})) - 1$$

(1)

In this equation,  $i$  represents the immovable element,  $\delta_p$  and  $\delta_w$  are the bulk density values of the parent rock and the altered rock, respectively, and  $C_{i,p}$  and  $C_{i,w}$  are the concentrations of the immobile element in the parent rock ( $C_{i,p}$ ) and in the altered rock ( $C_{i,w}$ ). In this study, TiO<sub>2</sub> was used as an immobile element.

The mass transport function  $\tau$  is used to calculate the gains and losses of each element in comparison to its concentration in the parent rock. This calculation is expressed by the following equation:

$$\tau = ((\delta_w C_{j,w}) / \delta_p C_{j,p})(\epsilon_{i,w} + 1) - 1 \quad (2)$$

where  $C_{j,w}$  is the concentration of a certain element in the altered sample and  $C_{j,p}$  is the concentration of the same element in the parent rock.

The value of  $\epsilon$  was calculated for each sample, in relation to the selected immovable element, using equation 1. After calculating  $\epsilon$ , equation 2 was applied to calculate mass transport ( $\tau$ ) for each lateritic horizon in each parent rock. The resulting mean values were displayed in bar graphs (Fig. 12) and spatialized in the study area (Fig. 13).

The values determined by mass balance were spatialized using the Leapfrog Geo software, version 6.0.4.

### 3.5. X-ray diffractometry

Thirteen samples were analyzed by X-ray diffractometry. The diffractograms were recorded in a D2 PHASER BRUKER AXS X-Ray Diffractometer at the Mineral Technology Laboratory - X-Rays, Federal University of Bahia (UFBA), using CuK $\alpha$  radiation, with wavelength  $\lambda = 1.54184 \text{ \AA}$  and a monochromator. The tests were performed in a  $2\theta$  angular scan range of  $2^\circ$ - $80^\circ$ . Measurements were performed at room temperature in continuous scan mode, with an angular step of  $0.014^\circ$  and counting time of 0.35 seconds. A PMMA sample spinner was used to minimize the preferred-direction effect. The voltage and current used in the tests were 30 kV and 10 mA, respectively. Fixed divergence slit was 0.6 mm for all cases. The software used to interpret the diffractograms was DIFFRAC.EVAV6.

### 3.6. Petrographic Analysis

The mineralogical and textural features were examined on 46 polished thin sections using a transmitted-reflected light optical microscope. The analysis used an Olympus BX51 trinocular microscope from the Mineral Analysis Laboratory (LAMIN) at the Geological Survey of Brazil – CPRM.

### 3.7. Scanning Electron Microscopy

Semiquantitative chemical analyses based on EDS (energy dispersive spectroscopy) coupled with a scanning electron microscope (SEM/EDS) and backscattered electron imaging (BSE) were performed on a Zeiss EVO LS15 scanning electron microscope (LAMIN). For these analyses, the samples had been previously metallized with carbon. The SEM-EDS analyses were performed for chemical and textural characterization, as well as for designing a map of the chemical distribution of nickel in the crystals of these minerals.

## 4. Results

### 4.1. Local Geology

#### 4.1.1. Mafic-ultramafic zones

The core of the intrusive massif is formed by greenish gray serpentized dunite with fine to medium grain size (Fig. 2b). The rock presents millimeter fractures, intensely branched and filled by Fe/Mn oxyhydroxides. Fresh rock outcrops are rare, and usually occur in the valley between the two topographic elevations. In the top areas and slopes of the elevations, blocks of intensely altered rock can be found; they are orange and composed of chalcedony percolating through fractures and composing boxwork texture (Fig. 2e, f, g). In drill holes, one can see less altered rock, greenish gray in color, with massive texture and fine to medium grain size (Fig. 3e). Chalcedony stockworks run along the rock, forming millimeter-size networks of veinlets.

The peridotite-pyroxenite zone surrounds the dunite core, forming a halo approximately 200 to 400m wide. Outcrops are rare, and fresh rock can only be seen through drill cores (Fig. 3l). It has a dark gray color and fine grains, Chalcedony stockworks with millimeter-sized networks of veinlets (Fig. 2i).

The gabbro zone occurs in the southern portion of the massif, forming an arc at the outer edge of the peridotite-pyroxenite zone. It has a light gray color, medium to coarse grain and phaneritic texture (Fig. 2c). Quartz-filled fractures occur.

Nepheline syenite (Fig. 2d) occurs on the east-northeast edge of the massif and has a pinkish brown color owing to the presence of K-feldspar, medium grain size and phaneritic texture. This unit was not analyzed in the present study.

#### 4.1.2 Lateritic profiles

Fig. 3 shows the typical lateritic profiles developed on the bedrock of each of the lithotypes that make up the Morro do Engenho zoned intrusive massif. This study analyzed eight lateritic horizons stacked upon one another from the bedrock (BDRK): saprock (SPRK), lower saprolite (SAP), ferruginous saprolite (FSAP), ocher saprolite (OSAP), plasma zone (PLSZ), lateritic duricrust (DRCR), chalcedony or silcrete crust (SLCR), and topsoil (TSL). In general, the profiles are structured into two domains: silica and oxy-hydroxide, defined by macroscopic characteristics with the aid of petrographic, chemical, XRD and SEM analyses.

Saprock (Fig. 3d, l, u) characterizes the alteration front on the bedrock (Fig. 3e, m). It is composed of semi-altered rock, brown in color, with an average level of fracture, and average thickness of 6 m.

Lower saprolite is characterized by altered rock with a clayey appearance and preserved fabric, greenish to brownish color, and composition dominated by silicates (Fig. 3c, j, k, q, r, s, t). Average thickness is 15 m, and the thickest profiles are found in the peridotite/pyroxenite and gabbro zones, where they can exceed 20 m.

Ferruginous saprolite is visually distinguished from lower saprolite by its reddish color (Fig. 3h, i, p, o). In this horizon, the original fabric of the parent rock remains preserved, but with a predominance of secondary Fe, Ti and Mn oxyhydroxides. At the base, there is a transition from the silicate domain to the oxide domain, marked by intercalated greenish and reddish clays (Fig. 3i, p). The average thickness of this interval is 6 m, reaching 8 m in the gabbro profile.

Ocher saprolite (Fig. 3b) effectively represents the domain of Fe and Mn oxyhydroxides. It occurs preferentially in association with its dunite parent rock; it is hardly ever found in zones peripheral to topographic elevations. It has a typical ocher color and an average thickness of 6 m.



Fig. 2 – General aspects of the Morro do Engenho alkaline ultramafic mafic complex with the main constituents of the outcrop zones. a) Perspective view of the two elevations that make up the core of the intrusive body; b) Semi-altered dunite in the core region, showing a serpentine veinlet; c) Semi-altered gabbro with medium to coarse grain; d) semi-altered nepheline syenite; e, f, g) alteration products present in the core zone; h) limonitic canga with botryoidal habit; i) Chalcidony stockworks in altered rock; j) limonitic canga block with chalcidony boxworks.



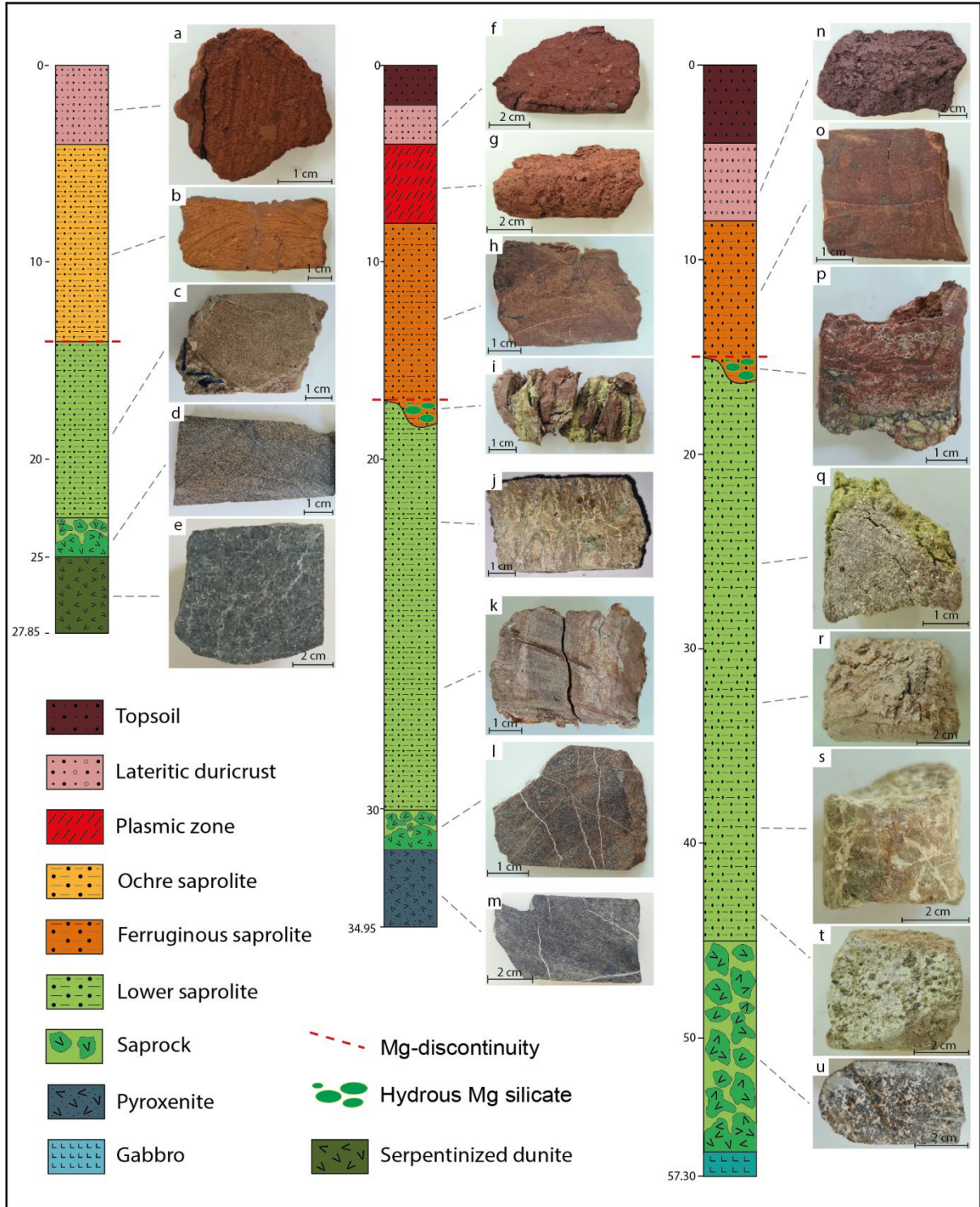


Fig. 3 – Toposequence of the lateritic profiles in the study holes, showing the evolution of alteration on each of the bedrocks belonging to the Morro do Engenho zoned intrusive body.

The interface between the lower horizons and the surface horizons that complement the lateritic profile is represented by the plasma zone (Fig. 3g). This horizon is on average 3 m thick and is composed of ferruginous clays with a mottled texture, normally kaolinitic, with red, pink or whitish color. Generally, the plasma zone is overlaid by the lateritic duricrust, composed of dark red laterites that are rich in hematite, quartz and Mn oxyhydroxides (Fig. 3a, f, n). This horizon is 4 m thick on average.

Chalcedony crusts or silcretes occur on the ridges of elevations and can be up to 12 m thick. They are composed of quartz and chalcedony, and they often present boxworks and silicified rock fragments. These crusts are responsible for preserving the relief and forming the terraces present in the region. They are usually covered by the topsoil horizon that also covers the dissected areas. With an average thickness of 3m, the topsoil has a dark brown to purple color, and granular texture formed by fine to medium sediments and pisolitic fragments. This horizon commonly contains fragments of limonitic canga with botryoidal habit (Fig. 2h).

#### *4.2 Textures and mineral properties of alteration profiles*

The arrangement of the x-ray diffractograms (Fig. 4) clearly shows the mineralogical evolution of the alteration profiles developed on each of the parent rocks that make up the Morro do Engenho zoned body. It also shows the transition of the silicate horizons at the base to the oxide horizons at the top of the profiles. The main characteristics of each profile are detailed below. A summary of the mineralogical variations in each profile can also be seen in Fig. 10.

##### *4.2.1 Alteration profile derived from serpentinized dunite*

In the diffractograms (Fig. 4a - CEA067), the samples of the alteration profile derived from the serpentinized dunite show a rock, in the saprock, essentially composed of serpentine, predominantly lizardite, with very low amounts of quartz. The analyses of petrographic sections and SEM images (Fig. 5a, d) show the presence of at least three stages of serpentinization. The primary phase (srp I), probably igneous, is composed of fibrous crystals, which form well-developed strips around the olivine and pyroxene cores, surrounding these minerals with straight to curved contacts and producing a mesh texture. The second serpentinization phase (srp II), certainly deriving from supergene processes, is formed by irregular fibrous aggregates that almost completely replace the olivine and pyroxene magmatic cores, forming a pseudomorphic texture on these minerals and affecting their contacts with the well-developed fibers of srp I. Obliteration of the primary serpentine crystals produces a new crystal fabric, dominated by extensive srp II development. Fractures are filled in the third phase of serpentinization (srp III), overlapping the previous phases. Magnetite is found to be associated with serpentine, forming longitudinal dark lines along the fibrous bands of srp I, reinforcing the hypothesis of an igneous serpentinization phase. Fe oxyhydroxides occur together with srp II, and they are mostly concentrated in the pseudomorphic cores. Chromite sparsely occurs in euhedral to subhedral grains. Quartz is found to fill cracks.

Mineralogical analysis by X-ray diffraction of the lower saprolite sample (Fig. 4a - CEA068) shows the presence of quartz, along with serpentine. Petrographic and SEM analyses (Fig. 5b, e) show the evolution of the alteration on the mineral features observed in the saprock, as evidenced by the formation of secondary phyllosilicates and a greater amount of Fe oxyhydroxides. In addition, iddingsite occurs as an alteration of the serpentine, making it brownish. Goethite occurs with skeletal habit and is surrounded by a mesh texture.

In the ocher saprolite, the mineralogical analysis (Fig. 4a - CEA069) shows the dominance of Fe and Mn oxyhydroxides, especially goethite, hematite and asbolane, in addition to the presence of chromite and chlorite, the latter as a probable product of supergene alteration of pyroxene. Because chlorite has very small amounts of Mg but is rich in Fe, as shown in specific SEM-EDS analyses (Fig. 19g, h), it can be classified as chamosite. Petrographic sections and BSE-MEV images (Fig. 5c, f, g, h, i) show a significant increase in quartz content, possibly owing to alteration of serpentine which, together with hematite, composes a silico-ferruginous plasma that extends throughout the matrix (Fig. 5C). Chlorite is the only silicate mineral that remains present, sometimes occurring together with Fe/Ti oxyhydroxides (Fig. 5g). Goethite is present as a magnetite alteration product that forms crowns

around chromite grains. Asbolane occurs together with goethite and hematite (Fig. 5h, i). The SEM-EDS spectra (Fig. 5j, k) show the presence of high levels of Ni (> 2%) associated with serpentine from different generations.

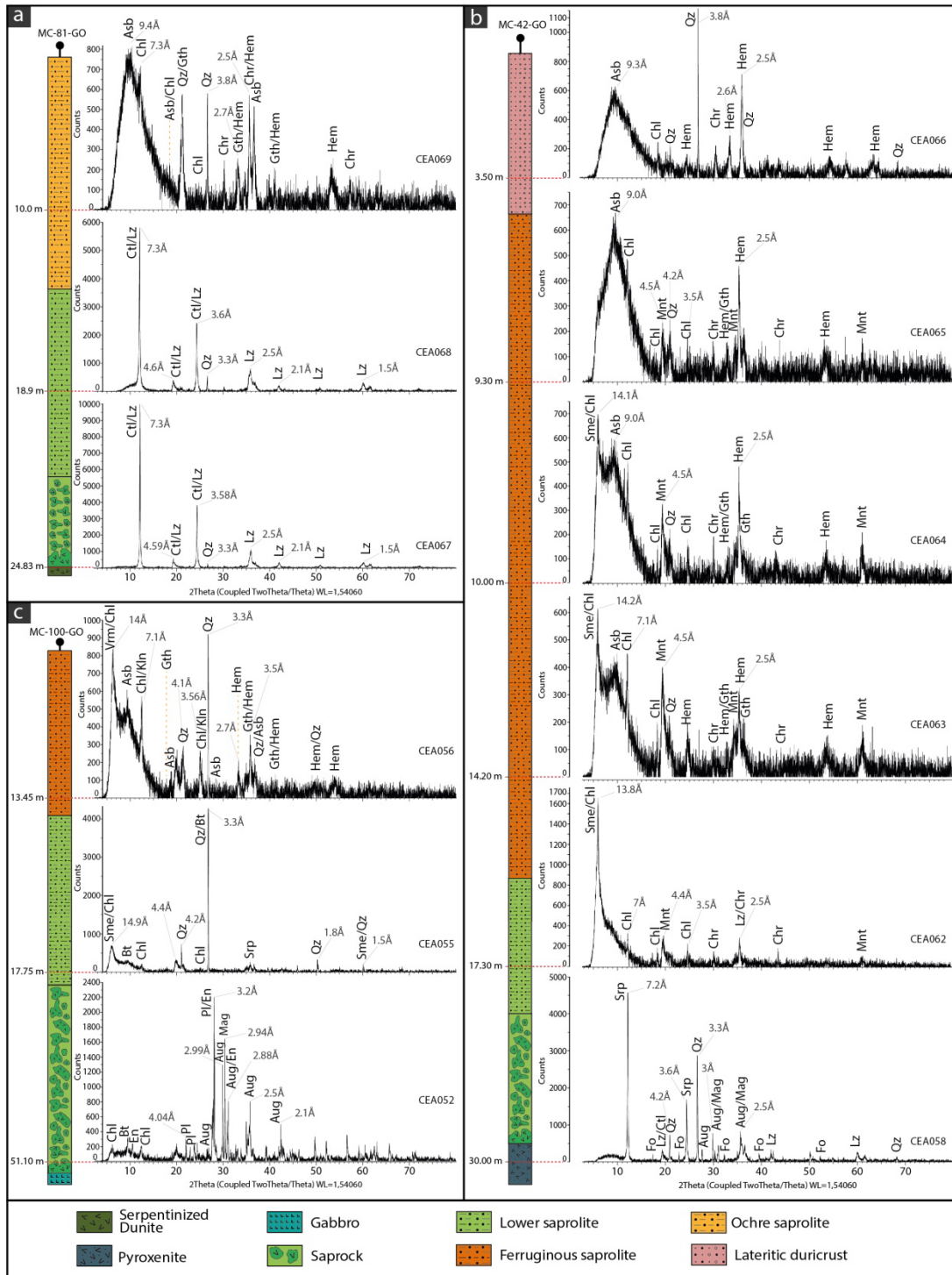


Fig. 4 – X-ray diffractograms (XRD) representing mineralogical variation in lateritic profiles derived from each of the parent rocks of the Morro do Engenho deposit. a) Profile derived from serpentinized dunite; b) Profile derived from pyroxenite; c) Profile derived from gabbro. Abbreviations: Asb – asbolane; Aug – augite; Bt – biotite; Chl – chlorite; Chr – chromite; Ctl – chrysotile; En – enstatite; Fo – forsterite; Gth – goethite; Hem – hematite; Kln – kaolinite; Lz – lizardite; Mag – magnetite; Mnt – montmorillonite; Pl – plagioclase; Qz – quartz; Sme – smectite; Srp – serpentine; Vrm – vermiculite (Warr, 2021).

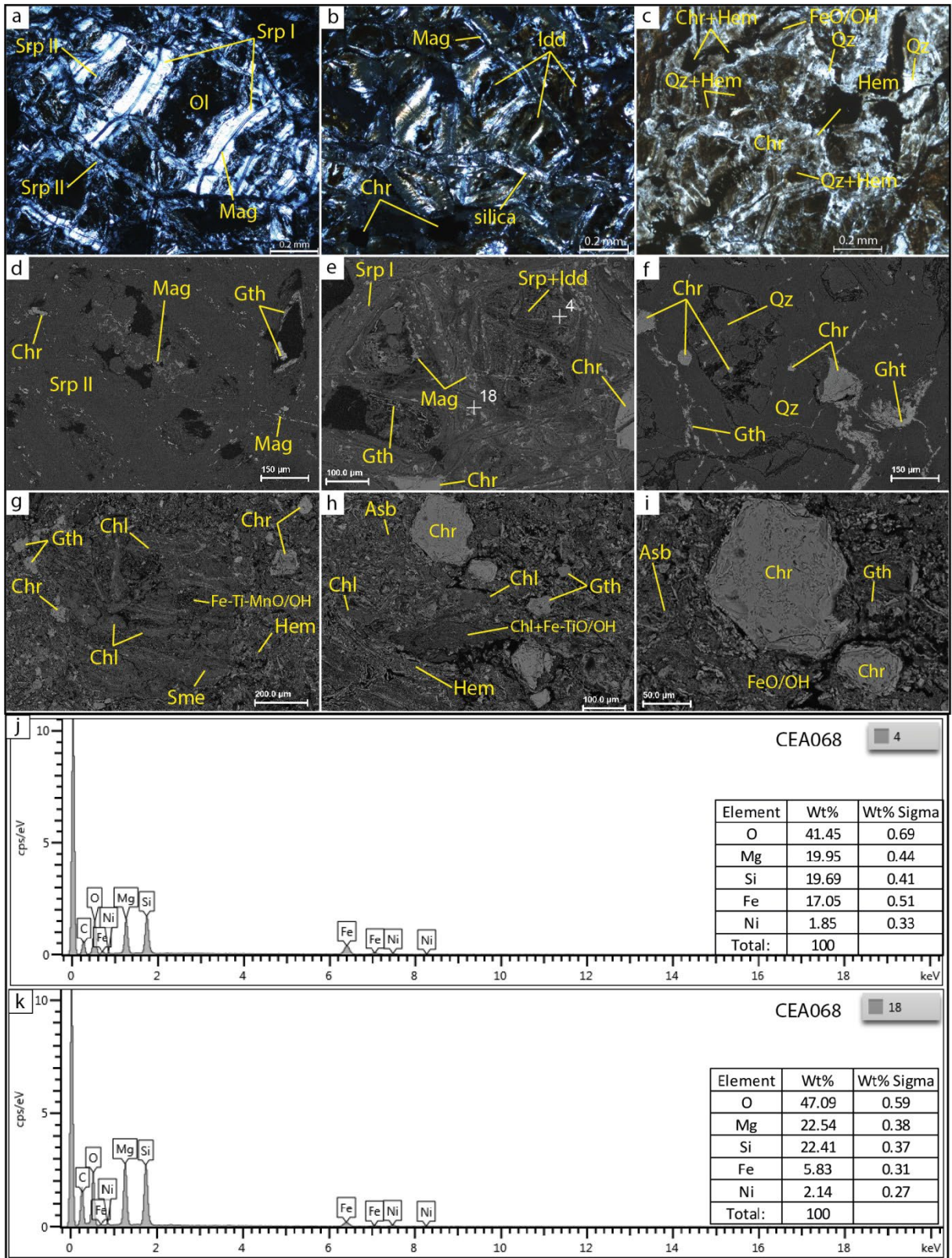


Fig. 5 – Photomicrographs, BSE images and spectra of spot SEM-EDS analysis of the alteration profile derived from serpentinized dunite. a) Serpentine composing a mesh texture in the saprock; b) Mesh-texture serpentine with alteration of iddingsite in the lower saprolite; c) Serpentine altered by hematite and composing amorphous silico-ferruginous plasma in the ferruginous saprolite; d) Magnetite associated with srp I, together with goethite and chromite in the saprock; e) Goethite with a skeletal habit surrounded by the mesh texture in the lower saprolite; f) Quartz and hematite composing amorphous silico-ferruginous plasma in the other saprolite; g)

Chlorite surrounded by amorphous silico-ferruginous plasma in the other saprolite; h - i) Chromite immersed in amorphous silico-ferruginous plasma in the other saprolite; j ) SEM-EDS spectrum of point 4, shown in Fig. 5e, indicating the presence of Ni in srp II. k) SEM-EDS spectrum of point 18, shown in Fig. 5e, indicating the presence of Ni in srp I. Abbreviations: Asb – asbolane; Chl – chlorite; Chr – chromite; Fe-Ti-MnO/OH - Fe/Ti/Mn oxyhydroxides; Gth – goethite; Hem – hematite; Idd – Iddingsite; Mag – magnetite; Ol – olivine; Qz – quartz; Sme – smectite; Srp - serpentine.

#### 4.2.2 *Pyroxenite-derived alteration profile*

Based on XRD analysis, the pyroxenite saprock sample shows mineralogy composition of augite, olivine, serpentine, quartz, magnetite and chromite (Fig. 4b- CEA058). In petrographic sections, the mesh texture, formed by fibrous serpentine halos around pyroxene and olivine cores with straight to curved contacts, characterizes the only serpentinization phase recognized in this presumably magmatic rock (Fig. 6a). Unlike dunite, the magmatic remnants of the parent rock (pyroxene and olivine) are preserved, i.e., no pseudomorphs were formed. Magnetite occurs as thin strands between the serpentine fibers, which run along the mesh texture (Fig. 6d). Chromite is sparsely present, with subhedral grains up to 0.2 mm thick.

In the lower saprolite, the mineralogical analysis (Fig. 4b - CEA062) shows that the parental mineralogy gives rise to chlorite and smectite with relevant amounts of Fe and Mn oxyhydroxides. The petrographic section and BSE-MEV images show total alteration of the serpentine and formation of pseudomorphic chlorite after pyroxene (Fig.6b). The serpentine is replaced by a mixture of montmorillonite and Fe and Mn oxyhydroxides, forming a ferruginous fabric that surrounds the pseudomorphic cores and covers some grains. Goethite, as well as asbolane, fill cracks and make up Ni- and Co-mineralized zones (Fig. 6e, f; Fig. 8).

In the ferruginous saprolite, XRD analyses (Fig. 4b – CEA063, CEA064, CEA065) indicate the domain of Fe and Mn oxyhydroxides, especially goethite, hematite and asbolane, with a decrease in the presence of smectite towards the top of the profile (Fig. 4b- CEA065). Chlorite, however, remains in the profile up to the top of the ferruginous saprolite (Fig. 4b- CEA065). The slides and BSE-MEV images show that ferruginous saprolite samples are formed by the predominance of Fe oxyhydroxides with silicate fragments composed of chlorite  $\pm$  smectite and smectite  $\pm$  hematite (Fig. 6c, g, h; Fig. 7a, b, c). Massive hematite forms ferruginous levels. Fe and Mn hydroxides are found to fill small cracks (Fig. 6i). The spot SEM-EDS analyses (Fig. 7d) enabled the identification of romanechite and asbolane. Chromite presents alteration to hematite, and quartz occurs in insignificant amounts. XRD mineralogical analysis shows that, in the lateritic duricrust samples (Fig. 4b - CEA066), hematite, asbolane and quartz are the major components.



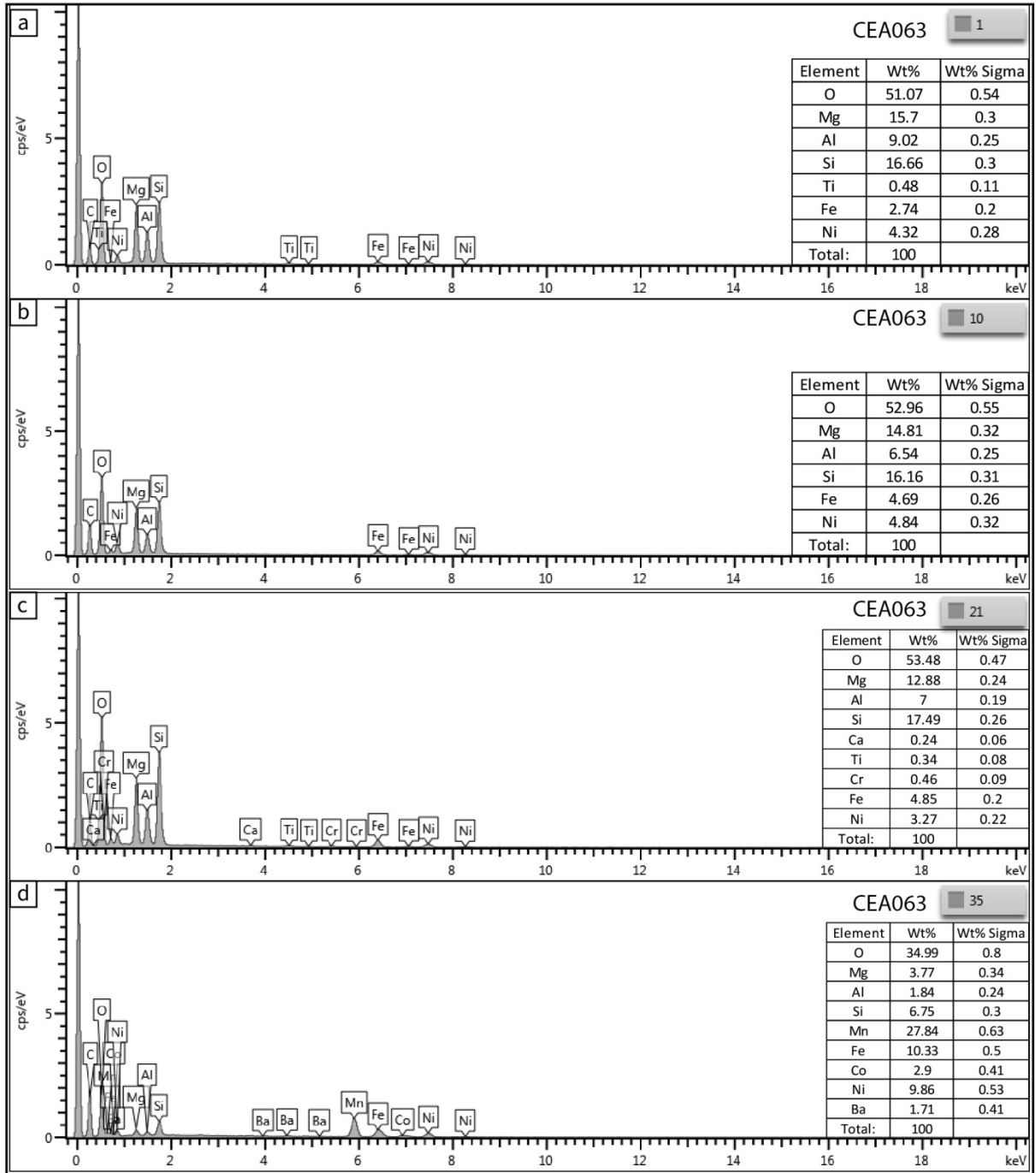


Fig. 7 – Spectra of spot SEM-EDS analyses at the points indicated in Fig. 6c, g). a, b) Spot analysis of chlorite ± smectite grains; c, d) Spot analysis in a zone formed by smectite and hematite.

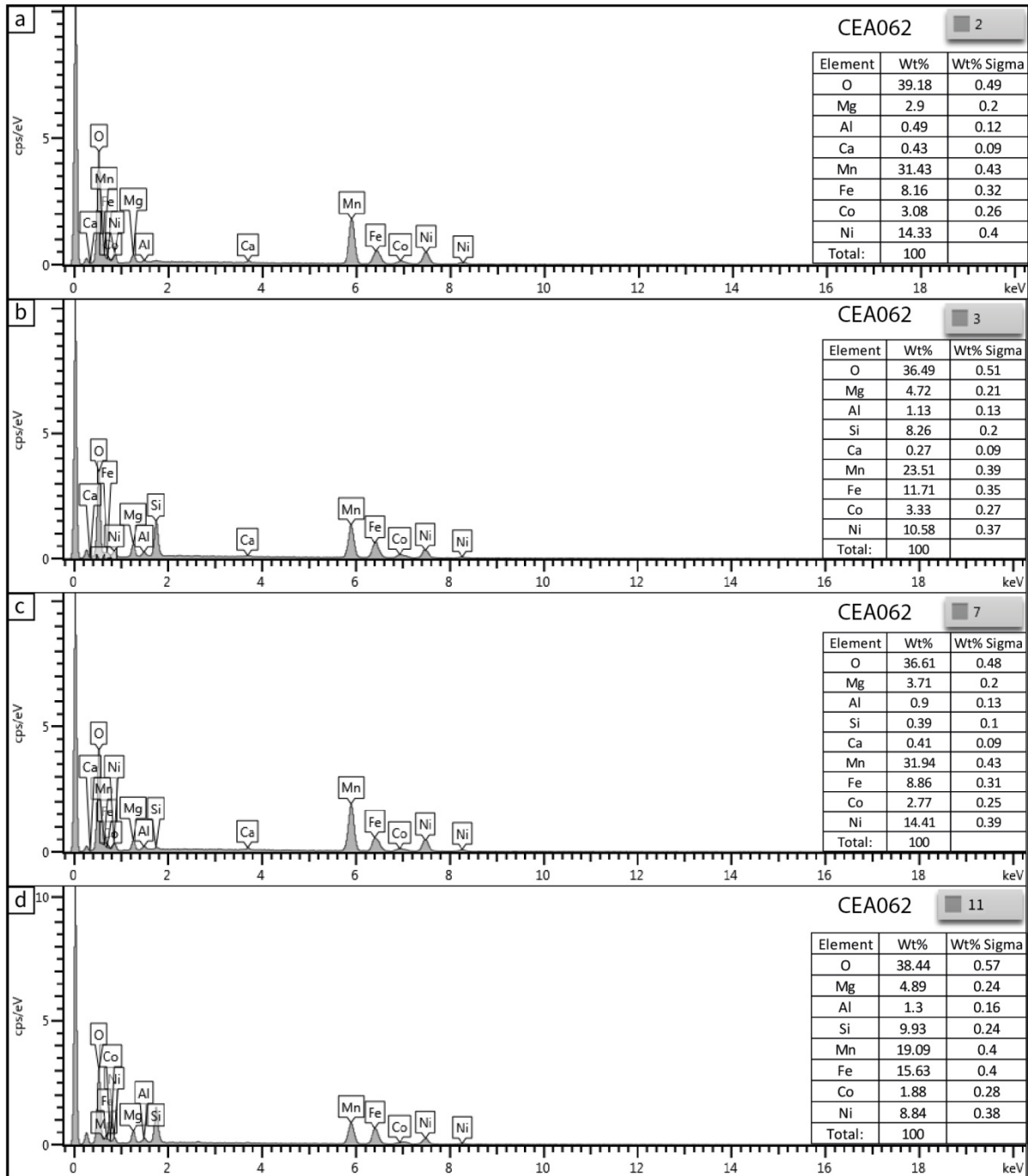


Fig. 8 – Spectra of spot SEM-EDS analyses at the points indicated in Fig. 6e, f, showing that asbolane is present and fills cracks, composing mineralized zones in Ni and Co.



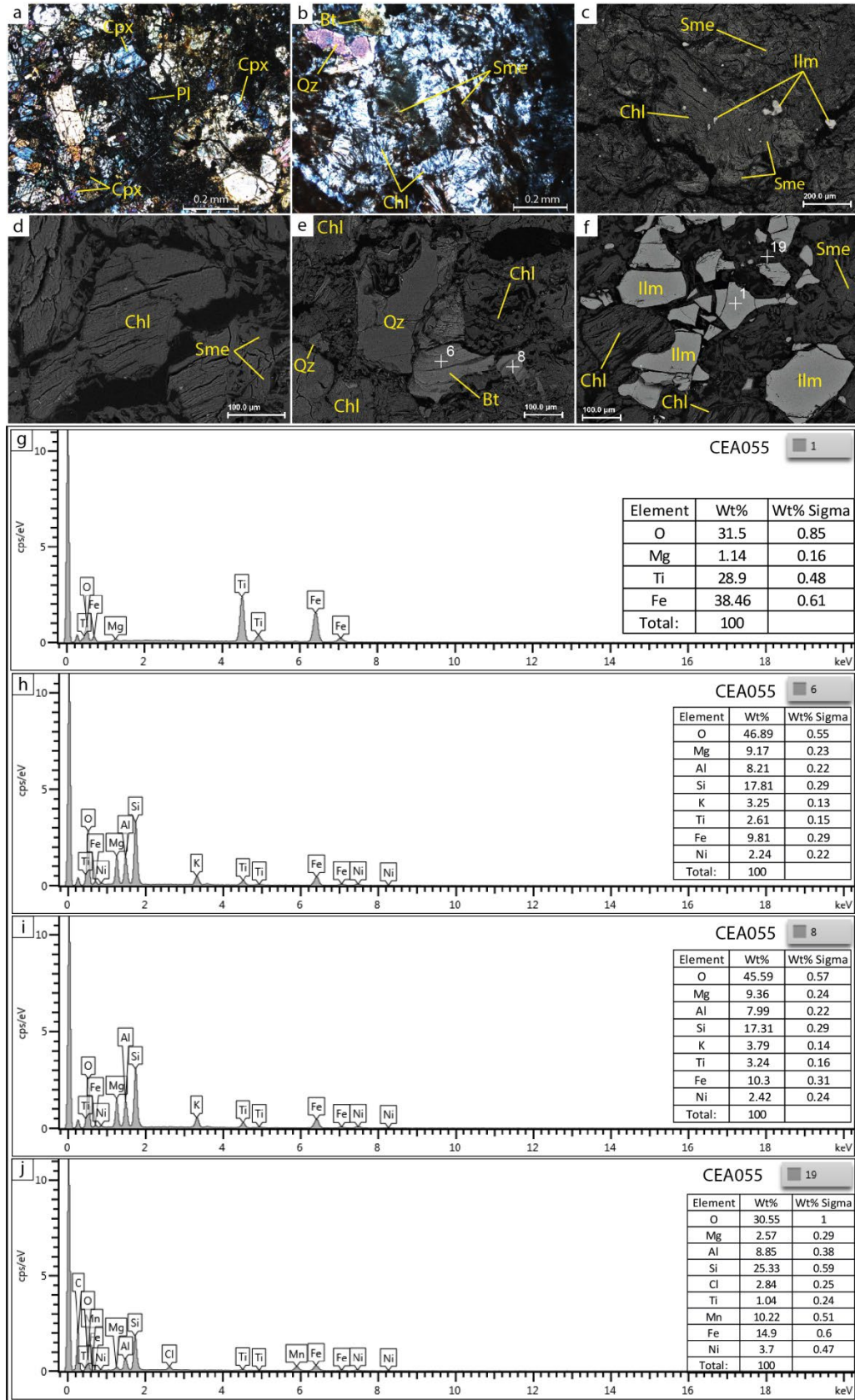


Fig. 9 – Photomicrographs, BSE images and spectra of SEM-EDS spot analysis of the gabbro-derived alteration profile samples. a) Incipient alteration in the saprock; b, c, d) Pseudomorphs of chlorite on pyroxene in the lower saprolite; e) Quartz, ilmenite and biotite occur sparsely in the lower saprolite; f) Chlorite, smectite and ilmenite in the lower saprolite. g) Spectra of spot SEM-EDS analysis of ilmenite at the points indicated in Fig. 9f; h, i)

Spectrum of spot SEM-EDS point analysis of biotite grain; j) Spectrum of spot SEM-EDS analysis of chlorite associated with Fe and Mn oxyhydroxides. Abbreviations: Bt – biotite; Chl – chlorite; Chr- chromite; Cpx – clinopyroxene; Ilm – ilmenite; Pl – plagioclase; Qz – quartz; Sme – smectite.

Parental rock	Mineral	BDRK	SAPRK	SAP	FSAP	OSAP	PLSZ	DRCR	LSL
Serpentinized Dunite	MnO/H	Abundant	Abundant	Minor	Trace	Trace	Trace	Trace	Trace
	Hem	Abundant	Abundant	Minor	Trace	Trace	Trace	Trace	Trace
	Gth	Abundant	Abundant	Minor	Trace	Trace	Trace	Trace	Trace
	Mag	Abundant	Abundant	Minor	Trace	Trace	Trace	Trace	Trace
	Chr	Abundant	Abundant	Minor	Trace	Trace	Trace	Trace	Trace
	Sme	Abundant	Abundant	Minor	Trace	Trace	Trace	Trace	Trace
	Chl	Abundant	Abundant	Minor	Trace	Trace	Trace	Trace	Trace
	Qz	Abundant	Abundant	Minor	Trace	Trace	Trace	Trace	Trace
	Srp	Abundant	Abundant	Minor	Trace	Trace	Trace	Trace	Trace
	Px	Abundant	Abundant	Minor	Trace	Trace	Trace	Trace	Trace
Pyroxenite	MnO/H	Abundant	Abundant	Minor	Trace	Trace	Trace	Trace	Trace
	Hem	Abundant	Abundant	Minor	Trace	Trace	Trace	Trace	Trace
	Gth	Abundant	Abundant	Minor	Trace	Trace	Trace	Trace	Trace
	Mag	Abundant	Abundant	Minor	Trace	Trace	Trace	Trace	Trace
	Sme	Abundant	Abundant	Minor	Trace	Trace	Trace	Trace	Trace
	Chl	Abundant	Abundant	Minor	Trace	Trace	Trace	Trace	Trace
	Qz	Abundant	Abundant	Minor	Trace	Trace	Trace	Trace	Trace
	Chr	Abundant	Abundant	Minor	Trace	Trace	Trace	Trace	Trace
	Srp	Abundant	Abundant	Minor	Trace	Trace	Trace	Trace	Trace
	Px	Abundant	Abundant	Minor	Trace	Trace	Trace	Trace	Trace
Gabbro	MnO/H	Abundant	Abundant	Minor	Trace	Trace	Trace	Trace	Trace
	Hem	Abundant	Abundant	Minor	Trace	Trace	Trace	Trace	Trace
	Ilm	Abundant	Abundant	Minor	Trace	Trace	Trace	Trace	Trace
	Gth	Abundant	Abundant	Minor	Trace	Trace	Trace	Trace	Trace
	Kln	Abundant	Abundant	Minor	Trace	Trace	Trace	Trace	Trace
	Vrm	Abundant	Abundant	Minor	Trace	Trace	Trace	Trace	Trace
	Sme	Abundant	Abundant	Minor	Trace	Trace	Trace	Trace	Trace
	Chl	Abundant	Abundant	Minor	Trace	Trace	Trace	Trace	Trace
	Qz	Abundant	Abundant	Minor	Trace	Trace	Trace	Trace	Trace
	Mag	Abundant	Abundant	Minor	Trace	Trace	Trace	Trace	Trace
	Bt	Abundant	Abundant	Minor	Trace	Trace	Trace	Trace	Trace
Pl	Abundant	Abundant	Minor	Trace	Trace	Trace	Trace	Trace	
		Abundant	Minor	Trace					

Figure 10 - Mineralogical succession of lateritic alteration profiles developed over each of the parent rocks. Abbreviations: Bt – biotite; Chl – chlorite; Chr – chromite; Gth – Goethite; Hem – hematite; Il – Ilmenite; Kln – kaolinite; MnO/H - Mn oxyhydroxides; Mag – magnetite; Ms – Muscovite; Ol – olivine; Px – pyroxene; Qz – quartz; Sme – smectite; Srp – serpentine; Tlc - talc; Vrm - vermiculite. SAPRK – saprock; SAP – lower saprolite; FSAP – ferruginous saprolite; OSAP – ocher saprolite; PLSZ – plasma zone; DRCR – lateritic duricrust; TSL – topsoil

#### 4.3. Geochemical characterization of lateritic profiles

Figs. 11 and 12 show the distribution of major, minor and trace elements along the typical lateritic profiles, derived from each of the lithologies of the zoned body. Table 1 to 3 shows the average chemical composition of each of the horizons in each lateritic profile.

Generally, the profiles show, from the parent rock to the top, a linear and continuous reduction of MgO, in contrast to a progressive increase in Fe<sub>2</sub>O<sub>3</sub>. The analysis of the geochemical profiles (Fig. 11 and 12) shows the transition zone between the silica and oxide domains in each profile, characterized by the MgO discontinuity zone (Freyssinet et al., 2005; Butt & Cluzel, 2013). In this zone, MgO content, which is around 40% in dunite and pyroxenite parent rocks and 25% in gabbroic rocks,

undergoes a drastic reduction to values below 10%. This effect can be associated with the replacement of silicate minerals with Fe and Mn oxyhydroxides, which occurs to a greater extent in the ferruginous saprolite horizon.

$\text{Fe}_2\text{O}_3$  content increases regularly towards the upper horizons of the lateritic profiles. In the parent rocks, the content ranges between 10% in dunite and pyroxenite and 17% in gabbro, reaching values of up to 50% in the horizons of ocher saprolite, plasma zone and duricrust particularly. The evolution of  $\text{Fe}_2\text{O}_3$  content in the lateritic profiles is accompanied by the UMIA index curve, reflecting increasing lateritization along the profiles. Elements such as Cr, Co and Mn follow a pattern similar to that of  $\text{Fe}_2\text{O}_3$ , with a progressive increase towards the top of the profiles.

$\text{SiO}_2$  distribution in the dunite profile shows a pattern similar to that of MgO, with a reduction in the transition from the silicatic domain to the oxide domain. In pyroxenitic and gabbroic profiles, there was a greater retention of  $\text{SiO}_2$  in the ferruginous saprolite, produced according to the composition of the alteration products of these lithologies.

$\text{Al}_2\text{O}_3$  contents in the parent rocks are lower than 1% in the dunite-derived profile and pyroxenite and 3% in the gabbro-derived profile. The distribution curves show a progressive increase in  $\text{Al}_2\text{O}_3$  towards the upper horizons, mostly from ferruginous saprolite, where it can reach up to 10%.

The increase in  $\text{Cr}_2\text{O}_3$  towards the top of the lateritic profile is constant and hardly significant. Chromite is present as an accessory mineral in the three parental lithologies, with greater emphasis in the dunite profile. It is poorly soluble and acts as a resistate mineral in the alteration profile; its highest concentrations are found in the lateritic duricrust.

MnO, in turn, presents higher contents, resulting from discontinuous MgO, and reflecting the presence of asbolane and associations with Fe and Ti oxyhydroxides.

$\text{TiO}_2$  distribution shows a slight increase towards the upper horizons, indicating the possible entry of allochthonous materials into the lateritic profile.

The variation of CaO contents is more prominent in the gabbro- and pyroxenite-derived profiles, with a reduction from the base to the top, owing to the greater presence of pyroxene and plagioclase in these rocks.

Co has a similar distribution to that of MnO, increasing in the oxide domain, reaching levels up to 800 ppm.

Ni distribution in the bedrock shows values close to 0.2% and significant increases in the lower saprolite and above. In the dunite-derived profile, a zone richer in Ni is formed between lower saprolite, ferruginous saprolite and ocher saprolite. The highest contents are found in this last horizon, reaching an average of 1.11%. In the pyroxenite-derived profile, the horizon with the highest contents is the ferruginous saprolite: up to 1.23% on average. In the gabbro-derived profile, the zone with the highest Ni contents is between lower saprolite and ferruginous saprolite; the highest contents are found in saprolite, where they can reach 0.83% on average.

The rare-earth elements (REE) show a light distribution from the transition to the oxide domain.

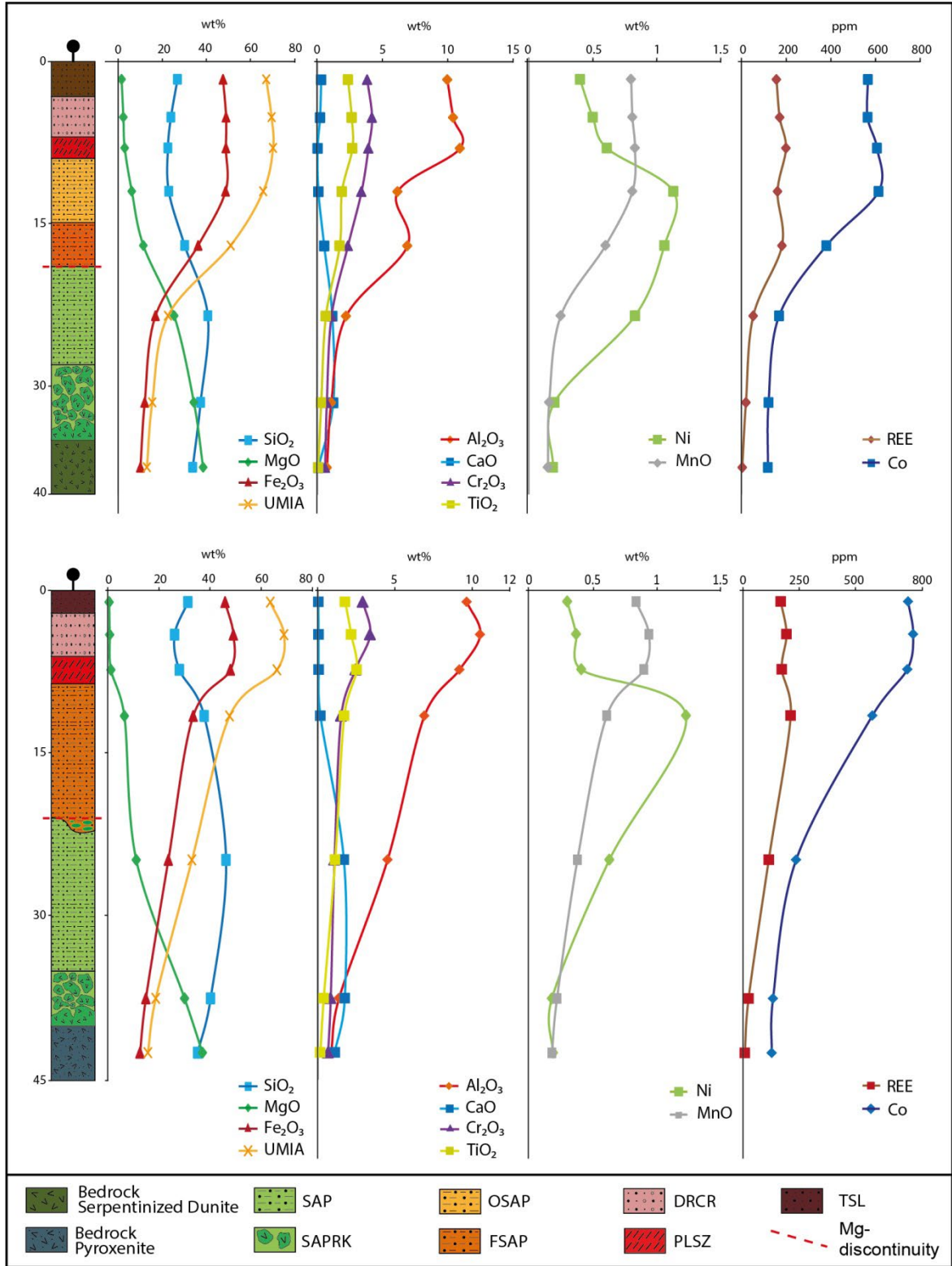


Fig. 11 – Distribution of chemical element contents in lateritic profiles developed on serpentinized dunite (MC-81-GO) and pyroxenite (MC-42-GO) rocks. Abbreviations: SAPRK – saprock; SAP – lower saprolite; FSAP – ferruginous saprolite; OSAP – ocher saprolite; PLSZ – plasma zone; DRCR – lateritic duricrust; LSL – topsoil.

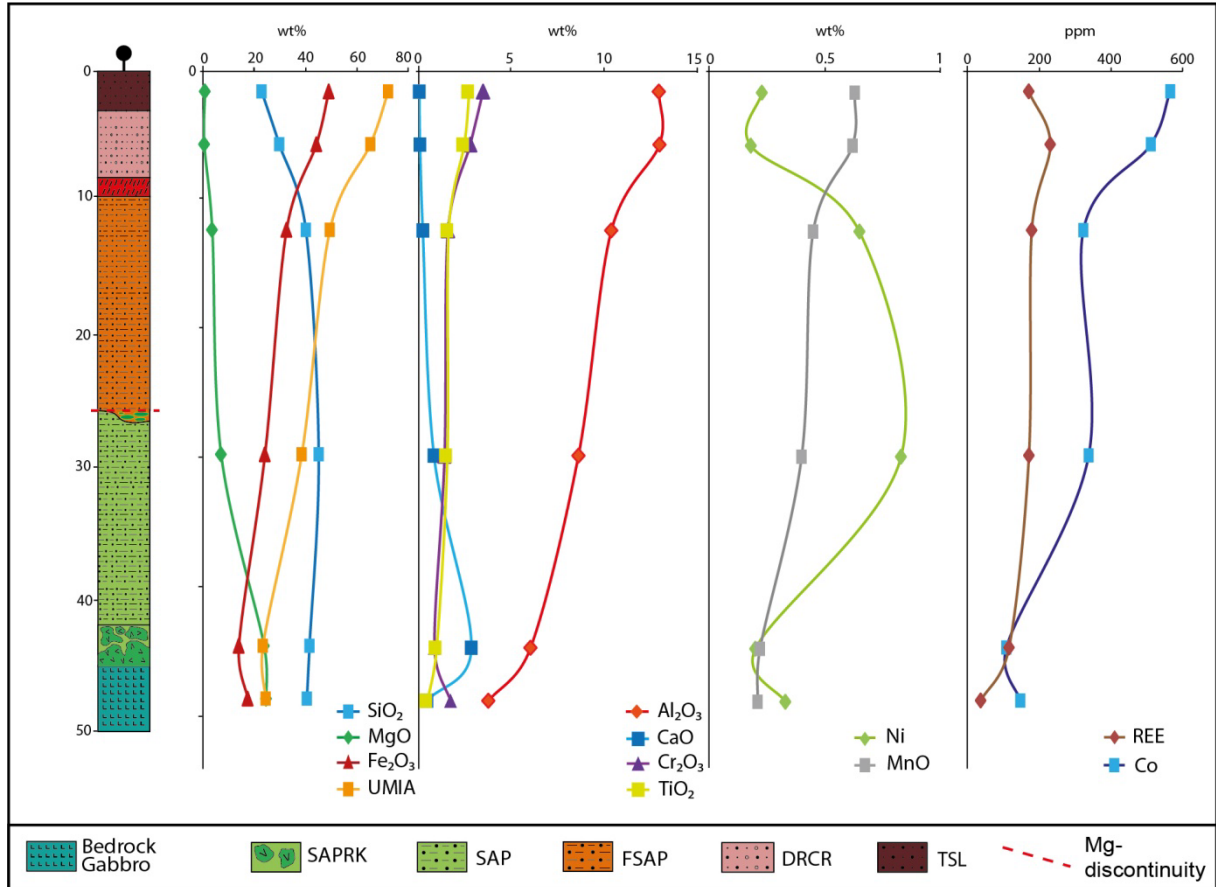


Fig. 12 – Distribution of chemical element contents in the lateritic profile developed on gabbro (MC-100-GO). Abbreviations: SAPRK – saprock; SAP – lower saprolite; FSAP – ferruginous saprolite; OSAP – ochre saprolite; PLSZ – plasma zone; DRCR – lateritic duricrust; TSL – topsoil.

Table 1. Average chemical composition of the horizons that make up the lateritic profiles developed over the dunite zone.

Horizon	Lateritic duricrust	Ochre saprolite	Ferruginous saprolite	Saprolite	Saprock	Bedrock
SiO <sub>2</sub> (%)	23.93	22.94	30.15	40.63	37.36	33.80
Al <sub>2</sub> O <sub>3</sub>	10.42	6.17	6.90	2.21	1.07	0.74
Fe <sub>2</sub> O <sub>3</sub>	48.92	48.66	36.22	16.92	12.03	10.10
MgO	2.23	6.20	11.42	25.39	34.32	38.50
CaO	0.21	0.08	0.53	1.15	1.21	0.08
Na <sub>2</sub> O	0.13	0.10	0.13	0.08	0.09	0.05
K <sub>2</sub> O	0.04	0.09	0.20	0.13	0.05	0.01
TiO <sub>2</sub>	2.64	1.89	1.72	0.66	0.30	0.07
P <sub>2</sub> O <sub>5</sub>	0.09	0.10	0.08	0.04	0.05	0.01
MnO	0.81	0.82	0.60	0.25	0.16	0.15
Cr <sub>2</sub> O <sub>3</sub>	4.19	3.39	2.35	1.09	0.73	0.60
LOI	5.79	8.05	8.25	10.44	12.61	16.39
Ni	0.50	1.13	1.06	0.83	0.20	0.19
Sc (ppm)	51.77	49.66	38.79	18.46	11.36	7.70
Ba	116.59	219.72	220.59	112.49	54.35	14.00
Co	564.09	613.46	379.95	168.09	120.98	118.00
Cs	0.45	0.45	0.90	0.46	0.33	0.03
Ga	19.06	13.93	12.38	4.98	3.01	2.10
Hf	5.53	3.24	3.18	1.18	0.49	0.07
Nb	34.34	19.88	26.76	7.56	2.41	0.03
Rb	2.91	5.24	11.70	3.31	0.60	0.50

Sn	1.39	1.17	1.18	0.89	0.30	0.15
Sr	18.66	35.82	47.06	70.71	77.80	5.00
Ta	1.90	1.39	1.85	0.66	0.17	0.03
Th	4.88	2.74	3.17	0.87	0.17	0.05
U	1.24	0.90	0.83	0.25	0.11	0.06
V	384.19	303.22	238.82	100.05	59.69	2.50
W	5.31	8.41	3.45	3.11	1.22	1.10
Zr	195.99	117.60	124.83	57.31	44.07	49.00
Y	14.31	17.13	21.70	5.85	2.34	0.32
La (ppm)	27.35	32.60	42.55	10.01	3.30	0.80
Ce	87.98	61.91	62.10	20.27	7.44	0.80
Pr	7.22	8.84	10.27	3.15	1.14	0.13
Nd	29.65	36.30	42.20	12.22	4.87	0.70
Sm	5.15	6.03	6.73	1.84	0.83	0.05
Eu	1.38	1.67	1.85	0.51	0.22	0.03
Gd	4.22	5.13	5.87	1.67	0.72	0.24
Tb	0.58	0.69	0.75	0.21	0.10	0.03
Dy	3.15	3.70	3.99	1.14	0.49	0.06
Ho	0.58	0.68	0.73	0.22	0.09	0.03
Er	1.59	1.75	1.93	0.53	0.22	0.07
Tm	0.22	0.23	0.24	0.07	0.04	0.03
Yb	1.41	1.46	1.51	0.42	0.18	0.05
Lu	0.20	0.21	0.22	0.06	0.04	0.03
UMIA	69.53	65.73	50.99	22.59	15.47	13.04
Samples	111	145	39	293	15	1

Table 2. Average chemical composition of the horizons that make up the lateritic profiles developed over the peridotite/pyroxenite zone.

Horizon	Lateritic duricrust	Ferruginous saprolite	Saprolite	Saprock	Bedrock
SiO <sub>2</sub> (%)	26.21	37.78	46.31	40.27	35.20
Al <sub>2</sub> O <sub>3</sub>	10.53	6.91	4.52	1.37	0.86
Fe <sub>2</sub> O <sub>3</sub>	49.18	33.47	23.77	15.00	12.70
MgO	0.86	6.59	11.24	30.10	37.10
CaO	0.04	0.16	1.68	1.74	1.09
Na <sub>2</sub> O	0.14	0.13	0.17	0.13	0.05
K <sub>2</sub> O	0.04	0.16	0.13	0.06	0.01
TiO <sub>2</sub>	2.16	1.71	1.12	0.37	0.16
P <sub>2</sub> O <sub>5</sub>	0.07	0.03	0.04	0.04	0.02
MnO	0.94	0.61	0.38	0.22	0.18
Cr <sub>2</sub> O <sub>3</sub>	3.39	1.51	1.07	0.83	0.66
LOI	5.92	9.05	8.73	10.22	10.25
Ni	0.37	1.23	0.63	0.18	0.19
Sc (ppm)	46.16	46.82	41.55	15.08	8.60
Ba	306.76	482.17	325.29	85.50	39.00
Co	763.00	579.89	237.78	134.08	127.90
Cs	0.55	0.50	0.54	0.33	0.14
Ga	18.60	12.28	8.48	3.83	3.20
Hf	5.82	2.98	2.00	0.62	0.21
Nb	35.28	29.19	10.18	2.86	0.24
Rb	2.89	10.68	5.78	2.37	0.40
Sn	1.39	1.00	0.86	0.58	0.15
Sr	23.27	70.44	49.54	42.50	17.00
Ta	1.93	1.86	1.23	0.12	0.03
Th	5.67	2.88	1.31	0.65	0.10
U	1.44	0.59	0.34	0.25	0.03
V	348.39	193.83	127.43	64.50	38.00
W	2.98	11.70	8.35	1.38	3.50
Zr	213.28	100.76	60.47	48.66	5.00
Y	12.74	22.30	15.46	2.85	1.43

La (ppm)	24.07	51.84	29.50	5.95	1.30
Ce	121.97	71.44	32.39	8.76	3.00
Pr	6.41	12.66	7.06	1.29	0.32
Nd	25.23	49.63	28.80	4.50	1.40
Sm	4.51	8.00	4.71	0.93	0.30
Eu	1.14	2.17	1.32	0.29	0.09
Gd	3.67	6.83	4.41	0.94	0.45
Tb	0.53	0.89	0.56	0.12	0.05
Dy	2.95	4.63	2.86	0.66	0.31
Ho	0.54	0.85	0.53	0.11	0.05
Er	1.53	2.21	1.37	0.30	0.14
Tm	0.22	0.28	0.17	0.04	0.03
Yb	1.43	1.74	1.00	0.26	0.10
Lu	0.21	0.26	0.15	0.03	0.03
UMIA	68.91	47.69	32.98	18.87	15.79
Samples	46	101	249	8	1

Table 3. Average chemical composition of the horizons that make up the lateritic profiles developed over the gabbro zone.

Horizon	Lateritic duricrust	Ferruginous saprolite	Saprolite	Saprock	Bedrock
SiO <sub>2</sub> (%)	29.79	40.20	45.21	42.83	40.60
Al <sub>2</sub> O <sub>3</sub>	12.93	10.34	8.57	6.76	3.73
Fe <sub>2</sub> O <sub>3</sub>	44.32	32.65	24.22	13.83	17.50
MgO	0.49	3.60	7.08	22.05	24.70
CaO	0.05	0.20	0.80	3.82	0.42
Na <sub>2</sub> O	0.14	0.15	0.13	0.59	0.05
K <sub>2</sub> O	0.03	0.11	0.17	0.15	0.04
TiO <sub>2</sub>	2.43	1.60	1.53	1.13	0.45
P <sub>2</sub> O <sub>5</sub>	0.08	0.04	0.06	0.18	0.02
MnO	0.62	0.45	0.40	0.22	0.21
Cr <sub>2</sub> O <sub>3</sub>	2.75	1.55	1.37	0.72	1.69
LOI	6.39	8.34	9.44	8.64	10.82
Ni	0.18	0.65	0.83	0.17	0.33
Sc (ppm)	28.16	46.83	33.63	25.38	13.00
Ba	193.07	383.57	478.31	326.33	173.00
Co	510.87	322.90	337.70	102.95	147.90
Cs	0.50	0.77	0.62	0.44	0.25
Ga	21.85	14.64	13.99	10.53	8.60
Hf	8.82	3.01	2.62	1.93	0.53
Nb	44.22	25.85	28.70	19.31	4.51
Rb	1.92	10.11	11.15	9.86	3.00
Sn	1.27	0.97	1.15	1.23	0.50
Sr	14.66	23.93	31.68	109.16	14.00
Ta	2.59	1.70	1.62	1.93	0.09
Th	8.38	3.28	3.12	2.08	0.50
U	2.03	0.82	0.58	0.44	0.22
V	352.36	216.70	161.52	176.66	87.00
W	2.75	3.69	9.45	0.66	0.05
Zr	339.36	98.22	117.29	80.80	5.00
Y	15.46	24.07	20.18	11.51	3.23
La (ppm)	26.11	39.56	34.74	18.03	5.20
Ce	155.11	63.05	70.32	47.26	23.30
Pr	7.05	10.37	8.82	5.22	1.15
Nd	26.15	42.68	34.18	19.80	5.00
Sm	4.75	7.44	5.94	3.76	0.50
Eu	1.20	2.18	1.66	1.08	0.21
Gd	3.85	6.94	5.19	3.37	0.78
Tb	0.58	0.94	0.71	0.49	0.10
Dy	3.35	5.05	3.91	3.02	0.56

Ho	0.65	0.93	0.74	0.47	0.11
Er	1.86	2.45	1.98	1.35	0.29
Tm	0.28	0.31	0.26	0.18	0.03
Yb	1.82	1.94	1.61	1.11	0.30
Lu	0.27	0.28	0.23	0.16	0.03
UMIA	65.44	49.60	38.61	24.10	24.53
Samples	14	30	51	6	1

The ternary diagram  $\text{SiO}_2$ ,  $\text{MgO}$ ,  $\text{Fe}_2\text{O}_3 + \text{Al}_2\text{O}_3$  m (Fig. 13a) shows the evolution path of lateritic profiles, from bedrock to topsoil, marked by loss of  $\text{MgO}$  and increase of  $\text{Fe}_2\text{O}_3 + \text{Al}_2\text{O}_3$ . The passage from bedrock/saprock to lower saprolite at the base of the pyramid reflects the alteration of the primary minerals of the parent rock, with compositions increasingly poor in  $\text{MgO}$ , and slightly enriched in  $\text{SiO}_2$ . At this stage, the alteration results in UMIA values between 20 and 40%.

The increase in  $\text{Fe}_2\text{O}_3 + \text{Al}_2\text{O}_3$  content is larger in the ferruginous saprolite, in which the variation in UMIA values is around 50%. Ocher saprolite shows even more intense alteration, reaching UMIA values between 50 and 90% and considerable increase in  $\text{Fe}_2\text{O}_3 + \text{Al}_2\text{O}_3$ . The evolution path of the lateritic profiles is complemented by the plasma zone, duricrust and topsoil horizons, which show extremely high  $\text{Fe}_2\text{O}_3 + \text{Al}_2\text{O}_3$  contents and UMIA values of up to 90%.

The correlation diagrams (Fig. 13b, c, d, e) show that Ni levels are positively correlated with UMIA (Fig. 13b), that is, lateritization is increased, with the exception of DRCCR, where Ni contents are reduced. Cobalt shows a strong positive correlation with UMIA (Fig. 13c), indicating increased contents as lateritization progresses. The highest values of Co are present in the oxide domain, especially in the ocher saprolite, plasma zone and duricrust. Ni is positively correlated with Mg in the domain of its low levels (Fig. 13d), while showing a negative correlation with high  $\text{MgO}$  contents. The correlation between Co and MnO (Fig. 13e) is positive and very significant; this finding highlights its association with Mn minerals, usually oxyhydroxides (asbolane).



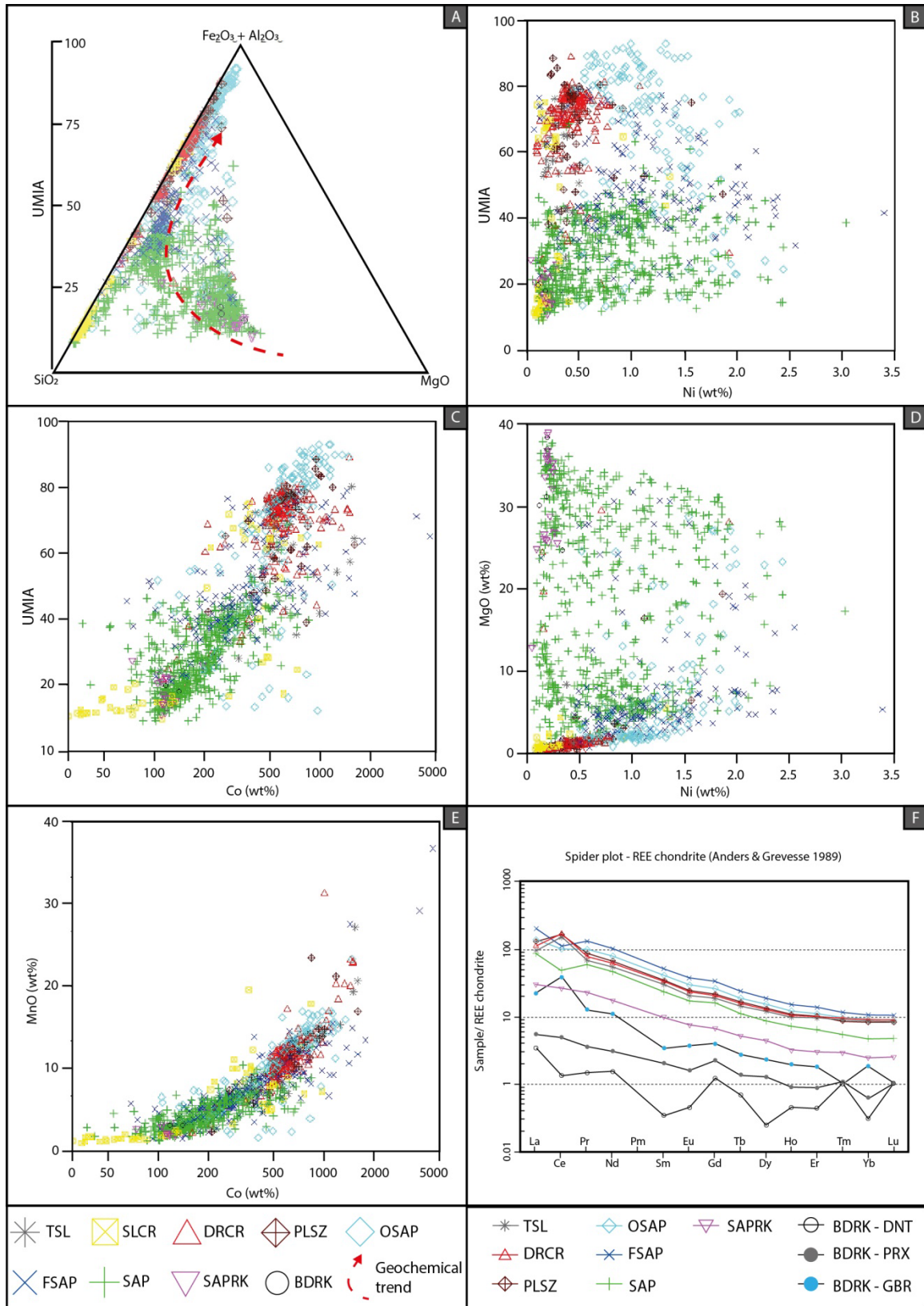


Fig. 13 – A) Diagram MgO - SiO<sub>2</sub> - Al<sub>2</sub>O<sub>3</sub>+Fe<sub>2</sub>O<sub>3</sub> (UMIA); B) Ni vs UMIA correlation diagram; C) Co vs UMIA correlation diagram; D) Ni vs MgO correlation diagram; E) Co vs MnO correlation diagram. F) REE patterns normalized to chondrites (Anders & Grevesse, 1989). BDRK – bedrock; SAPRK – saprock; SAP – lower saprolite; FSAP – ferruginous saprolite; OSAP – ocher saprolite; PLSZ – plasma zone; DRCR – lateritic duricrust; TSL – topsoil.

The analysis of the spider plot of the REEs (Fig. 13f) shows a gradual increase in contents along with increased lateritization. The increase in the contents from the bedrock reaches the apex in the horizons of the oxide domain, especially ferruginous saprolite, ocher saprolite and duricrust. In general, the dunitic rock shows a lower initial REE content than the pyroxenitic and gabbroic rocks. The patterns show steep slopes between the light rare earths, moving to a flattening trend, between Ho-Lu. There are positive Ce anomalies in the duricrust and the topsoil, as well as depletions in the same element in the lower saprolite and the ferruginous saprolite and in the ocher saprolite. On average, the lateritic horizon that contains the largest REE is the ferruginous saprolite.

#### 4.4 Mass Balance

Based on the methodology described by Brimhall and Dietrich (1987), the values of  $\epsilon$  and  $\tau$  were calculated. They showed the volume and mass transport variations in each alteration horizon, separately for each parent rock.

Fig. 14 shows the gains and losses in the bedrock, determined by mass transport calculation ( $\tau$ ) for each of the lateritic horizons, considering TiO<sub>2</sub> as an immobile element. Table 4 shows the values of  $\epsilon$  and  $\tau$ , together with the average values of apparent density, calculated for each horizon. The apparent density values found for the rocks considered as bedrock are significantly lower than those reported in the literature. This finding suggests that even in deep samples (e.g., 120m) weathering processes are influential. Therefore, it should be noted that the samples used for mass balance calculations reflect conditions more compatible with those of the saprock horizon.

In general, volume losses towards the top are common in the three profiles (dunite, peridotite/pyroxenite, gabbro), and reflect a gradual increase in the compaction of the altered material.

The diagrams in Figure 14 show that only Ni shows actual enrichment in comparison to the lithologies of the parent rock. This effect can be easily seen in the dunite diagram (Fig.14a), where there are Ni enrichments - associated with the lower saprolite - of up to 40%. The ocher saprolite also shows a peak in Ni but without positive enrichments.

In the pyroxenite-derived profile (Fig. 14b), the ferruginous saprolite shows an increase in Ni content, but it cannot be considered as positive enrichment. In this profile, from the plasma zone to the topsoil, Al<sub>2</sub>O<sub>3</sub> shows enrichment of up to 10%. In the gabbro-derived profile (Fig. 14c), Ni enrichment of up to 1% occurs in the lower saprolite.

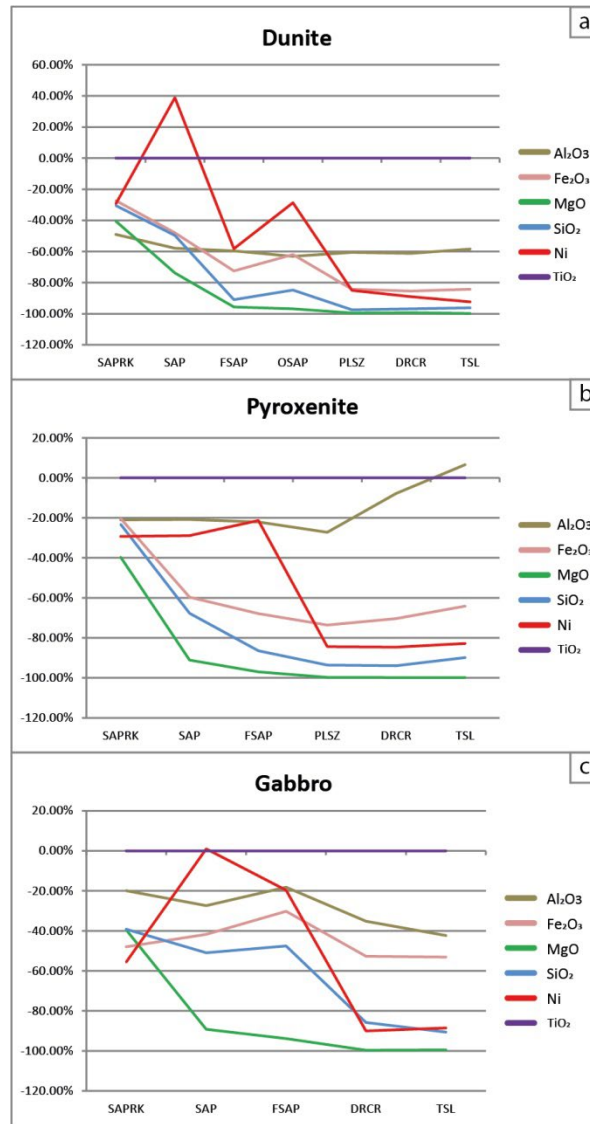


Fig. 14. Averages of gains and losses in comparison to the BDRK, using TiO<sub>2</sub> as an immovable element, determined by mass transport calculation ( $\tau$ ) for each of the lateritic horizons. SAPRK – saprock; SAP – lower saprolite; FSAP – ferruginous saprolite; OSAP – ocher saprolite; PLSZ – plasma zone; DRRCR – lateritic duricrust; TSL – topsoil.

Table 4. Average values of apparent density, volume variation ( $\varepsilon$ ) and mass transport ( $\tau$ ), determined for each of the lateritic horizons of each parent rock. SAPRK – saprock; SAP – lower saprolite; FSAP – ferruginous saprolite; OSAP – ocher saprolite; PLSZ – plasma zone; DRRCR – lateritic duricrust; TSL topsoil.

Parental rock	Horizon	Density (gm <sup>3</sup> )	$\varepsilon$	$\tau$
Dunite	LSL	1.71	-94.44%	-92.36%
	DRRCR	1.56	-94.06%	-89.04%
	PLSZ	1.48	-94.07%	-84.96%
	OSAP	1.32	-76.83%	-28.62%
	SAPF	1.28	-81.75%	-58.23%
	SAP	1.75	-44.95%	38.83%
	BDRK/SAPRK	2.54	-	-
Pyroxenite	LSL	2.60	-84.47%	-82.76%
	DRRCR	1.84	-87.44%	-84.64%

	PLSZ	1.98	-88.39%	-84.34%
	SAPF	1.72	-80.24%	-21.31%
	SAP	1.71	-63.97%	-28.90%
	BDRK/SAPRK	2.53	-	-
	LSL	2.14	-74.46%	-88.49%
	DRCR	1.83	-68.45%	-90.05%
Gabbro	SAPF	1.78	-31.65%	-19.66%
	SAP	1.79	-32.84%	0.99%
	BDRK/SAPRK	2.09	-	-

Fig. 15 shows the spatialization of the data collected by mass transport calculation, demonstrating areas where the greatest Ni enrichments are found in the Morro do Engenho deposit. Ni enrichments are concentrated in the valley region between the two topographic elevations. This aspect is indicative of possible controls for Ni mineralization in relation to its spatial distribution in the deposit.

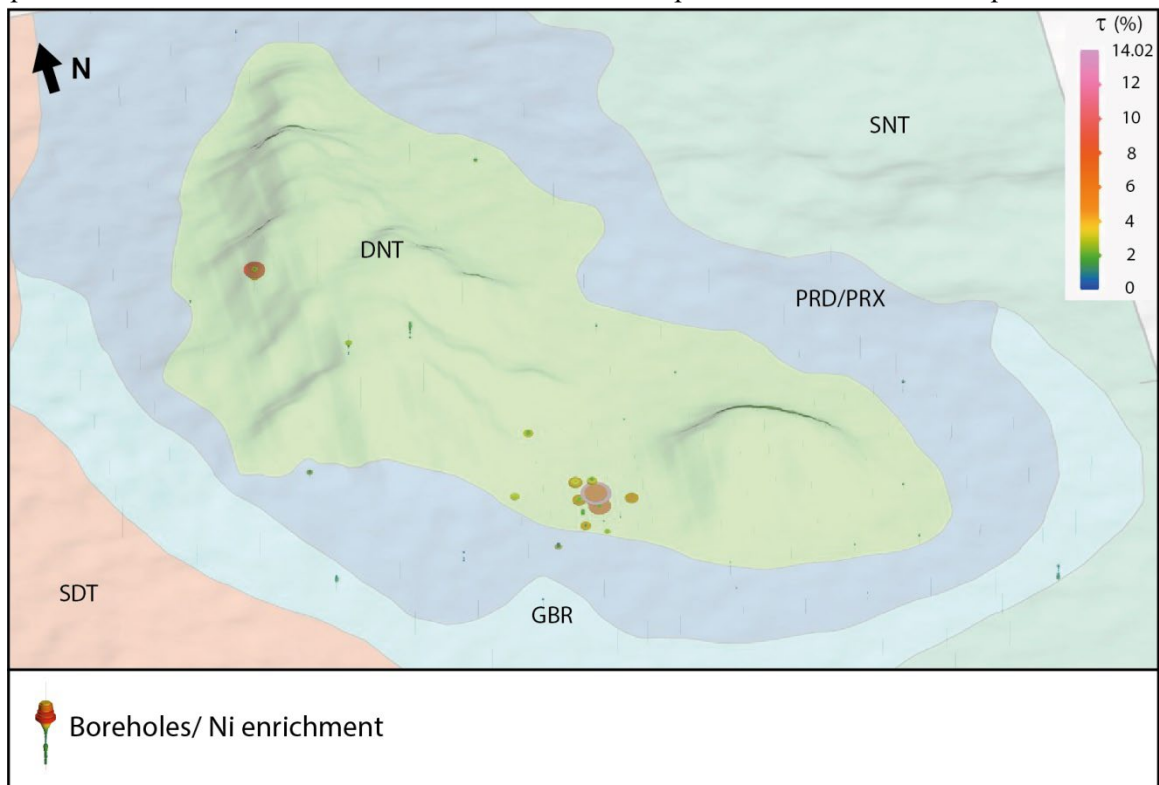


Fig. 15. 3D geological map of the Morro do Engenho deposit with the spatialization of the Ni enrichments in each drill hole, determined by mass transport calculation ( $\tau$ ). DNT – dunite zone; PRD/PRX – peridotite/pyroxenite zone; GBR – gabbro zone; SNT – syenite-nepheline zone; SDT – sandstone.

#### 4.5 Mineralization

Ni mineralization in the Morro do Engenho deposit mostly occurs in three main horizons: lower saprolite, ferruginous saprolite and ocher saprolite. In these horizons, Ni occurs in both silica and oxide phases, while keeping its own characteristics in each of them.

#### 4.5.1 Ni-bearing silicates

Ni-bearing silicates are found at different levels of the lateritic profile of the Morro do Engenho deposit. The main accumulations occur in the lower saprolite; however, they are also present in the horizons dominated by oxyhydroxides, represented by ferruginous saprolite and ocher saprolite. The main Ni-hosting silicate minerals are serpentine, chlorite and smectite. The Ni-rich serpentine is found more abundantly in the lower saprolite horizon of the profile derived from the serpentinized dunite and - to a lesser extent - in the profile derived from the peridotite/pyroxenite zone. In the dunite-derived profile, Ni is present in the serpentine (Fig. 16) at concentrations of up to 2.14%.

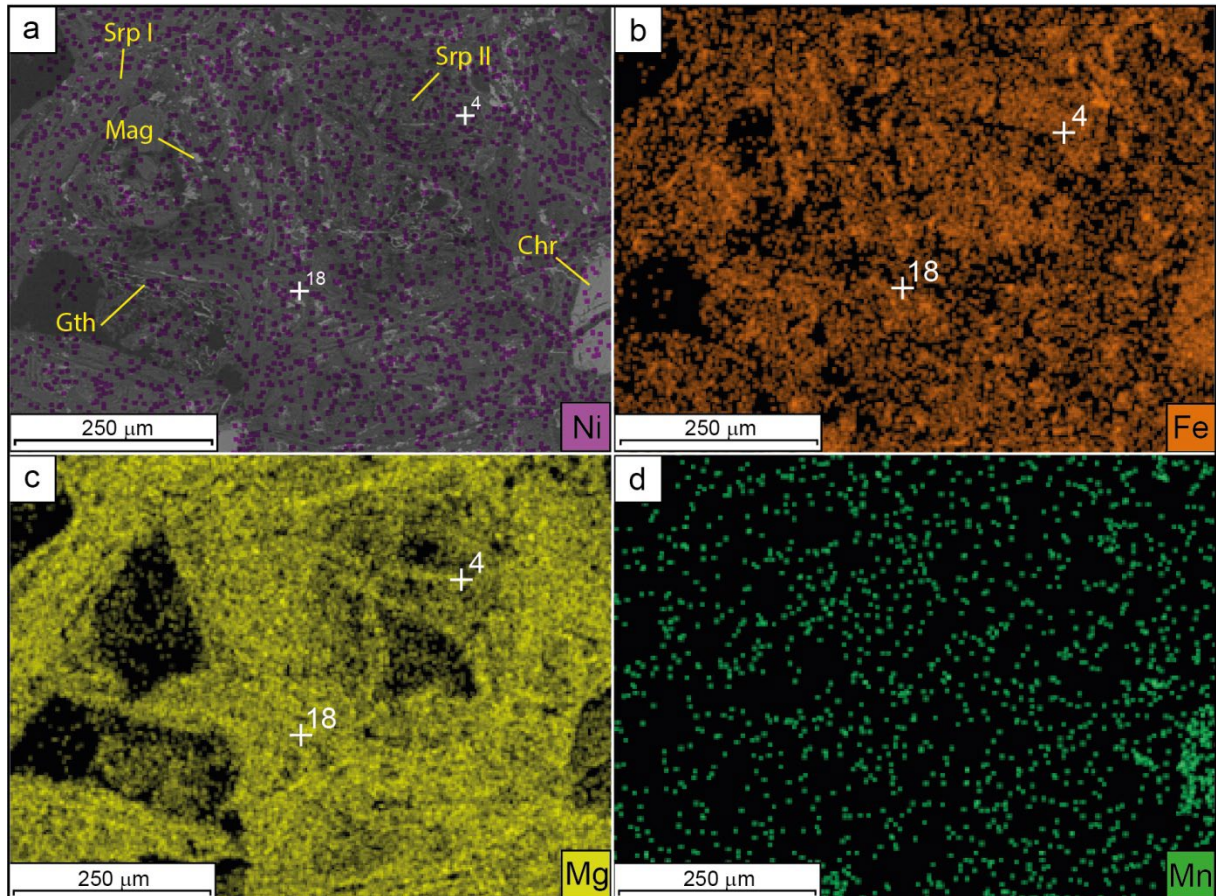


Fig. 16. a) Backscattered electron (BSE) photomicrograph of a representative lower saprolite sample in the dunite profile with overlapping SEM-EDS map for Ni. b, c, d) SEM-EDS maps for Fe, Mg and Mn. Sample CEA068. Spot SEM-EDS analyses indicated by the numbers in the images. Spectra are shown in Fig. 5. Abbreviations: Chr- chromite; Gth – goethite; Mag – magnetite; Srp I – phase I serpentine; Srp II – phase II serpentine.

Mineralization associated with chlorite is more common in the gabbro-derived profile. In this profile, chlorite occurs abundantly in the lower saprolite horizon with Ni contents of up to 3.7%. The EDS maps (Fig. 17) show the presence of Ni coinciding with Si- and Al-rich zones, associated with the presence of chlorite.

In the peridotite/pyroxenite-derived profile, chlorite occurs less prominently; however, it is part of important concentrations, especially in the ferruginous saprolite horizon (Fig. 18). In this horizon, chlorite shows a composition rich in Mg and poor in Fe, associated with Ni contents of up to 4.8% (Fig. 7b). The EDS maps (Fig. 18) show the presence of Ni replacing chlorite, as evidenced by the high levels of Mg and Al, to the detriment of Fe. Smectite also makes up a mineralized phase in this horizon, with Ni contents of up to 3.27% (Fig. 7c).

In the ocher saprolite, chlorite is present with the highest levels of Ni, up to 4.65%. It is associated with other Ni-mineralized phases composed of smectite and Fe and Mn oxyhydroxides. The EDS maps (Fig. 19) show the concentrations of Ni in silicate minerals, chlorite and smectite, as well as the composition in Mg, Si and Al, in contrast to the Fe-rich ferruginous matrix.

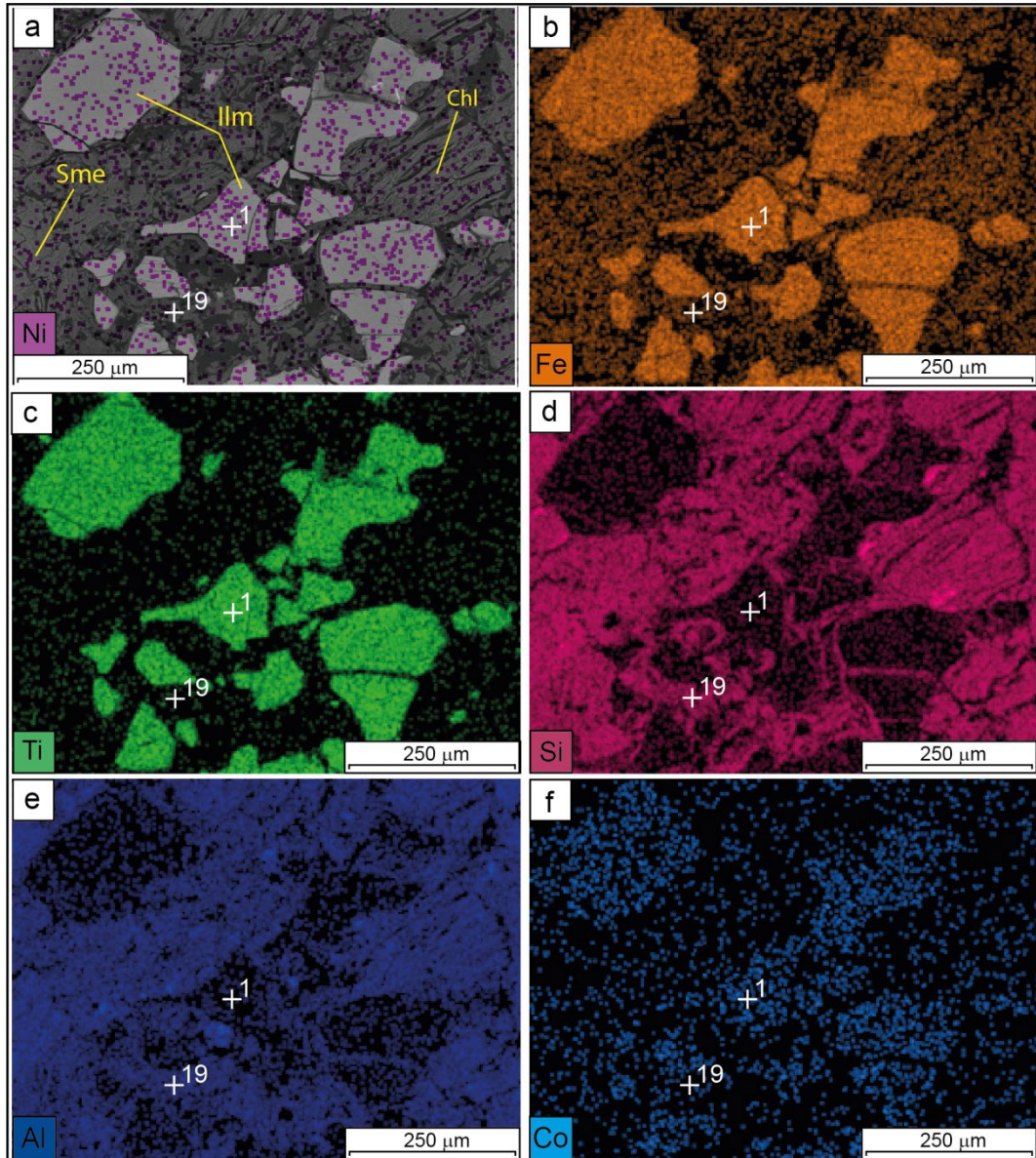


Fig. 17. a) Backscattered electron (BSE) image of a representative sample of lower saprolite in the gabbro profile with overlapping SEM-EDS map for Ni. b, c, d, e, f) SEM-EDS maps for Fe, Ti, Si, Al and Co. Sample CEA055. Spot SEM-EDS analyses indicated by the numbers in the images. Spectra are shown in Fig. 8. Abbreviations: Chl – chlorite; Ilm – ilmenite; Sme – smectite.

Smectite-related Ni mineralization occurs essentially in peridotite/pyroxenite- and gabbro-derived profiles. In addition to occurring with chlorite in the lower saprolite, smectite is intergrown, in the ferruginous saprolite, with Fe and Mn oxides (Fig. 6h) that contain high levels of Ni (Fig. 18a). More rarely, biotite occurred with contents of up to 2.4% of Ni in the ferruginous saprolite of the gabbro-derived profile (Fig. 20). EDS maps show that this mineral also hosts Ti in large amounts (Fig. 20c).

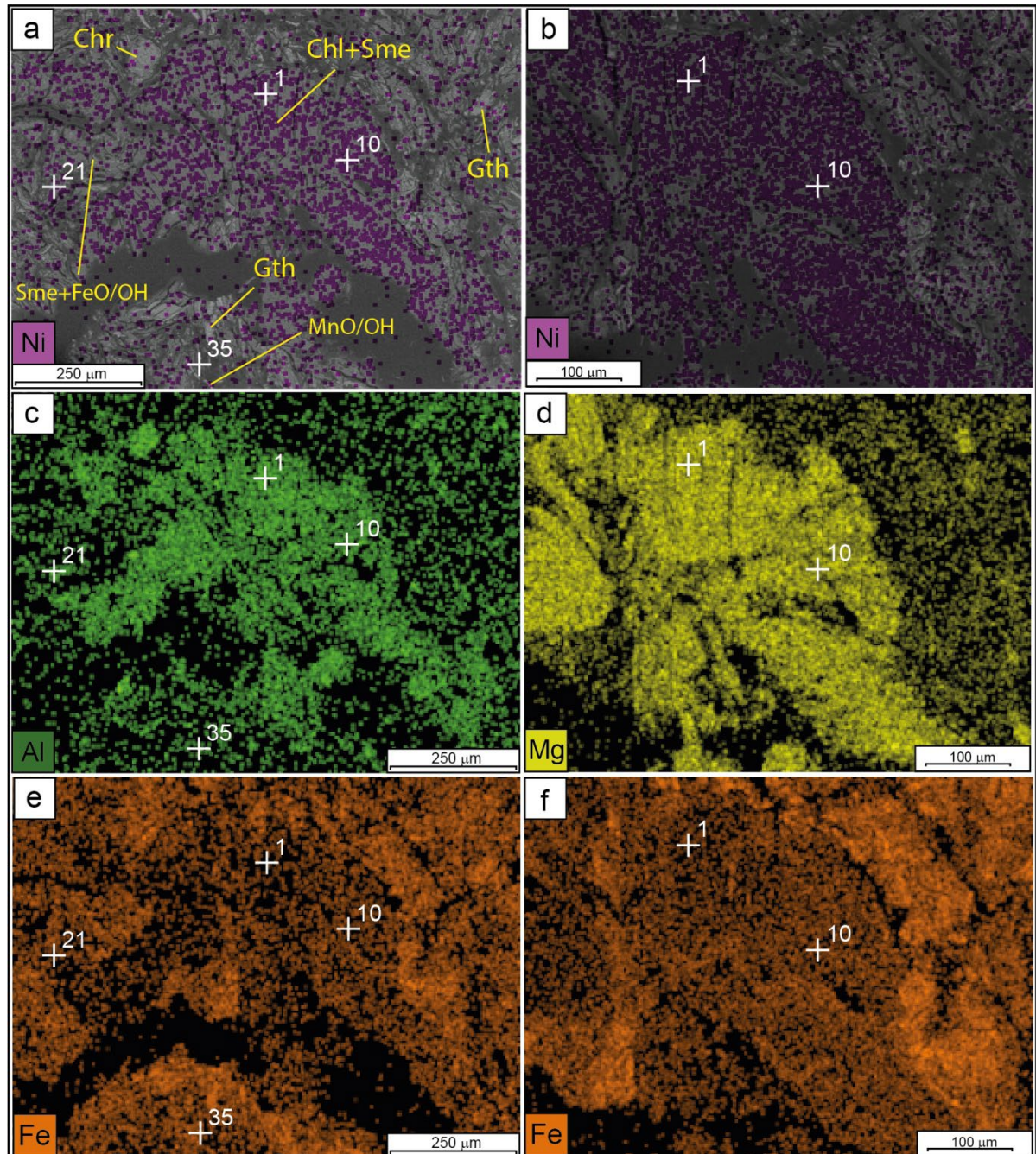


Fig. 18. a, b) Backscattered electron (BSE) image of a representative ferruginous saprolite sample in the pyroxenite profile with overlapping SEM-EDS map for Ni. c, d, e, f) SEM-EDS maps for Al, Mg and Fe. Sample CEA063. Spot SEM-EDS analyses indicated by the numbers in the spectra images are shown in Figs. 7 and 8. Abbreviations: Chr – chromite; FeO/OH - Fe oxyhydroxide; Gth – goethite; MnO/OH - Mn oxyhydroxide; Sme – smectite.

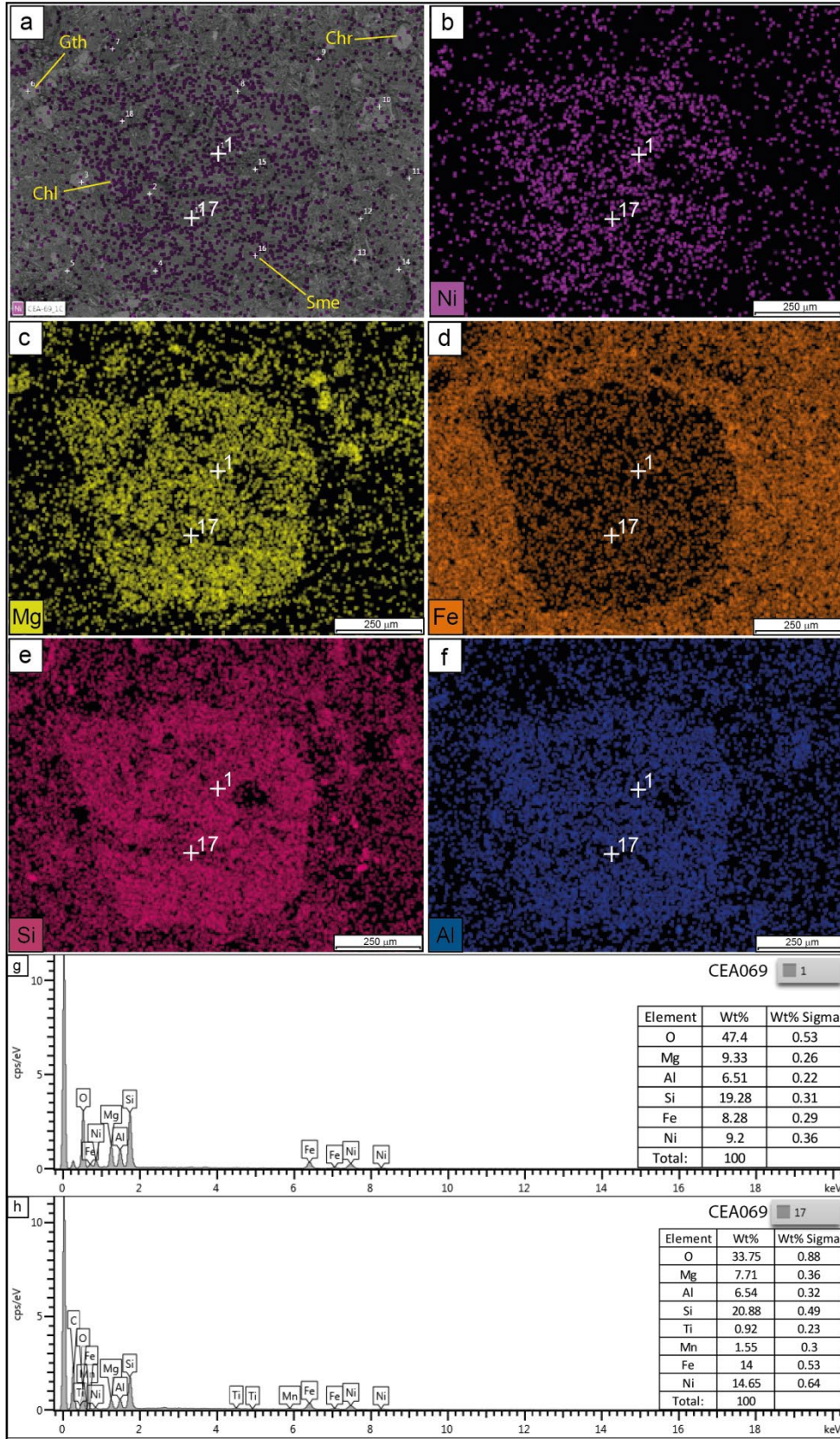


Fig. 19. a) Backscattered electron (BSE) image of a representative ocher saprolite sample in the dunite profile with overlapping SEM-EDS map for Ni. b, c, d, e, f) SEM-EDS maps for Ni, Mg, Fe, Si and Al. g, h) Spectra of spot analyses indicated by the numbers in the images. Sample CEA069. Abbreviations: Chl – chlorite; Chr – chromite; Gth – goethite; Sme – smectite.



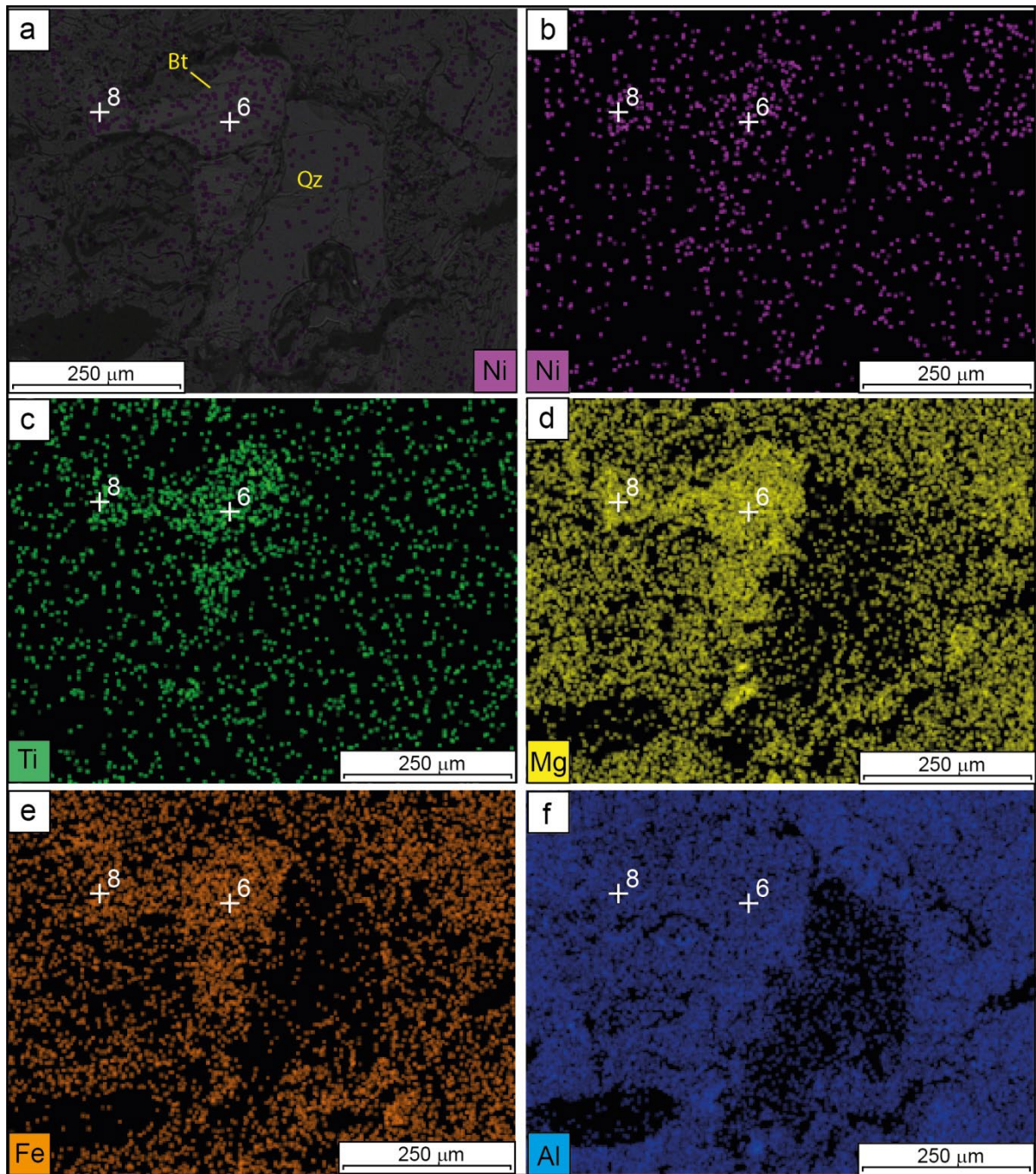


Fig. 20. a) Backscattered electron (BSE) image of a representative lower saprolite sample of the gabbro profile with overlapping SEM-EDS map for Ni. b, c, d, e, f) SEM-EDS maps for Ni, Ti, Mg, Fe and Al. Spot SEM-EDS analyses indicated by the numbers in the images. Spectra are shown in Fig. 9. Sample CEA055. Abbreviations: Bt – biotite; Qz - quartz.

#### 4.5.2 Ni-bearing oxyhydroxides

Oxyhydroxide-related mineralization occurs mostly in the oxide domain, represented by ferruginous saprolite and ocher saprolite. However, they are also found in the silicate domain; they are present in the lower saprolite. Fe and Mn oxyhydroxides are the main components of this type of mineralization, although chromite-related concentrations also occur.

In the lower saprolite of the dunite profile, there are small concentrations of Ni in association with goethite (Fig. 16a). In the other saprolite (Fig. 19), Ni occurs together with goethite or with ferruginous plasma that composes the regolith matrix.

In the pyroxenitic profile, oxyhydroxides are part of important concentrations of Ni (Fig. 21). These mineralized zones fill micro fractures and voids in the matrix between grains. In addition to Ni, Mn oxyhydroxides also contain high levels of Co. In Morro do Engenho, the composition of Mn oxyhydroxides, as found in the spot SEM-EDS analyses, indicates the dominant presence of asbolane with small amounts of romanechite. There were Ni contents of up to 14.68% associated with Mn oxyhydroxides, together with Co contents of up to 5.83%. There were other less important occurrences together with ilmenite and chromite (Fig. 16a; 17a).

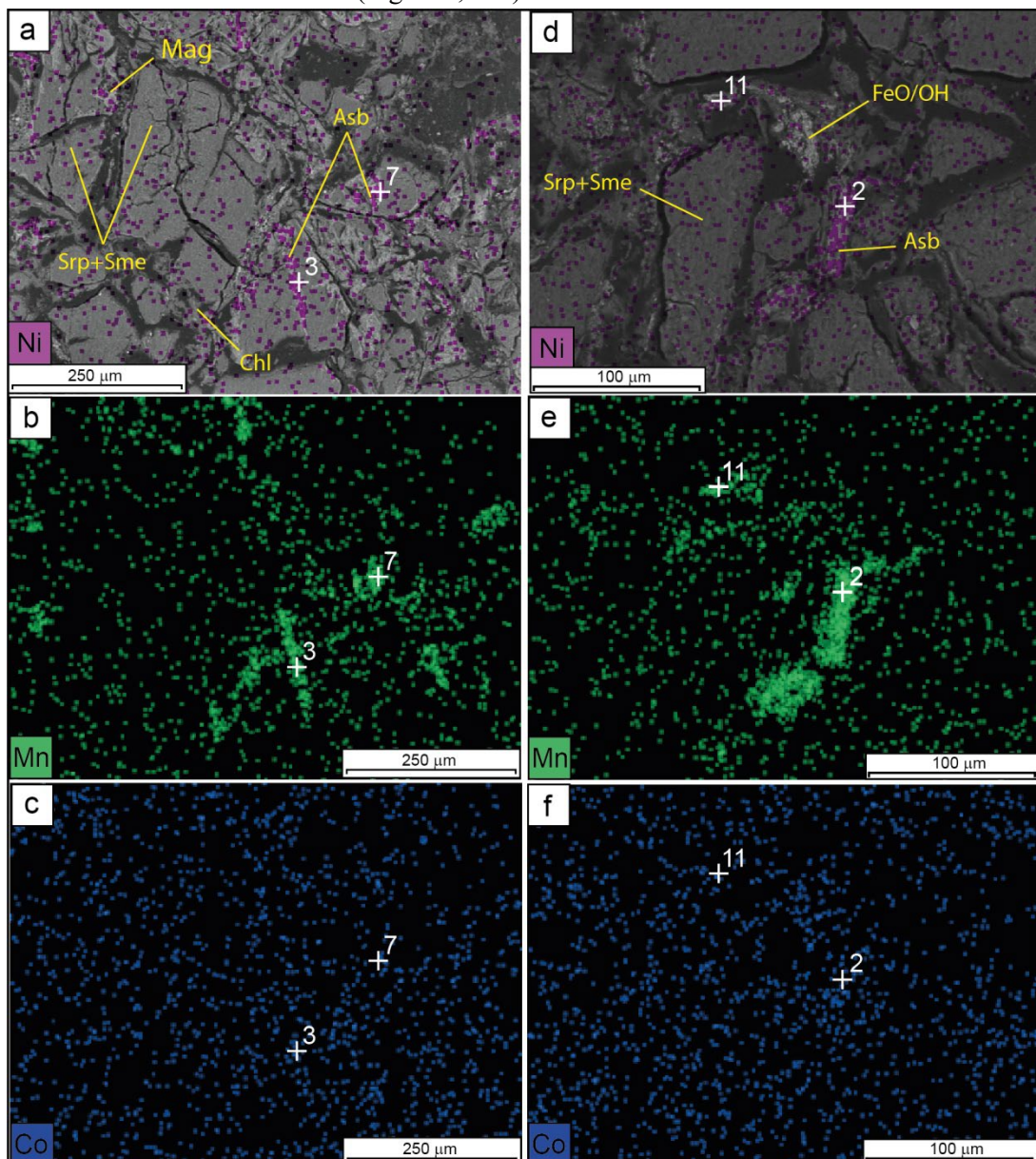


Fig. 21. a, c) Backscattered electron photomicrograph (BSE) of a representative lower saprolite sample in the pyroxenitic profile with overlapping SEM-EDS map for Ni. c, d) SEM-EDS maps for Mn. Sample CEA062. Spot SEM-EDS analyses indicated by numbers. Spectra are shown in Fig. 8. Abbreviations: Asb – asbolane; Chl – chlorite; FeO/OH - Fe oxyhydroxide; Mag – magnetite; Sme – smectite; Srp - serpentine.

## 5. Discussions

### 5.1 Geomorphological features, climate and relief

The geomorphological evolution of the Morro do Engenho lateritic Ni deposit plays a fundamental role in the current configuration of the deposit, as well as its mineralization.

According to Golightly (2010), the region of the Morro do Engenho deposit is part of a scenario referred to as “Dry to Wet”. In this scenario, high peneplanes that characterize the paleorelief remnants are commonly generated. This configuration favors enrichment in the lower saprolite zone along with Co and Mn rich zones.

According to Scherer (2000), from the Permian to the Mesozoic, the central portion of the South American platform was covered by extensive deposits of aeolian sands that formed the Botucatu desert, under an arid climate scenario. In this context, the advance of active erosive processes during the South American cycle, in the Paleogene, occurred in parallel to an increase in rainfall volume, which justifies the classification adopted by Golightly (2010).

As demonstrated by Freyssinet et al. (2005), deposits formed in humid savanna environments, when subjected to changes caused by tectonic uplift, undergo changes in their water regime, which directly affects the type of mineralization produced. Under a new phreatic level, Ni is then carried to the base of the profile, promoting enrichments in the lower saprolite horizon and forming silicate mineralization.

The change from dry to humid climate certainly caused variations in the water regime of Morro do Engenho. However, according to Thorne et al. (2012), lateritic Ni deposits develop in regions where rainfall exceeds 1000 mm/year and average monthly temperatures range from 22 to 31 °C in summer and 15 to 27 °C in winter. In this context, it can be assumed that the advance of the alteration front in Morro do Engenho started after the increase in regional precipitation, with a strong influence of pH variations caused by the infiltration of tropical acid rain water with an average pH of 5.6 (Myagkiy et al., 2017).

### 5.2 Ni mineralization phases

The findings in this study show that the Ni mineralization of the Morro do Engenho deposit is not restricted to just one mineral phase, i.e., it can be present in both silicate and oxide phases.

Among the silicate phases, the concentrations of Ni associated with the serpentine represent the predominant mineralization in the region of the dunite core. According to Freyssinet et al. (2005), Ni is accommodated in the serpentine structure through Mg substitution. The correlation graph in Fig. 13d shows a negative correlation between Ni and Mg in the domain with high Mg content up to the lower saprolite limit; from this point onwards, it shows a positive correlation. This effect demonstrates the initial presence of Ni in Mg minerals, with low Ni contents and high Mg contents; after Ni is replaced with Mg in these minerals, there is an increase in Ni contents and a decrease in Mg contents. The positive correlation between Ni and Mg is found to occur in the domain with low Mg contents, together with the horizons of the oxide domain of the lateritic profile, represented by Fe (Mn) oxyhydroxides.

The presence of Ni-rich serpentine suggests the formation of (1:1) garnierite, forming hydrosilicate minerals through the lizardite – nepouite series (Brindley and Hang, 1973; Brindley and Maksimovic, 1974; Wells et al., 2009; Galí et al., 2012; Villanova-de-Benavent et al., 2014; Cathelineau et al., 2017). This type of mineralization typically occurs in tectonically active environments, where concentrations are controlled by fractures, faults, or shear zones. However, in the Morro do Engenho deposit, there is no evidence of important structures that could accommodate garnierite mineralization. Golightly (1981) demonstrates that fully serpentinized rocks are less

susceptible to weathering and fracturing and, thus, do not favor garnierite accumulation. Given the high degree of serpentinization of the dunite in Morro do Engenho, it can be assumed that this characteristic represents a determining factor for the low level of garnieritic mineralization found in this study. A similar situation was described by Machado et al. (2021) in the Santa Fé deposit. The authors suggested that the scarcity of faults or deep structures in the parent rock would be the main reason for the absence of substantial garnierite mineralization, concentrated in fracture zones or fault planes.

The mineralized silicate phases present in the peridotite/pyroxenite and gabbro zones are represented by chlorite and smectite, which make up clay minerals (Butt & Cluzel, 2013). According to Oliveira and Melfi (1979), the generation of smectite is favored by the greater presence of pyroxene in the parent rocks. For Colin et al. (1990), the composition of smectites is affected by groundwater movement through the regolith, which in turn is controlled by the degree of fracturing.

Table 1 shows that the gabbro parent rock is richer in  $Al_2O_3$  than other lithologies of the zoned body. The lithogeochemical profile shows that the  $Al_2O_3$  content is continuously increased towards the top of the profile. It can be assumed that the supergene alteration of the primary minerals of the gabbro parent rock provided enough  $Al_2O_3$  to generate large amounts of smectite and chlorite in this profile. In addition, one should also consider the presence of primary chlorite, which could have been reworked in the regolith. The occurrence of chlorite containing high levels of Ni also in the ferruginous saprolite and ocher saprolite coincides with increases in levels in the pyroxenite and dunite profiles.

The oxide mineralized phases are concentrated in Fe and Mn oxyhydroxides, especially asbolane and goethite. This type of mineralization is mostly present in the ferruginous saprolite and ocher saprolite, and may also occur in the lower saprolite when cracks are filled. As suggested by Golightly (2010) in the Santa Fé deposit, mineralization in the limonite domain of Morro do Engenho can be associated with vertical fluctuations in the water table that are influenced by a similar type of climate to the current one, i.e., there is a wet season and a dry season.

Myagkiy et al. (2017) demonstrated that type of mineralization (silicate or oxide) is influenced by the alteration front in the lateritic profile over time and on the basis of rainfall. As rainwater with acidic pH infiltrates the profile, the boundary between the oxide and silicate domains migrates downwards vertically. The advance of the more acidic pH front causes goethite precipitation, favoring the oxide mineralization; also, it affects the precipitation/dissolution of newly-formed silicates and regulates the transport of elements in the lateritic profile.

Weathering of olivine and serpentine leads to the formation of goethite and silico-ferruginous plasma residues in the oxide horizons. The association between Ni and goethite was summarized by Myagkiy et al. (2017), who described three possibilities for this type of mineralization, namely through isomorphic replacement of Fe with Ni in the mineral structure, association of Ni with poorly crystallized phases or adsorption of Ni to the surface of goethite.

It is noteworthy that the transformation of goethite into hematite promotes the release by dehydration of Ni present in goethite. According to (Nahon & Tardy, 1992; Machado et al., 2021), the limited ability of hematite to retain Ni allows the metal to be carried through solutions to the base of the profile, further enriching the lower saprolite.

Mineralogical associations with oxyhydroxides and Mn have been widely discussed by Ostwald, (1984) and Putzolu et al. (2018) in their studies of laterite deposits from Australia. According to the authors, Ni, as well as Co, can replace Al in the lithiophorite structure. This replacement, when complete, causes the transformation of lithiophorite into asbolane. Putzolu et al., (2021) described the presence of three mineral species of Mn oxyhydroxides in the Santa Fé deposit, with asbolane being

the most Ni-rich variety. In the Morro do Engenho deposit, there is a dominant presence of asbolane with very small amounts of romanechite.

### 5.3 Hydrodynamic and Mechanical Transport Factors

The *per descensum* lateritic model of fluid circulation is commonly used in an attempt to explain the geometry and distribution of mineralization of Ni laterite deposits (Trescases, 1975; Cathelineau et al., 2016; Quesnel et al., 2017). In this model, Mg, Si and Ni, among other mobile elements, are transported vertically and concentrated in deep zones of the saprolite.

Myagkiy et al. (2019) demonstrated, through simulations in 2-D models, the role of hydrodynamic factors in the remobilization of Ni. In contrast to the *per descensum* model, the tested model shows the concentration of Ni in topographically low regions. According to the authors, the remobilization of Ni is particularly due to the dissolution of Ni-bearing secondary silicates in saprolite and the dissolution of olivines partially preserved in the saprock/bedrock. pH plays a fundamental role in the dissolution and precipitation of silicates, and their migration is shaped by topography. The remobilization of Ni through the dissolution of goethite, present in lateritic covers, plays an insignificant role in the nickel reconcentration process.

The concentration of the highest Ni enrichments in a topographically depressed zone, as seen in the map in Figure 22, demonstrates that the processes that form the Morro do Engenho deposit are compatible with the model for Ni remobilization through hydrodynamic factors. The geomorphology of the deposit suggests two major lateral flow directions, one in the SE direction and one in the SW direction, which would have converged to the lowest zone between the two elevations (Fig. 22a). The dissolution/precipitation of Ni-bearing silicates in the bedrock/saprock/lower saprolite of the serpentinized dunite could then have caused the remobilization of Ni, through the migration of the pH towards the topography, favoring the enrichment of the lower saprolite in the flat area between the elevations and producing concentrations of up to 3.0% Ni.

The geometry of the Morro do Engenho deposit shows that lateral redistribution through hydrodynamic factors could also explain the mineralization of areas peripheral to the dunite core, composed of pyroxenite- and gabbro-derived lateritic profiles (Fig. 22b). Regional groundwater flow direction, strongly influenced by topography, would be an important factor in the remobilization of Ni dissolved in the saprolite horizons of the dunite zone, for precipitation in the lower saprolite of the peripheral region of Ni-enriched silicates, which are mostly composed of chlorite and smectite.

Several studies (Trescases, 1975; Cathelineau et al., 2016) have reported that Ni-mineralized areas are not always spatially associated with the main Ni source rock. Colin et al. (1990) proposed that in the Jacuba deposit, in Niquelândia, the action of groundwater would have transported Ni in solution from dunite, positioned at higher levels, to pyroxenite located topographically below, thus producing mineralization in the lateritic profile developed on this lithology. A similar process was described by Machado et al. (2021) in the Santa Fe deposit. According to the authors, lateral migration of Ni from a dunite source promoted enrichments in peripheral pyroxenites, in which smectite and serpentine are the main Ni-bearing minerals. In the Vermelho deposit, in Carajás, unlike what happens in Niquelândia, Silva & Oliveira (1995) suggested that migration of enriched solutions would have occurred only vertically and, for this reason, pyroxenite would not have been mineralized, remaining sterile.

Additionally, Quesnel et al. (2017) proposed that the mechanical transport of lateritic materials in slope zones can also produce local enrichments in the saprolite zone. This possibility is supported by whole-rock chemical data (Tables 1, 2, 3), which show evidence of mechanical transport, particularly in samples from higher horizons. In these samples, anomalous values in TiO<sub>2</sub> and Al<sub>2</sub>O<sub>3</sub>, suggest some contribution of allochthonous lateritic materials. Thus, it is likely that the mechanical transport of

lateritic materials also played a role in the mineralization of gabbro- and pyroxenite-derived profiles, favoring the concentration of Ni in the alteration products of these rocks.

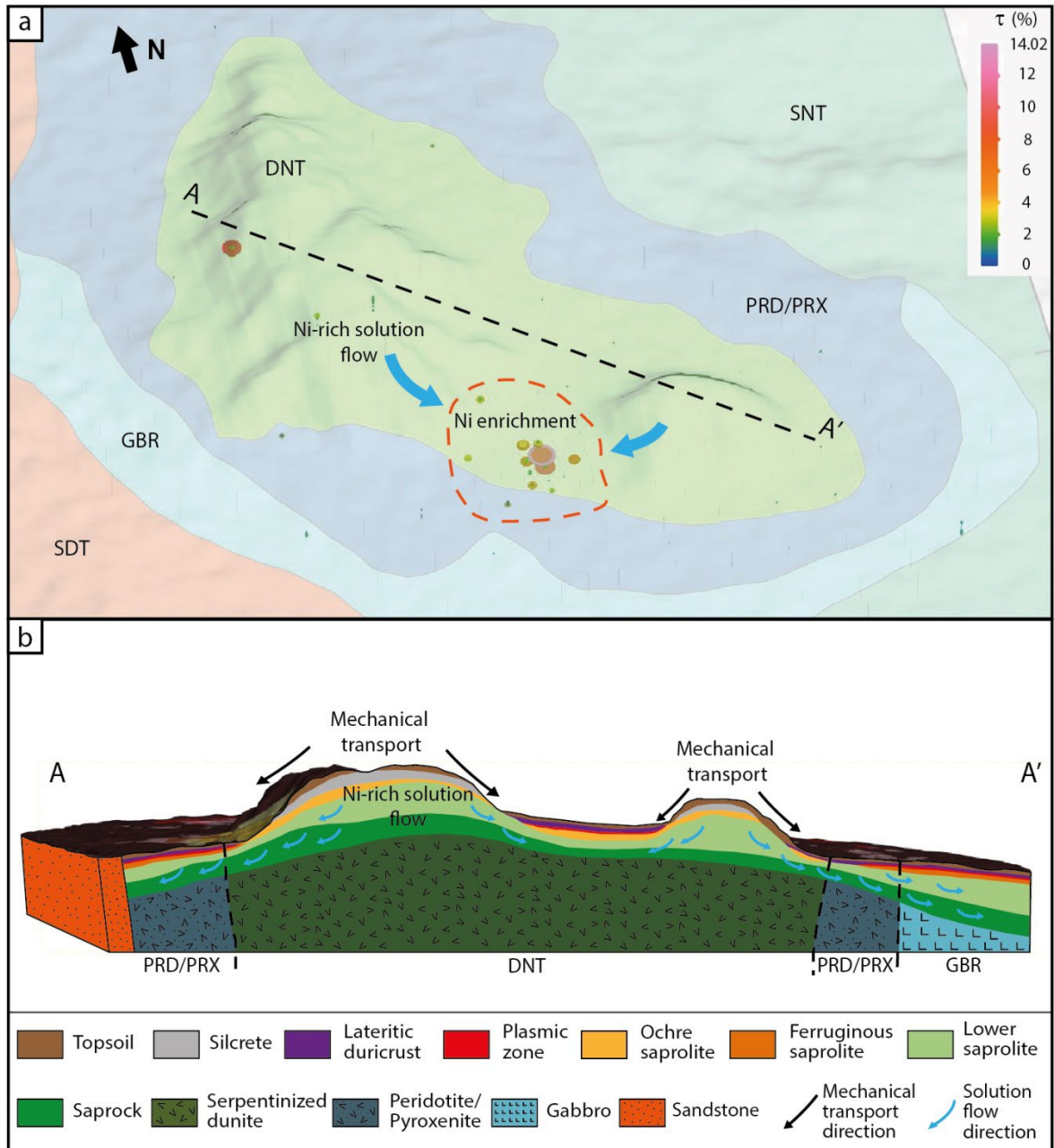


Fig. 22. a) Probable flow directions of the Ni-enriched solutions, responsible for the concentration of the metal in the depressed zone between the two topographic elevations, where the greatest Ni enrichments are present. Abbreviations: DNT – Dunite zone; PRD/PRX - peridotite/pyroxenite zone; GBR – gabbro zone; SNT - syenite-nepheline zone; SDT – sandstone. B) Cross-section A-A' schematically showing the lateral Ni remobilization flows and probable directions of mechanical transport of lateritic materials. The dissolution/precipitation of Ni-bearing silicates in the bedrock/saprock/lower saprolite zone of the serpentinized dunite is interpreted as being responsible for the remobilization of Ni, through the migration of the pH towards the topography, favoring the enrichment of lower saprolite in the flat area between the elevations, as well as in the peripheral zones, composed of gabbro- and pyroxenite-derived profiles.

#### 5.4 Deposit classification

The classification of lateritic Ni deposits is based on the mineralogy bearing the dominant mineralization (Brand et al., 1998; Gleeson et al., 2003; Golyghtly, 2010; Butt & Cluzel, 2013;

Freyssinet et al., 2005). According to Butt & Cluzel (2013), this definition has important implications for the economic use of the deposit, especially in terms of the type of ore processing to be adopted. However, Ni laterite deposits rarely show only one type of mineralization; therefore, knowledge of the mineralogy and chemistry of the mineralized phases is required to determine the best ore processing routes (Putzolu et al., 2020).

Morro do Engenho has been historically classified as a silicate deposit (Chaban et al., 1975). However, the results of this study show that mineralization is also present in oxide phases, which encourages a broader analysis of the mineralization characteristics of Morro do Engenho.

There is a similar scenario in the Santa Fé deposit, where Machado et al. (2021) reported the difficulty in classifying the deposit into one of the three conventional types existing in the literature. In this case, the authors considered the presence of nickel-bearing chlorites in association with Fe oxyhydroxides as a fundamental factor, which allowed classifying the deposit as an oxide type. Such characteristics are also found in Morro do Engenho, particularly with regard to the presence of chlorite with high levels of Ni in the oxide domain. However, in terms of thickness, the silicate horizon, represented by lower saprolite, is significantly thicker than oxide horizons, which generally reflects a higher volume of silicate ore compared to the oxide ore. This aspect is extremely relevant from the point of view of using the ore from Morro do Engenho and broadens the understanding of the dominant mineralization. Thus, the data analyzed in this study favor the classification of the Morro do Engenho as a predominantly silicate deposit with relevant occurrence of oxide mineralization.

## 6. Conclusions

- Lateritic Ni mineralization in the Morro do Engenho deposit is present in the alteration profiles derived from the dunite core and peripheral rocks formed by peridotites, pyroxenites and gabbros.
- Mass balance shows that Ni presents enrichments in relation to the parent rock, especially in the lower saprolite of the dunite-derived profile, where it reaches up to 40% and in the lower saprolite of the gabbro profile, with values of up to 1%.
- The correlation diagrams show that Ni levels are positively correlated with UMIA, that is, with increasing degree of lateritization, except for DRCCR, where Ni levels are reduced. Ni is positively correlated with Mg in the domain of its low levels, while it has a negative correlation at the high levels of MgO.
- Cobalt shows a strong positive correlation with UMIA, indicating an increase in contents as lateritization progresses. The highest values of Co are present in the oxide domain, especially in the ocher saprolite, plasma zone and duricrust. The correlation between Co and MnO is positive and very significant, which highlights its connection with Mn minerals, usually oxyhydroxides (asbolane).
- The REE contents show a gradual increase together with an increase in the degree of lateritization. The increase in the contents from the bedrock reaches the apex in the horizons of the oxide domain, especially ferruginous saprolite, ocher saprolite and duricrust. In general, the dunitic rock shows a lower initial REE content than the pyroxenitic and gabbroic rocks. On average, the lateritic horizon that contains the largest levels of REE is the ferruginous saprolite.
- The main silicate minerals that host Ni are serpentine, chlorite and smectite. The Ni-rich serpentine is found more abundantly in the lower saprolite horizon of the profile derived from the serpentized dunite and - to a lesser extent - in the profile derived from the peridotite/pyroxenite zone. Mineralization associated with chlorite is more common in the gabbro-derived profile, where it occurs abundantly in the lower saprolite with contents up to

3.7% Ni. In the peridotite/pyroxenite-derived profile, chlorite is responsible for important concentrations, especially in the ferruginous saprolite horizon, exhibiting Ni contents of up to 4.8%. Smectite also composes a mineralized phase in this horizon with contents of up to 3.27% of Ni. In the ocher saprolite horizon, chlorite associated with smectite and Fe and Mn oxyhydroxides has Ni contents of up to 4.65%.

- Oxyhydroxide mineralization occurs preferably in the oxide domain, represented by ferruginous saprolite and ocher saprolite. However, oxyhydroxides are also found in the silicate domain, with the presence of Mn oxyhydroxides (Fe) that fill micro fractures and matrix voids. Goethite, asbolane and, secondarily, romanechite are the main Ni minerals of this type of mineralization.
- The change from dry to humid climate caused variations in the water regime of Morro do Engenho; however, it can be assumed that the advance of the alteration front in Morro do Engenho started after an increase in regional rainfall rates, with a strong influence of variations in pH caused by the infiltration of acidic tropical rainwater with acidic pH.
- The concentration of the highest Ni enrichments in a topographically depressed zone demonstrates that the processes that form the Morro do Engenho deposit are compatible with the model for remobilization of Ni through hydrodynamic factors. The geomorphological features of the deposit suggest two main lateral flow directions: one in the SE direction and one in the SW direction, which would have converged to the lowest zone between the two topographic elevations.
- The geometric characterization of the Morro do Engenho deposit shows that lateral redistribution through hydrodynamic factors could also account for the mineralization of areas peripheral to the dunite core, composed of lateritic pyroxenite- and gabbro-derived profiles. Regional groundwater flow direction, strongly influenced by topography, would be an important factor in the remobilization of Ni dissolved in the saprolite horizons of the dunite zone, for precipitation in the lower saprolite of the peripheral region of Ni-enriched silicates, which are mostly composed of chlorite and smectite.
- It is likely that the mechanical transport of lateritic materials also played a role in the mineralization of the profiles derived from gabbro and pyroxenite, favoring the concentration of Ni in the alteration products of these rocks.
- The data analyzed in this study favor the classification of Morro do Engenho as a predominantly silicate deposit with an important presence of oxide-type mineralization.

## ACKNOWLEDGMENTS

This work is part of the results of the Project Reevaluation of the *Mineral Heritage of CPRM-Niquel de Morro do Engenho*. It was developed and published with the permission of the Geological Survey of Brazil – CPRM. We are thankful to the entire project team that somehow helped us to achieve our objectives. We express our special thanks to the 3D Modeling group of GSB-CPRM, geologist Ricardo Wosniak; geologist Daniel Augusto de Miranda; geophysicist Ricardo Cavalcanti Santiago; geologist Marcelo Lacerda Vasquez, from the Mineral Analysis Laboratory of GSB-CPRM; geologist Jonathan Nereu Lisboa Rojas, from the Regional Rock Collection of GSB-CPRM; and the Laboratory of Mineral Technology - X-Rays - Federal University of Bahia.



## REFERENCES

- AIGLSPERGER, T.; PROENZA, J.; LEWIS, J.; LABRADOR, M.; SVOJTKA, M.; ROJAS P.; ARTURO, L.; LONGO, F.; ĎURIŠOVÁ, J. Critical metals (REE, Sc, PGE) in Ni laterites from Cuba and the Dominican Republic. **Ore Geology Reviews**. v. 73, p. 127-147, 2016. DOI: 10.1016/j.oregeorev.2015.10.010.
- ALEVA, G.J.J. **Laterites: concepts, geology, morphology and chemistry**. Wageningen: ISRIC, 1994. 169 p.
- ALMEIDA F.F.M. Relações tectônicas das rochas alcalinas mesozoicas da Região Meridional da Plataforma Sul-Americana. **Revista Brasileira de Geociências**, v. 13, n. 3, p. 139-158, 1983.
- ALMEIDA F.F.M. Distribuição regional e relações tectônicas do magmatismo pós-Paleozóico no Brasil. **Revista Brasileira de Geociências**, v. 16, n. 4, p. 325-349, 1986.
- ANAND, R.R.; PAINE, M. Regolith geology of the Yilgarn Craton, Western Australia: Implications for exploration. **Australian Journal of Earth Sciences**. v. 49, n. 1, p. 3-162, 2002. DOI: 10.1046/j.1440-0952.2002.00912.x
- ALVARES, C.A.; STAPE, J.L.; SENTELHAS, P.C.; GONÇALVES, J.L. M.; SPAROVEK, G. Köppen's climate classification map for Brazil. **Meteorologische Zeitschrift**, v. 22, n. 6, p. 711-728, 2013.
- ASSUMPCÃO, M.; BIANCHI, M.; JULIÀ, J.; DIAS, F.L.; FRANÇA, G.S.; NASCIMENTO, R.; DROUET, S.; PAVÃO, C.G.; ALBUQUERQUE, D.F.; LOPES, A.E.V. Crustal thickness map of Brazil: Data compilation and main features. **Journal of South American Earth Sciences**, v. 43, p. 74-85, 2013.
- BABECHUK, M.G.; WIDDOWSON, M.; KAMBER, B.S. Quantifying chemical weathering intensity and trace element release from two contrasting basalt profiles, Deccan Traps, India. **Chemical Geology**. v. 363, p. 56-75, 2014.
- BARBOUR, A.P.; GIRARD, V.A.V.; KAWASHITA, K.; SOUZA, A.M.S. Geocronologia do Complexo Máfico-Ultramáfico Alcalino de Santa Fé, Goiás. **Boletim do Instituto de Geociências**, v. 10, p. 11-18, 1979.
- BARDET, M.G. Géologie du diamante. Troisième partie: Gisements de diamants d'Asie, d'Amérique, d'Europeet d'Australasie. **Mémoires du Bur. Recherches Geol. Min.**, n. 83, 169 p, 1977.
- BERBERT, C.O. O Deposito de Níquel Laterítico de Morro do Engenho, Goiás. *In*: SCHOBENHAUS, C. & COELHO, C.E.S. **Principais Depósitos Mineraiis do Brasil**. Brasília: Ministério das Minas e Energia, 1986. V. 11, P. 335-340.
- BIONDI, J.C. **Processos metalogenéticos e os depósitos mineraiis brasileiros**. São Paulo: Oficina de Textos, 2003. p. 383-406.

BIZZI, L.A.; VIDOTTI, R.M. Condicionamento do magmatismo Pós-Gondwana. *In*: BIZZI, L.A.; SCHOBENHAUS, C.; VIDOTTI, R.M.; GONÇALVES, J.H. (org.) **Geologia, tectônica e recursos minerais do Brasil**: texto, mapas e SIG. Brasília: CPRM, 2003. p. 335-361.

BRAND, N.W.; BUTT, C.R.; ELIAS, M. Nickel laterites: classification and features. **AGSO Journal of Australian Geology e Geophysics**, Symonston ACT, v. 17, n. 4, p. 81-88. 1998.

BRAUN, O.P.G. Contribuição à geomorfologia do Brasil central. **Revista Brasileira de Geografia**, v. 32, p. 3-39, 1971.

BRIMHALL G.H.; DIETRICH W.E. Constitutive mass balance relations between chemical composition, volume, density, porosity, and strain in metasomatic hydrochemical systems: results on weathering and pedogenesis. **Geochimica et Cosmochimica Acta**, v. 51, p. 567-587, 1987.

BRIMHALL, G.H.; LEWIS, C.J.; FORD C.; BRATT, J.; TAYLOR, G.; WARIN, O. Quantitative geochemical approach to pedogenesis: importance of parent material reduction, volumetric expansion, and eolian influx in lateritization. **Geoderma**, v. 51, p. 51-91, 1991.

BRINDLEY, G.W.; HANG, P.T. The Nature of Garnierites —I Structures, Chemical Compositions and Color Characteristics. **Clays and Clay Minerals**, v. 21, p. 27-40, 1973.

BRINDLEY, G.; MAKSIMOVIC, Z. The nature and nomenclature of hydrous nickel-containing silicates. **Clay Minerals**, v.10, n.4, p. 271-277, 1974. DOI: 10.1180/claymin.1974.010.4.05.

BUTT C.R.M.; CLUZEL D. Nickel laterite ore deposits: weathered serpentinites. **Elements**, v. 9, n. 2, p.123–128, 2013.

CATHELINEAU, M.; QUESNEL, B.; GAUTIER, P.; BOULVAIS, P.; COUTEAU, C.; DROUILLET, M. Nickel dispersion and enrichment at the bottom of the regolith: formation of pimelite target-like ores in rock block joints (Koniambo Ni deposit, New Caledonia). **Mineral Deposita** v. 51, p. 271–282, 2016. DOI: <https://doi.org/10.1007/s00126-015-0607-y>.

CATHELINEAU, M.; MYAGKIY, A.; QUESNEL, B. et al. Multistage crack seal vein and hydrothermal Ni enrichment in serpentinitized ultramafic rocks (Koniambo massif, New Caledonia). **Miner Deposita**, v. 52, p. 945–960, 2017. DOI: <https://doi.org/10.1007/s00126-016-0695-3>.

CHABAN, N.; SANTOS, J.F.; TAKAHASHI, A.T.; OLIVEIRA, J.A.; BERBERT, C.O.; TRIGUIS, J.A.; ARAUJO, A.G. **Projeto Morro do Engenho**: relatório único de pesquisa de níquel realizada nos municípios de Montes Claros de Goiás e Jussara, estado de Goiás. Goiânia: CPRM, 1975. 16 v.

COLIN, F.; NAHON, D.; TRESCASES, J.J.; MELFI, A.J. Lateritic Weathering of Pyroxenites at Niquelandia, Goiás, Brazil: the supergene behavior of nickel. **Economic Geology**, v. 85, n. 05, p.1010-1023, 1990.

COSTA, M.L. O níquel no Brasil e seus depósitos lateríticos. *In*: MELFI, A.J.; MISI, A.; CAMPOS, D.A.C.; CORDANI, U.G. (org.) **Recursos Minerais no Brasil: problemas e desafios**. Rio de Janeiro: Academia Brasileira de Ciências, 2016. Cap. 01, p.124-132.

- DANNI, J.C.M. Os picritos alcalinos da região de Iporá: implicações na gênese dos complexos do tipo central do sul de Goiás. **Revista Brasileira de Geociências**, v. 24, n. 2, p. 112–119, 1994.
- DUTRA, A.C.; MARANGONI, Y.R. Gravity and magnetic 3D inversion of Morro do Engenho complex, Central Brazil, **Journal of South American Earth Sciences**, v. 28, n. 2, p. 193-203, 2009.
- EGLINGTON, R.A. **The regolith glossary – surficial geology, soils and landscapes**. Canberra: Cooperative Research Centre for Landscape Evolution and Mineral Exploration, 2001. 144p.
- ELIAS, M. Nickel lateritic deposits – Geological overview, resources and exploitation. In: COOKE, D.; PONGRATZ, J. (ed.) **Giant Ore Deposits: characteristics, genesis and exploration**. Hobart: University of Tasmania, 2002. p. 205-220.
- FERRARI, A.; RICCOMINI, C. Campo de esforços plio-pleistocênico na ilha da Trindade (Oceano Atlântico Sul, Brasil) e sua relação com a tectônica regional. **Revista Brasileira de Geociências**, v. 29, p. 195-202, 1999. DOI: 10.25249/0375-7536.199929195202.
- FREYSSINET, P.H.; BUTT, C.R.M.; MORRIS, R.C.; PIANTONE, P. Ore-forming processes related to lateritic weathering. **Economic Geology**, 100th Anniv, p. 681-722, 2005.
- GALÍ, S.; SOLER, J.M.; PROENZA, J.A. et al. Ni Enrichment and Stability of Al-Free Garnierite Solid-Solutions: A Thermodynamic Approach. **Clays Clay Miner**, v. 60, p. 121–135, 2012. DOI: <https://doi.org/10.1346/CCMN.2012.0600203>.
- GIBSON, S.A.; THOMPSON, R.N.; LEONARDOS, O.H.; DICKINSON, A.P.; MITCHELL, J.G. The Late Cretaceous Impact of the Trindade Mantle Plume: Evidence from large-volume, mafic, potassic magmatism in SE Brazil. **Journal of Petrology**, v. 36, n. 1, p. 189-229, fev. 1995.
- GLEESON, S.A.; BUTT, C.R.M.; ELIAS, M.; Nickel Laterites: A Review. **SEG Discovery**, v. 54, p. 1–18, 2003. DOI: <https://doi.org/10.5382/SEGnews.2003-54.fea>.
- GOLIGHTLY J.P. Nickeliferous laterite deposits. **Economic Geology**, 75th Anniv, p.710–735, 1981.
- GOLIGHTLY J.P. Progress in understanding the evolution of nickel laterite. **Society of Economic Geologists**, Inc. Special Publication, v. 15, p. 451–485, 2010.
- GOMES, C.B.; COMIN-CHIARAMONTI, P. An introduction to the alkaline and alkaline-carbonatitic magmatism in and around the Paraná Basin. In: GOMES, C.B. & COMIN-CHIARAMONTI, P. **Mesozoic to Cenozoic Alkaline Magmatism in the Brazilian Platform**. São Paulo: Edusp, 2005. P. 21-29.
- JUNQUEIRA-BROD, T.C.; GASPAR, J.C.; BROD, J.A.; JOST, H.; BARBOSA, E.S.R.; KAFINO, C.V. Emplacement of kamafugite lavas from the Goiás alkaline province, Brazil: constraints from whole-rock simulations, **Journal of South American Earth Sciences**, v. 18, n. 3–4, p. 323-335, 2005.

JUNQUEIRA-BROD, T.C.; ROIG, H.L.; GASPAR, J.C.; BROD, J.A.; MENESES, P.R. A Província Alcalina de Goiás e a Extensão do seu Vulcanismo Kamafugítico. **Revista Brasileira de Geociências**, v. 32, n. 4, p. 559-566, 2002.

KING, L.C. A Geomorfologia do Brasil Oriental. **Revista Brasileira de Geografia**, v. 18, n. 2, p. 147-266, 1956.

KÖNIG, U. Nickel Laterites — Mineralogical Monitoring for Grade Definition and Process Optimization. **Minerals**, v. 11, p. 1178, 2021. DOI: <https://doi.org/10.3390/min1111178>.

LACERDA FILHO, J.V.; GOLLMAN, K.; SANTOS, D.V.; MARTINS, F.R.; SOUZA, J.O.; CARNEIRO, J.S.M.; MENEGHINI, P.F.V.; HATTINGH, K.; SILVA, E.R.; EBERHARDT, D.B. Projeto geologia e metalogenia da porção oeste de Goiás. Programa geologia, mineração e transformação mineral do Brasil. Levantamento geológico e de potencial mineral de novas fronteiras. Goiânia: CPRM, 2021. 424 P.

LELONG, F.; TARDY, Y.; GRANDIN, G.; TRESCASES, J. J.; BOULANGE, B. Pedogenesis, chemical weathering and processes of formation of some supergene ore deposits. In: WOLF, K. H. (ed.). **Handbook of Strata-bound and Stratiform Ore Deposits**. Amsterdam, Elsevier, v. 3, P. 93–174, 1976.

MACHADO, M.; PORTO, C.; SANTORO, L.; PUTZOLU, F.; NEUMANN, R.; BASTOS NETO, A.; POLIVANOV, H.; HERRINGTON, R. The origin of supergene nickeliferous chlorite in the Santa Fé Ni-Laterite Deposit, GO, Brazil. **Brazilian Journal of Geology**, v. 51, 2021. DOI: 10.1590/2317-4889202120200119.

MARSH, E.E.; ANDERSON, E.D.; GRAY, F. **Nickel-cobalt laterites - a deposit model**: chapter H in mineral deposit models for resource assessment. Reston: USGS, 2013. (USGS Scientific Investigations Report 2010–5070–H).

MAURIZOT, P.; SEVIN, B.; ISEPPI, M.; GIBAND, T. Nickel-Bearing Laterite Deposits in Accretionary Context and the Case of New Caledonia: From the Large-Scale Structure of Earth to Our Everyday Appliances, **GSA Today**, v. 29, n. 5, p. 4–10, 2019.

MIZUSAKI, A.M.P.; THOMAZ-FILHO, A. O Magmatismo Pós-Paleozóico no Brasil. In: Mantesso Neto, V.; Bartorelli, A.; Carnerio, C.D.R.; Brito-Neves, B.B. **Geologia do Continente Sul-Americano: Evolução da obra de Fernando Flávio Marques de Almeida**. São Paulo: Ed. Beca. 2004, 673p. P. 281-291.

MYAGKIY, A.; TRUCHE, L.; CATHELINÉAU, M.; GOLFIER, F. Revealing the conditions of Ni mineralization in the laterite profiles of New Caledonia: Insights from reactive geochemical transport modelling. **Chemical Geology**, v. 466, p. 274-284, 2017. DOI: <https://doi.org/10.1016/j.chemgeo.2017.06.018>.

MYAGKIY, A.; GOLFIER, F.; TRUCHE, L.; CATHELINÉAU, M. Reactive transport modeling applied to Ni laterite ore deposits in New Caledonia: Role of hydrodynamic factors and geological

structures in Ni mineralization. **Geochemistry, Geophysics, Geosystems**, v. 20, p. 1425–1440, 2019. DOI: <https://doi.org/10.1029/2018GC007606>

NAHON, D.; TARDY, Y. The Ferruginous Laterites. *In*: Butt, C.R.M. ; Zeegers, H. **Regolith exploration geochemistry in tropical and subtropical terrains**. Handbook of Exploration Geochemistry, Elsevier Science B.V., v. 4, 1992, P. 41-55. DOI: <https://doi.org/10.1016/B978-0-444-89095-5.50010-9>.

NASCIMENTO, E.L.C. **Geologia, Geoquímica e Mineralogia do Complexo Carbonatítico Morro Preto – GO**. 2018. 199 f., il. Thesis (PhD in Applied Geosciences) — Universidade de Brasília, Brasília, 2018.

OLIVEIRA, S.M.B.; MELFI, A.J. Considerações sobre a origem das esmectitas nos níveis de alteração dos piroxenitos de Santa Fé, GO. **Boletim IG-USP**, v. 10, p. 91-96, 1979.

OLIVEIRA, S.B. **Alteração intempérica das rochas ultrabásicas de Santa Fé (GO) e gênese do depósito níquelífero**. 1980. 238f. Thesis (Doctorate) - Instituto de Geociências, Universidade de São Paulo, São Paulo, 1980.

OSTWALD, J. Two varieties of lithiophorite in some Australian deposits. **Mineralogical Magazine**, v. 48, p. 385-392, 1984.

PUTZOLU, F.; BALASSONE, G., BONI, M., MACZURAD, M., MONDILLO, N., NAJORKA, J.; PIRAJNO, F. Mineralogical association and Ni-Co department in the Wingellina oxide-type laterite deposit (Western Australia). **Ore Geology Reviews**, v. 97, p. 21–34, 2018.

PUTZOLU, F.; ABAD, I.; BALASSONE, G.; BONI, M.; CAPPELLETTI, P.; GRAZIANO, S.; MACZURAD, M.; MONDILLO, N.; NAJORKA, J. Santoro, L. Parent rock and climatic evolution control on the genesis of Ni-bearing clays in Ni-Co laterites: New inferences from the Wingellina deposit (Western Australia). **Ore Geology Reviews**, v. 120:103431, 2020. DOI: [10.1016/j.oregeorev.2020.103431](https://doi.org/10.1016/j.oregeorev.2020.103431).

PUTZOLU, F.; SANTORO, L.; PORTO, C.; MONDILLO, N.; MACHADO, M.; SAAR, B.A.; BASTOS, A; HERRINGTON, R. The Influence of the Magmatic to Postmagmatic Evolution of the Parent Rock on the Co Department in Lateritic Systems: The Example of the Santa Fé Ni-Co Deposit (Brazil). **Economic Geology**, v. 116, n. 4, p. 837–861, 2021. DOI: <https://doi.org/10.5382/econgeo.4819>.

QUESNEL, B.; de VESLUD, C.L.C.; BOULVAIS, P.; GAUTIER, P.; CATHELINÉAU, M.; DROULLET, M. 3D modeling of the laterites on top of the Koniambo Massif, New Caledonia: refinement of the per descensum lateritic model for nickel mineralization. **Miner Deposita**, v. 52, p. 961–978, 2017. DOI: <http://dx.doi.org/10.1016/j.chemgeo.2017.06.018>.

SILVA, M.L.M.C., OLIVEIRA, S.B., As fases portadoras de níquel do minério laterítico de níquel do vermelho, Serra do Carajás (PA). **Revista Brasileira de Geociências**, v. 25, n. 1, p. 69-78, 1995.

SONOKI I.K.; GARDA G.M. Idades K-Ar de rochas alcalinas do Brasil Meridional e Paraguai Oriental: compilação e adaptação as novas constantes de decaimento. **Boletim IG-USP, Série Científica**, v.19, p. 63-85, 1988.

TAULER, E.; LEWIS, J.F.; VILLANOVA-DE-BENAVENT, C.; AIGLSPERGER, T.; PROENZA, J.A.; DOMÈNECH, C.; GALLARDO, T.; LONGO, F.; GALÌ, S. Discovery of Ni-smectite-rich saprolite at Loma Ortega, Falcondo mining district (Dominican Republic): geochemistry and mineralogy of an unusual case of “hybrid hydrous Mg silicate – clay silicate” type Ni-laterite. **Miner Deposita**, v. 52, p. 1011–1030, 2017. DOI: <https://doi.org/10.1007/s00126-017-0750-8>.

TRESCASES, J.J. Géochimie des altérations et des eaux de surface dans le massif ultrabasique du Sud de la Nouvelle-Calédonie. *In: Bulletin du Service de la carte géologique d'Alsace et de Lorraine*, v. 22, n. 4, p. 329-354, 1969. DOI: <https://doi.org/10.3406/sgeol.1969.1361>

VILLANOVA-DE-BENAVENT, C.; PROENZA, J.A.; GALÍ, S.; GARCÍA-CASCO, A.; TAULER, E.; LEWIS, J.F.; LONGO, F. Garnierites and garnierites: textures, mineralogy and geochemistry of garnierites in the Falcondo Ni-laterite deposit, Dominican Republic. **Ore Geology Reviews**, v. 58, p.91–109, 2014.

WARR, L. IMA–CNMNC approved mineral symbols. **Mineralogical Magazine**, v. 85(3), p. 291-320, 2021. DOI:10.1180/mgm.2021.43.

WATLING, H.R.; ELLIOT, A.D.; FLETCHER H.M.; ROBINSON D.J.; SULLY, D.M. Ore mineralogy of nickel laterites: controls on processing characteristics under simulated heap-leach conditions, **Australian Journal of Earth Sciences**, v. 58, n.7, p. 725-744, 2011. DOI: 10.1080/08120099.2011.602986

WELLS, M.A.; RAMANAIDOU, E.R.; VERRALL, M.; TESSAROLO, C.; Mineralogy and crystal chemistry of “garnierites” in the Goro lateritic nickel deposit, New Caledonia. **European Journal of Mineralogy**, v. 21, n. 2, p. 467–483, 2009. DOI: <https://doi.org/10.1127/0935-1221/2009/0021-1910>.

ZALÁN, A.M.P.; THOMAZ-FILHO, A. Evolução Fanerozóica Das Bacias Sedimentares Brasileiras. *In: Mantesso Neto, V.; Bartorelli, A.; Carnerio, C.D.R.; Brito-Neves, B.B. Geologia do Continente Sul-Americano: Evolução da obra de Fernando Flávio Marques de Almeida*. São Paulo: Ed. Beca. 2004, 673p. P. 595-612.

SCHERER, C.M.S. Eolian dunes of the Botucatu Formation (Cretaceous) in southernmost Brazil: Morphology and origin. **Sedimentary Geology**, v. 137, n. 1–2, p. 63–84, 2000.

THORNE, R.L.R.L., ROBERTS, S.S., HERRINGTON, R.R. Climate change and the formation of nickel laterite deposits. **Geology**, v. 40, p. 331–334, 2012.

## CAPÍTULO 3 CONCLUSÕES

---

Dentre os principais apontamentos que este estudo forneceu, pode-se destacar alguns tópicos principais que caracterizam as principais conclusões obtidas diante dos resultados apresentados.

- A mineralização de Ni laterítico do depósito de Morro do Engenho está presente nos perfis de alteração derivados do núcleo dunítico e rochas periféricas formadas por peridotitos, piroxenitos e gabros.
- O balanço de massa mostra que o Ni apresenta enriquecimentos em relação à rocha parental, principalmente no saprólito inferior do perfil derivado do dunito, aonde chega até 40% e no saprólito inferior do perfil gabroico, com valores de até 1%.
- Os diagramas de correlação mostram que os teores de Ni se correlacionam positivamente com UMIA, ou seja, com o aumento do grau da lateritização, com exceção na DRCR, onde os teores de Ni são reduzidos. Ni correlaciona-se positivamente com Mg no domínio de seus baixos teores, enquanto apresenta correlação negativa nos altos teores de MgO.
- Cobalto mostra forte correlação positiva com UMIA, indicando o aumento dos teores a medida com que a lateritização avança. Os valores mais elevados de Co estão presentes no domínio óxido, principalmente no saprólito ocre, zona plasmática e duricrosta. A correlação entre Co e MnO é positiva e muito significativa, ressaltando a sua ligação com os minerais de Mn, em geral oxi-hidróxidos (asbolana).
- Os teores de REE exibem um aumento gradual juntamente com o aumento do grau de lateritização. O avanço dos teores desde o bedrock atinge o ápice nos horizontes do domínio óxido, principalmente saprólito ferruginoso, saprólito ocre e duricrosta. De modo geral, a rocha dunítica mostra-se com conteúdo inicial de REE menor que as rochas piroxenítica e gabroica. Em média, o horizonte laterítico que contém os maiores de REE é o saprólito ferruginoso.
- Os principais minerais silicáticos que hospedam o Ni são serpentina, clorita e esmectita. A serpentina rica em Ni é observada com maior abundância no horizonte do saprólito inferior do perfil derivado do dunito serpentizado e em menor expressão no perfil derivado da zona peridotito/piroxenítica. A mineralização associada à clorita é mais comum no perfil derivado de gabro, onde ocorre em abundância no saprólito inferior com teores de até 3,7% de Ni. No perfil derivado de peridotito/piroxenito, a clorita forma concentrações importantes, principalmente no horizonte de saprólito ferruginoso, exibindo teores de Ni de até 4,8%. Esmectita também compõe fase mineralizada neste horizonte com teores de até 3,27% de Ni. No saprólito ocre, clorita associada com esmectita e oxi-hidróxidos de Fe e Mn apresenta teores de Ni de até 4,65%.
- A mineralização relacionada a oxi-hidróxidos ocorre, preferencialmente, no domínio óxido, representado pelo saprólito ferruginoso e saprólito ocre. Contudo, também estão presentes no domínio silicático, com presença de oxi-hidróxidos de Mn (Fe) no preenchimentos de micro fraturas e interstícios da matriz. Goethita, asbolana e, secundariamente, romanechita são os principais minerais de Ni deste tipo de mineralização
- A passagem do clima seco para úmido provocou variações no regime hídrico de Morro do Engenho, entretanto, é possível supor que o avanço do front de alteração em Morro do Engenho

tenha sido iniciado a partir do aumento da precipitação regional, com forte influência das variações de pH ocasionadas pela infiltração de águas de chuva tropical ácida com pH ácido.

- A concentração dos maiores enriquecimentos em Ni em uma zona deprimida topograficamente demonstra que os processos formadores do depósito Morro do Engenho são compatíveis com o modelo de remobilização de Ni através de fatores hidrodinâmicos. A geomorfologia do depósito permite sugerir duas direções principais de fluxo lateral, uma no sentido SE e outra no sentido SW, que teriam convergido para a zona mais baixa entre as duas elevações topográficas.
- A geometria do depósito Morro do Engenho mostra que a redistribuição lateral através dos fatores hidrodinâmicos poderia também explicar a mineralização de áreas periféricas ao núcleo dunítico, compostas por perfis lateríticos derivados de piroxenito e gabro. A direção do fluxo regional de águas subterrâneas, influenciada fortemente pela topografia, seria um fator importante na remobilização do Ni dissolvido nos horizontes saprolíticos da zona dunítica, para a precipitação no saprolito inferior da região periférica de silicatos enriquecidos em Ni, compostos principalmente por clorita e esmectita.
- É provável que o transporte mecânico de materiais lateríticos também tenha exercido algum papel na mineralização dos perfis derivados de gabro e piroxenito, favorecendo a concentração de Ni nos produtos de alteração destas rochas.
- Os dados analisados neste estudo favorecem a classificação do depósito de Morro do Engenho como do tipo predominantemente silicático com participação importante de mineralização do tipo óxido.



## **APÊNDICE A – JUSTIFICATIVA DA PARTICIPAÇÃO DOS COAUTORES**

---

Participaram deste estudo como coautores o Prof. Pedro Maciel de Paula Garcia, como coorientador do projeto de pesquisa, o Prof. Aroldo Misi, orientador da dissertação, e a geóloga Alice dos Santos Dias.

O Prof. Pedro Maciel de Paula Garcia atuou como coorientador da pesquisa e participou nas discussões de resultados geoquímicos, petrográficos e MEV, estruturação da publicação, correções e revisão final.

O Prof. Aroldo Misi, orientador da pesquisa, contribuiu com a concepção da pesquisa, discussões dos resultados e das conclusões, correções do texto e revisão final.

A geóloga Alice dos Santos Dias teve participação nas fases de amostragem, caracterização petrográfica e geoquímica.

# ANEXO A – REGRAS DE FORMATAÇÃO DA REVISTA

## JOURNAL OF SOUTH AMERICAN EARTH SCIENCES

---

AUTHOR INFORMATION PACK 19 Apr 2022 [www.elsevier.com/locate/jsames](http://www.elsevier.com/locate/jsames)

### PREPARATION

#### *NEW SUBMISSIONS*

Submission to this journal proceeds totally online and you will be guided stepwise through the creation and uploading of your files. The system automatically converts your files to a single PDF file, which is used in the peer-review process.

As part of the Your Paper Your Way service, you may choose to submit your manuscript as a single file to be used in the refereeing process. This can be a PDF file or a Word document, in any format or layout that can be used by referees to evaluate your manuscript. It should contain high enough quality figures for refereeing. If you prefer to do so, you may still provide all or some of the source files at the initial submission. Please note that individual figure files larger than 10 MB must be uploaded separately.

#### *References*

There are no strict requirements on reference formatting at submission. References can be in any style or format as long as the style is consistent. Where applicable, author(s) name(s), journal title/book title, chapter title/article title, year of publication, volume number/book chapter and the article number or pagination must be present. Use of DOI is highly encouraged. The reference style used by the journal will be applied to the accepted article by Elsevier at the proof stage. Note that missing data will be highlighted at proof stage for the author to correct.

#### *Formatting requirements*

There are no strict formatting requirements but all manuscripts must contain the essential elements needed to convey your manuscript, for example Abstract, Keywords, Introduction, Materials and Methods, Results, Conclusions, Artwork and Tables with Captions.

If your article includes any Videos and/or other Supplementary material, this should be included in your initial submission for peer review purposes.

Divide the article into clearly defined sections.

#### *Figures and tables embedded in text*

Please ensure the figures and the tables included in the single file are placed next to the relevant text in the manuscript, rather than at the bottom or the top of the file. The corresponding caption should be placed directly below the figure or table.

#### *Peer review*

This journal operates a single anonymized review process. All contributions will be initially assessed by the editor for suitability for the journal. Papers deemed suitable are then typically sent to a minimum of two independent expert reviewers to assess the scientific quality of the paper. The Editor is responsible for the final decision regarding acceptance or rejection of articles. The Editor's decision is final. Editors are not involved in decisions about papers which they have written themselves or have been written by family members or colleagues or which relate to products or services in which the editor has an interest. Any such submission is subject to all of the journal's usual procedures, with peer review handled independently of the relevant editor and their research groups. [More information on types of peer review.](#)

#### *REVISED SUBMISSIONS*

##### *Use of word processing software*

Regardless of the file format of the original submission, at revision you must provide us with an editable file of the entire article. Keep the layout of the text as simple as possible. Most formatting codes will be removed and replaced on processing the article. The electronic text should be prepared in a way very similar to that of conventional manuscripts (see also the [Guide to Publishing with Elsevier](#)). See also the section on Electronic artwork.

To avoid unnecessary errors you are strongly advised to use the 'spell-check' and 'grammar-check' functions of your word processor.

**LaTeX**

You are recommended to use the Elsevier article class [elsarticle.cls](#) to prepare your manuscript and [BibTeX](#) to generate your bibliography.

Our [LaTeX site](#) has detailed submission instructions, templates and other information.

**Article structure****Subdivision - numbered sections**

Divide your article into clearly defined and numbered sections. Subsections should be numbered 1.1 (then 1.1.1, 1.1.2, ...), 1.2, etc. (the abstract is not included in section numbering). Use this numbering also for internal cross-referencing: do not just refer to 'the text'. Any subsection may be given a brief heading. Each heading should appear on its own separate line.

**Introduction**

State the objectives of the work and provide an adequate background, avoiding a detailed literature survey or a summary of the results.

**Material and methods**

Provide sufficient details to allow the work to be reproduced by an independent researcher. Methods that are already published should be summarized, and indicated by a reference. If quoting directly from a previously published method, use quotation marks and also cite the source. Any modifications to existing methods should also be described.

**Theory/calculation**

A Theory section should extend, not repeat, the background to the article already dealt with in the Introduction and lay the foundation for further work. In contrast, a Calculation section represents a practical development from a theoretical basis.

**Results**

Results should be clear and concise.

**Discussion**

This should explore the significance of the results of the work, not repeat them. A combined Results and Discussion section is often appropriate. Avoid extensive citations and discussion of published literature.

**Conclusions**

The main conclusions of the study may be presented in a short Conclusions section, which may stand alone or form a subsection of a Discussion or Results and Discussion section.

**Data Availability**

Authors are encouraged to include a 'Data Availability' section in their manuscript which is visible in ALL reading formats and may refer to data hosted in ANY repository. It should be placed before the references to provide readers with information about where they can obtain the research data required to reproduce the work reported in the manuscript, and typically consists of a simple sentence giving the URL(s) of and citation(s) to the dataset(s). Full information can be found [here](#).

**Appendices**

If there is more than one appendix, they should be identified as A, B, etc. Formulae and equations in appendices should be given separate numbering: Eq. (A.1), Eq. (A.2), etc.; in a subsequent appendix, Eq. (B.1) and so on. Similarly for tables and figures: Table A.1; Fig. A.1, etc.

**Essential title page information**

- **Title.** Concise and informative. Titles are often used in information-retrieval systems. Avoid abbreviations and formulae where possible.
- **Author names and affiliations.** Please clearly indicate the given name(s) and family name(s) of each author and check that all names are accurately spelled. You can add your name between parentheses in your own script behind the English transliteration. Present the authors' affiliation addresses (where the actual work was done) below the names. Indicate all affiliations with a lowercase superscript letter immediately after the author's name and in front of the appropriate address.  
Provide the full postal address of each affiliation, including the country name and, if available, the e-mail address of each author.
- **Corresponding author.** Clearly indicate who will handle correspondence at all stages of refereeing and publication, also post-publication. This responsibility includes answering any future queries about Methodology and Materials. **Ensure that the e-mail address is given and that contact details are kept up to date by the corresponding author.**
- **Present/permanent address.** If an author has moved since the work described in the article was done, or was visiting at the time, a 'Present address' (or 'Permanent address') may be indicated as a footnote to that author's

name. The address at which the author actually did the work must be retained as the main, affiliation address. Superscript Arabic numerals are used for such footnotes.

### **Highlights**

Highlights are mandatory for this journal as they help increase the discoverability of your article via search engines. They consist of a short collection of bullet points that capture the novel results of your research as well as new methods that were used during the study (if any). Please have a look at the examples here: [example Highlights](#). Highlights should be submitted in a separate editable file in the online submission system. Please use 'Highlights' in the file name and include 3 to 5 bullet points (maximum 85 characters, including spaces, per bullet point).

### **Abstract**

A concise and factual abstract is required. The abstract should state briefly the purpose of the research, the principal results and major conclusions. An abstract is often presented separately from the article, so it must be able to stand alone. For this reason, References should be avoided, but if essential, then cite the author(s) and year(s). Also, non-standard or uncommon abbreviations should be avoided, but if essential they must be defined at their first mention in the abstract itself.

### **Graphical abstract**

Although a graphical abstract is optional, its use is encouraged as it draws more attention to the online article. The graphical abstract should summarize the contents of the article in a concise, pictorial form designed to capture the attention of a wide readership. Graphical abstracts should be submitted as a separate file in the online submission system. Image size: Please provide an image with a minimum of 531 × 1328 pixels (h × w) or proportionally more. The image should be readable at a size of 5 × 13 cm using a regular screen resolution of 96 dpi. Preferred file types: TIFF, EPS, PDF or MS Office files. You can view [Example Graphical Abstracts](#) on our information site.

Authors can make use of Elsevier's [Illustration Services](#) to ensure the best presentation of their images and in accordance with all technical requirements.

### **Keywords**

Immediately after the abstract, provide a maximum of 6 keywords, using American spelling and avoiding general and plural terms and multiple concepts (avoid, for example, 'and', 'of'). Be sparing with abbreviations: only abbreviations firmly established in the field may be eligible. These keywords will be used for indexing purposes.

### **Abbreviations**

Define abbreviations that are not standard in this field in a footnote to be placed on the first page of the article. Such abbreviations that are unavoidable in the abstract must be defined at their first mention there, as well as in the footnote. Ensure consistency of abbreviations throughout the article.

### **Acknowledgements**

Collate acknowledgements in a separate section at the end of the article before the references and do not, therefore, include them on the title page, as a footnote to the title or otherwise. List here those individuals who provided help during the research (e.g., providing language help, writing assistance or proof reading the article, etc.).

### **Formatting of funding sources**

List funding sources in this standard way to facilitate compliance to funder's requirements:

Funding: This work was supported by the National Institutes of Health [grant numbers xxxx, yyyy]; the Bill & Melinda Gates Foundation, Seattle, WA [grant number zzzz]; and the United States Institutes of Peace [grant number aaaa].

It is not necessary to include detailed descriptions on the program or type of grants and awards. When funding is from a block grant or other resources available to a university, college, or other research institution, submit the name of the institute or organization that provided the funding.

If no funding has been provided for the research, it is recommended to include the following sentence:

This research did not receive any specific grant from funding agencies in the public, commercial, or not-for-profit sectors.

### **Units**

Follow internationally accepted rules and conventions: use the international system of units (SI). If other units are mentioned, please give their equivalent in SI.

### **Math formulae**

Please submit math equations as editable text and not as images. Present simple formulae in line with normal text where possible and use the solidus (/) instead of a horizontal line for small fractional terms, e.g., X/Y. In

principle, variables are to be presented in italics. Powers of  $e$  are often more conveniently denoted by  $\exp$ . Number consecutively any equations that have to be displayed separately from the text (if referred to explicitly in the text).

#### **Footnotes**

Footnotes should be used sparingly. Number them consecutively throughout the article. Many word processors build footnotes into the text, and this feature may be used. Should this not be the case, indicate the position of footnotes in the text and present the footnotes themselves separately at the end of the article.

#### **Electronic artwork**

##### *General points*

- Make sure you use uniform lettering and sizing of your original artwork.
- Preferred fonts: Arial (or Helvetica), Times New Roman (or Times), Symbol, Courier.
- Number the illustrations according to their sequence in the text.
- Use a logical naming convention for your artwork files.
- Indicate per figure if it is a single, 1.5 or 2-column fitting image.
- For Word submissions only, you may still provide figures and their captions, and tables within a single file at the revision stage.
- Please note that individual figure files larger than 10 MB must be provided in separate source files.

A detailed [guide on electronic artwork](#) is available.

**You are urged to visit this site; some excerpts from the detailed information are given here.**

##### *Formats*

Regardless of the application used, when your electronic artwork is finalized, please 'save as' or convert the images to one of the following formats (note the resolution requirements for line drawings, halftones, and line/halftone combinations given below):

EPS (or PDF): Vector drawings. Embed the font or save the text as 'graphics'.

TIFF (or JPG): Color or grayscale photographs (halftones): always use a minimum of 300 dpi.

TIFF (or JPG): Bitmapped line drawings: use a minimum of 1000 dpi.

TIFF (or JPG): Combinations bitmapped line/half-tone (color or grayscale): a minimum of 500 dpi is required.

##### **Please do not:**

- Supply files that are optimized for screen use (e.g., GIF, BMP, PICT, WPG); the resolution is too low.
- Supply files that are too low in resolution.
- Submit graphics that are disproportionately large for the content.

##### *Color artwork*

Please make sure that artwork files are in an acceptable format (TIFF (or JPEG), EPS (or PDF) or MS Office files) and with the correct resolution. If, together with your accepted article, you submit usable color figures then Elsevier will ensure, at no additional charge, that these figures will appear in color online (e.g., ScienceDirect and other sites) in addition to color reproduction in print. [Further information on the preparation of electronic artwork.](#)

##### **Figure captions**

Ensure that each illustration has a caption. A caption should comprise a brief title (**not** on the figure itself) and a description of the illustration. Keep text in the illustrations themselves to a minimum but explain all symbols and abbreviations used.

##### **Tables**

Please submit tables as editable text and not as images. Tables can be placed either next to the relevant text in the article, or on separate page(s) at the end. Number tables consecutively in accordance with their appearance in the text and place any table notes below the table body. Be sparing in the use of tables and ensure that the data presented in them do not duplicate results described elsewhere in the article. Please avoid using vertical rules and shading in table cells.

##### **References**

###### *Citation in text*

Please ensure that every reference cited in the text is also present in the reference list (and vice versa). Any references cited in the abstract must be given in full. Unpublished results and personal communications are not recommended in the reference list, but may be mentioned in the text. If these references are included in the reference list they should follow the standard reference style of the journal and should include a substitution of the publication date with either 'Unpublished results' or 'Personal communication'. Citation of a reference as 'in press' implies that the item has been accepted for publication.

### ***Web references***

As a minimum, the full URL should be given and the date when the reference was last accessed. Any further information, if known (DOI, author names, dates, reference to a source publication, etc.), should also be given. Web references can be listed separately (e.g., after the reference list) under a different heading if desired, or can be included in the reference list.

### ***Data references***

This journal encourages you to cite underlying or relevant datasets in your manuscript by citing them in your text and including a data reference in your Reference List. Data references should include the following elements: author name(s), dataset title, data repository, version (where available), year, and global persistent identifier. Add [dataset] immediately before the reference so we can properly identify it as a data reference. The [dataset] identifier will not appear in your published article.

### ***References in a special issue***

Please ensure that the words 'this issue' are added to any references in the list (and any citations in the text) to other articles in the same Special Issue.

### ***Reference management software***

Most Elsevier journals have their reference template available in many of the most popular reference management software products. These include all products that support [Citation Style Language styles](#), such as [Mendeley](#). Using citation plug-ins from these products, authors only need to select the appropriate journal template when preparing their article, after which citations and bibliographies will be automatically formatted in the journal's style. If no template is yet available for this journal, please follow the format of the sample references and citations as shown in this Guide. If you use reference management software, please ensure that you remove all field codes before submitting the electronic manuscript. [More information on how to remove field codes from different reference management software.](#)

### ***Reference Formatting***

There are no strict requirements on reference formatting at submission. References can be in any style or format as long as the style is consistent. Where applicable, author(s) name(s), journal title/book title, chapter title/article title, year of publication, volume number/book chapter and the pagination must be present. Use of DOI is highly encouraged. The reference style used by the journal will be applied to the accepted article by Elsevier at the proof stage. Note that missing data will be highlighted at proof stage for the author to correct. If you do wish to format the references yourself they should be arranged according to the following examples:

[dataset] Oguro, M., Imahiro, S., Saito, S., Nakashizuka, T., 2015. Mortality data for Japanese oak wilt disease and surrounding forest compositions. Mendeley Data, v1. <http://dx.doi.org/10.17632/xwj98nb39r.1>.

### ***Reference style***

All publications cited in the text should be presented in a list of references following the text of the manuscript. In the text refer to the author's name (without initials) and year of publication (e.g. "Since Condie (2001) has shown that..." or "This is in agreement with results obtained later (Meert, 2003; Burrett and Berry, 2000)."

For three or more authors use the first author followed by "et al.", in the text. The list of references should be arranged alphabetically by authors' names. The manuscript should be carefully checked to ensure that the spelling of authors' names and dates are exactly the same in the text as in the reference list.

References should be given in the following form:

Kusky, T.M., Stern, R.J., Tucker, R.D., 2003. Evolution of East African and related orogens, and the assembly of Gondwana. *Precambrian Research*, 123, 81–85. Pili, E., Sheppard, S.M.F., Lardeaux, J.M., 1999. Fluid–rock interaction in the granulites of Madagascar and lithospheric transfer of fluids. *Gondwana Research*, 2, 341–350.

Suzuki, K., Adachi, M., 1992. Middle Precambrian detrital monazite and zircon from Hida gneiss in Oki- Dogo island, Japan: their origin and implications for the correlation of basement gneiss of Southwest Japan and Korea. *Tectonophysics*, 235, 277–292.

Touret, J.L.R., 1985. Fluid regime in southern Norway, the record of fluid inclusions. In: Tobi, A.C., Touret, J.L.R. (Eds.), *The Deep Proterozoic Crust in the North Atlantic Provinces*. Reidel, Dordrecht, 517–549.

Kinny, P. D., Collins, A. S., Razakamanana, T., 2004. Provenance hints and age constraints of metasedimentary gneisses of Southern Madagascar from SHRIMP U–Pb zircon data. In: Chetty, T.R.K. and Bhaskar Rao, Y.J. (Eds.), *International Field Workshop on the Southern Granulite Terrane*. National Geophysical Research Institute, Hyderabad, India, 97–98.

Rogers, J.J.W. and Santosh, M., 2004. *Continents and Supercontinents*. Oxford University Press, New York. Li, Z.X., Metcalfe, I., Powell, C.M. (Eds.), 1996. Breakup of Rodinia and Gondwanaland and Assembly of Asia. *Australian Journal of Earth Sciences* 43.

Albee, H.F., Cullins, H.L., 1975. Geologic map of the Alpine Quadrangle, Bonneville County, Idaho, and Lincoln County Wyoming. United States Geological Survey Geologic Quadrangle Map GQ–1259, scale 1:24,000.

Sajeev, K., 2003. Evolution and metamorphic zoning of Highland Complex, Sri Lanka: a comparison with Madurai Block, southern India. Ph.D. thesis, Okayama University.

### **Video**

Elsevier accepts video material and animation sequences to support and enhance your scientific research. Authors who have video or animation files that they wish to submit with their article are strongly encouraged to include links to these within the body of the article. This can be done in the same way as a figure or table by referring to the video or animation content and noting in the body text where it should be placed. All submitted files should be properly labeled so that they directly relate to the video file's content. In order to ensure that your video or animation material is directly usable, please provide the file in one of our recommended file formats with a preferred maximum size of 150 MB per file, 1 GB in total. Video and animation files supplied will be published online in

the electronic version of your article in Elsevier Web products, including [ScienceDirect](#). Please supply 'stills' with your files: you can choose any frame from the video or animation or make a separate image. These will be used instead of standard icons and will personalize the link to your video data. For more detailed instructions please visit our [video instruction pages](#). Note: since video and animation cannot be embedded in the print version of the journal, please provide text for both the electronic and the print version for the portions of the article that refer to this content.

### **Data visualization**

Include interactive data visualizations in your publication and let your readers interact and engage more closely with your research. Follow the instructions [here](#) to find out about available data visualization options and how to include them with your article.

### **Supplementary material**

Supplementary material such as applications, images and sound clips, can be published with your article to enhance it. Submitted supplementary items are published exactly as they are received (Excel or PowerPoint files will appear as such online). Please submit your material together with the article and supply a concise, descriptive caption for each supplementary file. If you wish to make changes to supplementary material during any stage of the process, please make sure to provide an updated file.

Do not annotate any corrections on a previous version. Please switch off the 'Track Changes' option in Microsoft Office files as these will appear in the published version.

### **Research data**

This journal requires and enables you to share data that supports your research publication where appropriate, and enables you to interlink the data with your published articles. Research data refers to the results of observations or experimentation that validate research findings. To facilitate reproducibility and data reuse, this journal also encourages you to share your software, code, models, algorithms, protocols, methods and other useful materials related to the project.

Below are a number of ways in which you can associate data with your article or make a statement about the availability of your data when submitting your manuscript. When sharing data in one of these ways, you are expected to cite the data in your manuscript and reference list. Please refer to the "References" section for more information about data citation. For more information on depositing, sharing and using research data and other relevant research materials, visit the [research data page](#).

#### **Data linking**

If you have made your research data available in a data repository, you can link your article directly to the dataset. Elsevier collaborates with a number of repositories to link articles on ScienceDirect with relevant repositories, giving readers access to underlying data that gives them a better understanding of the research described.

There are different ways to link your datasets to your article. When available, you can directly link your dataset to your article by providing the relevant information in the submission system. For more information, visit the [database linking page](#).

For [supported data repositories](#) a repository banner will automatically appear next to your published article on ScienceDirect.

In addition, you can link to relevant data or entities through identifiers within the text of your manuscript, using the following format: Database: xxxx (e.g., TAIR: AT1G01020; CCDC: 734053; PDB: 1XFN).

#### **Mendeley Data**

This journal supports Mendeley Data, enabling you to deposit any research data (including raw and processed data, video, code, software, algorithms, protocols, and methods) associated with your manuscript in a free-to-use,

open access repository. During the submission process, after uploading your manuscript, you will have the opportunity to upload your relevant datasets directly to *Mendeley Data*. The datasets will be listed and directly accessible to readers next to your published article online.

For more information, visit the [Mendeley Data for journals page](#).

**To maximise the visibility of your data, authors are invited to add a citation to their datasets by including a data reference in their Reference List as per the 'Data References' instructions elsewhere on this page.**

### ***Data in Brief***

You have the option of converting any or all parts of your supplementary or additional raw data into a data article published in *Data in Brief*. A data article is a new kind of article that ensures that your data are actively reviewed, curated, formatted, indexed, given a DOI and made publicly available to all upon publication (watch this [video](#) describing the benefits of publishing your data in *Data in Brief*). You are encouraged to submit your data article for *Data in Brief* as an additional item directly alongside the revised version of your manuscript. If your research article is accepted, your data article will automatically be transferred over to *Data in Brief* where it will be editorially reviewed, published open access and linked to your research article on ScienceDirect. Please note an [open access fee](#) is payable for publication in *Data in Brief*. Full details can be found on the [Data in Brief website](#). Please use [this template](#) to write your *Data in Brief* data article.

### ***MethodsX***

You have the option of converting relevant protocols and methods into one or multiple *MethodsX* articles, a new kind of article that describes the details of customized research methods. Many researchers spend a significant amount of time on developing methods to fit their specific needs or setting, but often without getting credit for this part of their work. *MethodsX*, an open access journal, now publishes this information in order to make it searchable, peer reviewed, citable and reproducible.

Authors are encouraged to submit their *MethodsX* article as an additional item directly alongside the revised version of their manuscript. If your research article is accepted, your methods article will automatically be transferred over to *MethodsX* where it will be editorially reviewed. Please note no open access fee is payable for publication in *MethodsX*. Full details can be found on the [MethodsX website](#). Please use the [methods template](#) or [protocol template](#) to prepare your *MethodsX* article.

### ***Data statement***

To foster transparency, we require you to state the availability of your data in your submission if your data is unavailable to access or unsuitable to post. This may also be a requirement of your funding body or institution. You will have the opportunity to provide a data statement during the submission process. The statement will appear with your published article on ScienceDirect. For more information, visit the [Data Statement page](#).



# ANEXO B – COMPROVANTE DE SUBMISSÃO DO ARTIGO

08/08/2022 16:26

E-mail de COMPANHIA DE PESQUISA DE RECURSOS MINERAIS CPRM - Confirming submission to Journal of South Am...



Eduardo Moussalle Grissolia &lt;eduardo.grissolia@cprm.gov.br&gt;

## Confirming submission to Journal of South American Earth Sciences

**Journal of South American Earth Sciences** <em@editorialmanager.com>

8 de agosto de 2022 16:25

Responder a: Journal of South American Earth Sciences <support@elsevier.com>

Para: EDUARDO MOUSSALLE GRISSOLIA <eduardo.grissolia@cprm.gov.br>

\*This is an automated message.\*

MINERALOGY AND GEOCHEMISTRY OF THE MORRO DO ENGENHO LATERITIC NICKEL DEPOSIT, GOIÁS  
ALKALINE PROVINCE, BRAZIL

Dear Mr. GRISSOLIA,

We have received the above referenced manuscript you submitted to Journal of South American Earth Sciences.

To track the status of your manuscript, please log in as an author at <https://www.editorialmanager.com/sames/>, and navigate to the "Submissions Being Processed" folder.

Thank you for submitting your work to this journal.

Kind regards,  
Journal of South American Earth Sciences

More information and support

You will find information relevant for you as an author on Elsevier's Author Hub: <https://www.elsevier.com/authors>

FAQ: How can I reset a forgotten password?

[https://service.elsevier.com/app/answers/detail/a\\_id/28452/supporthub/publishing/](https://service.elsevier.com/app/answers/detail/a_id/28452/supporthub/publishing/)

For further assistance, please visit our customer service site: <https://service.elsevier.com/app/home/supporthub/publishing/>

Here you can search for solutions on a range of topics, find answers to frequently asked questions, and learn more about Editorial Manager via interactive tutorials. You can also talk 24/7 to our customer support team by phone and 24/7 by live chat and email

This journal uses the Elsevier Article Transfer Service. This means that if an editor feels your manuscript is more suitable for an alternative journal, then you might be asked to consider transferring the manuscript to such a journal. The recommendation might be provided by a Journal Editor, a dedicated Scientific Managing Editor, a tool assisted recommendation, or a combination. For more details see the journal guide for authors.

#AU\_SAMES#

To ensure this email reaches the intended recipient, please do not delete the above code

In compliance with data protection regulations, you may request that we remove your personal registration details at any time. (Use the following URL: <https://www.editorialmanager.com/sames/login.asp?a=r>). Please contact the publication office if you have any questions.